Investigating the structure of chromatin *in vitro*: the roles of H4 K16 acetylation, linker histone H5, and the DNA template.

by

Alison Calestagne-Morelli
B.Sc. University of Victoria, 2004

A Dissertation Submitted in Partial Fulfillment of the Requirements for the Degree of

MASTER OF SCIENCE

in the Department of Microbiology and Biochemistry

Investigating the structure of chromatin *in vitro*: the roles of H4 K16 acetylation, linker histone H5, and the DNA template.

by

Alison Calestagne-Morelli
B.Sc. University of Victoria, 2004

Supervisory Committee

Juan Ausio

Supervisor

Terry W. Pearson

Departmental Member

John Taylor

Outside Member

Supervisory Committee

Juan Ausio

Supervisor

Terry W. Pearson

Departmental Member

John Taylor

Outside Member

Abstract

It has been frequently postulated that genome or domain-wide histone post-translational modifications induce structural changes to chromatin. Until recently, however, experimental evidence for this hypothesis was lacking. H4 K16 acetylation is the first, and only, of all of the possible post-translational modifications to be directly linked to changes in chromatin conformation. I was interested in clarifying the mechanism by which H4 K16Ac exerts its modulatory effect. To characterize the role of this modification I reconstituted mononucleosomes with H4 K16Ac isolated from chicken erythrocytes by weak cation-exchange HPLC. Analytical ultracentrifuge (AUC) and $MgCl_2$ solubility data suggested that H4 K16Ac structurally relaxes the association of nucleosomal DNA with the histone octamer by weakening intra-nucleosomal DNA-histone electrostatic interaction.

Similar to early studies on H4 K16 acetylation, evidence suggests that the phosphorylation of linker histones promotes chromatin decondensation and increases DNA accessibility. In an effort to initiate a study characterizing the structural effects of chromatin fibers containing phosphorylated linker histones, I have optimized a method of

purification for nonphosphorylated and monophosphorylated linker histone H5 from erythrocytes of anemic chickens. Preliminary AUC data of oligonucleosomes containing the nonphosphorylated control linker histones (manipulated to the same degree as the experimental monophosphorylated linker histones) showed a salt-dependent sedimentation trend that was consistent with expected values at low ionic concentrations. The purification method described is valuable as it results in a high yield of pure post-translationally modified H5 product suitable for oligonucleosome reconstitutions.

In the third component of this thesis, I describe the creation of a DNA template, Pbsn-208(10), which contains a *Rattus norvegicus* probasin promoter nucleosome positioning sequence flanked on both sides by 5 tandem repeats of the *Lytechinus variegatus* nucleosome positioning sequence. Unlike other DNA templates used in the study of chromatin compaction *in vitro*, the Pbsn-208(10) allows not only the reconstitution of homogenous chromatin fibers but also the differentiation of the middle of the fiber from its flanking ends. Thus, the effects of PTMs on histone-DNA interactions and nucleosome conformation in the center of a chromatin fiber can now be easily investigated. In addition, the Pbsn-208(10) template can help to identify the precise location of H1/H5 within the nucleosome.

Table of Contents

List of Tables

Acknowledgements

I am very grateful for all the help, encouragement, support, and inspiration I received throughout my time as a grad student. Thanks to every one of the Ausio lab members for all their help, support, and shared laughs over these two years. Thanks to all of my friends and family for putting up with me, and supporting me through good times and sometimes more difficult times. Thanks to UVIC for the financial support (Fellowship) that provided me with the opportunity to excel. Thanks to Deb and Melinda in the Bioc. office for all of their work and for helping me make it to the finish line. A special thanks to my supervisor, Dr. Ausio, for always making time for me despite his very busy schedule: Dr. Ausio thanks for your support, for your guidance, and for always sharing ideas, inspiration, and motivation. I had a great and memorable experience as a grad student in the Ausio lab. I would also like to thank my committee members, Dr. Taylor, and Dr. Pearson, for their guidance and support. Thanks to my Dad, for his words of wisdom and for encouraging me to persevere. Thanks to my partner, Chris, for your love and support through floods, power-outages, and everything else! See you at 'firsts' (soon enough anyways). Finally, thanks to my mom who taught me how to face a challenge.

1.0 INTRODUCTION

DNA within eukaryotic cells is tightly compacted into a highly conserved nucleoprotein complex called chromatin. The nucleosome core particle is the fundamental unit of chromatin and consists of 146 base pairs of DNA wrapped around a heterotypic histone octamer [$(H3\text{-}H4)_2 \cdot 2(H2A\text{-}H2B)$] in a left handed superhelix (Luger et al. 1997). Neighboring nucleosomes are connected by 30-40 base pairs of linker DNA to which linker histones bind and facilitate chromatin condensation into transcriptionally repressive 30-100 nm fibers (Ausio and Abbott 2004).

Gene expression is controlled in part by regulated changes to the nuclear organization of DNA. Chromatin that is highly compact is inaccessible to transcriptional activators. Conversely, gene activation is made possible following the targeted decondensation of specific chromosomal domains. Transitions from one structural and functional state of chromatin to another are correlated to changes in covalent histone modifications (Spotswood and Turner 2002). Histone posttranslational modifications (PTMs) include acetylation, methylation, phosphorylation, ADP-ribosylation, and ubiquitination (Ausio and Abbott 2004). Numerous families of enzymes are responsible for catalyzing the addition and removal of modifying groups to highly conserved sites on histone N-terminal tails.

The histone code hypothesis predicts that unique patterns of PTMs are connected to specific biological outcomes by forming a language read by many other regulatory factors (Strahl and Allis 2000). The total number of possible combinations of histone modifications is extremely high and is representative of a vast amount of epigenetic

information. For instance, there are 50 unique acetylated histone isoforms alone (Spotswood and Turner 2002). Recently, a new histone modification nomenclature has been proposed with a goal of establishing unambiguous designations for complex higher-order combinations (Turner 2005).

Of all the histone post-translational modifications, acetylation has generated the most interest and has been extensively studied since it was first linked to gene activity (Strahl and Allis 2000). In 1964, it was reported that nuclear histone acetylation—which occurs on the e-amino group of lysines in the four core histones—was associated with an increase in transcriptional activity (Allfrey et al. 1964). Moreover, although histone tails contain multiple modifiable lysine residues, it was found that only specific ones are subject to acetylation and that this trend is highly conserved among species (van Holde 1989).

Histone acetylation is a highly reversible process catalyzed by cellular histone acetyltransferases (HATs) and histone deacetylases (HDACs) respectively. Evidence suggests that some HATs can be further subdivided into two classes; the first acts locally modifying only neighboring nucleosomes (Korzus et al. 1998; Kuo et al. 2000; Parekh and Maniatis 1999; Vignali et al. 2000), while the second acetylates histones on a more global level or over considerable distances (Krebs et al. 2000; Vignali et al. 2000; Vogelauer et al. 2000). Concomitantly, acetylated tails may exert their modulatory effects in two non-mutually exclusive ways. First, acetylated residues and/or synergistic combinations of posttranslational modifications (PTMs) can recruit, or mediate interactions with other regulatory factors. This type of acetylation is targeted to enhancers, promoters, and /or other regulatory elements, and is generally associated with

gene activation. It is believed that these modifications are part of the histone code and are recognized by transactivating factors resulting in distinct downstream events (Jenuwein and Allis 2001; Strahl and Allis 2000). Second, histone acetylation has also been correlated to the establishment of broad regions of chromatin (several kilobases) that are more sensitive to DNAse I and therefore considered to be in a more open conformation. This type of domain- or genome-wide acetylation is not considered part of the histone code. Rather, it is associated with fiber decondensation which, structurally poises chromatin for transcriptional activity (Eberharter and Becker 2002; Forsberg et al. 2000; Hebbes et al. 1994; Perry and Chalkley 1982; Schubeler et al. 2000). The molecular mechanism of acetylation induced chromatin decondensation, however, remains unclear.

1.1 Global and long-range histone acetylation: genomic views

In yeast, targeted histone acetylation takes place among simultaneously occurring genome-wide HAT and HDAC activity (Vogelauer et al. 2000). Similar to localized acetyl-transfer activity, genome-wide steady-state levels of *Saccharomyces cerevisiae*'s histone acetylation are strictly regulated and maintained (Katan-Khaykovich and Struhl 2002; Reid et al. 2004; Topalidou et al. 2003). A recent study using the genome-wide mapping technique (GMAT) indicates that general levels of histone acetylation in *Saccharomyces cerevisiae*'s entire genome are high (Roh et al. 2004). These results are in agreement with previous work by Waterborg (2000) and most likely reflect the fact that in this organism most of the genome exists as euchromatin (Waterborg 2000). Further enrichment is generally found at the 5' end of a gene's coding region—usually within the first 500 bp of the open reading frame (Roh et al. 2004).

In more highly differentiated eukaryotic cells, the majority of the genome is characterized as inactive heterochromatin populated by hypoacetylated nucleosomes. GMAT data indicates that the majority of acetylation is localized to euchromatic promoter regions and/or regulatory elements, and does not commonly span entire active domains the way it does in yeast (Roh et al. 2005). However, genomic characterization of various euchromatic regions in more highly differentiated eukaryotes has revealed that domain-wide acetylation (over several kilobases) does indeed occur at a range of loci including individual genes (Zhou et al. 2004), gene family clusters (Chambeyron and Bickmore 2004; Elefant et al. 2000; Hebbes et al. 1994) compound clusters (Baxter et al. 2005; Chowdhury and Sen 2001) and more general clusters of unrelated genes (Litt et al. 2001). Among these loci are a wide variety of eukaryotic gene types such as tissue specific, housekeeping, and colinear and developmentally regulated genes (Chambeyron and Bickmore 2004; Chowdhury and Sen 2001; Litt et al. 2001; Myers et al. 2001; Rastegar et al. 2004).

Domain-wide acetylation across gene clusters is typically non-uniform. Patterns characterized by peaks and valleys of hyperacetylation are established across domains in a strictly conserved manner within each unique cellular system (Calestagne-Morelli and Ausio 2006). Evidence suggests that acetylation patterns conserved over distinct loci reflect biological variability in the regulation of genes expression. Acetylation patterns were observed to vary across biologically related genes in *Saccharomyces cerevisiae* (Kurdistani et al. 2004). In this study, ChIP-microarray profiling of intergenic regions (IGRs) and open reading frames (ORFs) was used to determine genome-wide acetylation

at lysine residues on the four core histones in *S. cerevisiae* (Kurdistani et al. 2004). Subsequent statistical and clustering algorithm analysis revealed strong positive correlations between distinct combinations of histone acetylation among biologically related genes. Consistent patterns of modifications were observed on the same or different histones within promoter and coding regions among groups of coexpressed genes that share cis-regulatory elements, bind specific transcription factors, and function in similar physiological processes. It is not known whether or not the same trend is found among biologically related genes in higher eukaryotes.

Regions of conserved synteny within the a–globin cluster in human, mouse and chicken, do however, exhibit a similar pattern of domain-wide histone acetylation (Anguita et al. 2001). Anguita et al (2001) propose that this pattern makes up part of a histone code that has marked the a–globin cluster as an erythroid specific transcriptionally competent domain throughout evolution (Anguita et al. 2001). The establishment of distinct long-range patterns of histone post-translational modification at orthologous loci is not limited to acetylation. Recently, genomic mapping and comparative analysis of histone methylation on chromosomes 21 and 22 in human and mouse also show strongly conserved patterns of this modification at orthologous loci (Bernstein et al. 2005). Thus, it is not unlikely that selective pressures play a primary role in shaping the mechanisms involved in the establishment of domain-wide non-uniform patterns of histone post-translational modifications throughout evolution.

Patterns of histone acetylation across a given domain in highly differentiated eukaryotes may be characteristic of transcriptional regulation where cell lineage-restricted HATs are key players in distinct gene activation pathways. Studies show that the

establishment of domain-wide acetylation patterns requires specific transcription factors and that changes in these patterns coincide with changes in gene expression (Letting et al. 2003; Litt et al. 2001). The recruitment of the transcription factor GATA-1 and the CBP histone acetyltransferase, for instance, is required for the formation of tissue-specific and developmentally regulated histone acetylation patterns and proper lineage specific gene expression at the ß-globin gene cluster (Letting et al. 2003). Alternatively, domain-wide acetylation is also believed to be a developmental marker for stimulus-specific transcription within the same tissue (Chang and Aune 2005). For example, two distinct hyperacetylation patterns across the *Ifng* gene can result from two different transcriptional signaling pathways in mouse natural killer cells (Chang and Aune 2005). In short, context dependent domain-wide acetylation appears to reflect each unique system's mode of gene regulation. Furthermore, acetylation may not only establish transcriptional potential across a domain but also transmit that epigenetic information to subsequent cellular generations (Turner 1993).

An important consideration, however regarding studies of long range and global acetylation patterns has to do with the high rates of acetylation turnover. With some half-lives as short as a few minutes (Clayton et al. 2006; Waterborg 2002), differential occupation by bromo-domain-containing proteins has the potential to mask the acetylated state of histone residues. Also, ChIP results may represent genome averages of acetylation across a domain rather than reflect the variability of acetylation due to rapid turnover of the modification within a population of cells growing asynchronously.

1.2 The structural implications for domain-wide histone acetylation

Given the common relationship between structure and function and that eukaryotic cells have evolved to maintain domain wide hyperacetylation, it is important to consider what purpose it is serving beyond the histone code (Jenuwein and Allis 2001; Strahl and Allis 2000). In particular, it is necessary to understand how histone acetylation impacts chromatin's structural integrity and in turn, modulates chromatin accessibility (Gorisch et al. 2005). Within the nucleosome, histone N-terminal tails are highly basic, lysine rich, relatively unstructured, and interact with negatively charged DNA. It has been proposed in the past that histone acetylation results in the release of histone tails from nucleosomal DNA which effectively leads to a more open chromatin structure and allows for increased transcription factor access (Turner 2005). Mutskov et al. (1998) demonstrate, however, that while acetylation reduces NH_2 tail lysine-positive charges under physiological ionic conditions, it does not result in the release of histone tails from DNA. Results from their study show that the efficiency of UV-induced hyperacetylated histone tail-DNA cross-linking is very similar to that of their hypoacetylated counterparts (Mutskov et al. 1998). In addition, greater than 50% of hyperacetylated histone tail-DNA interactions for H2B and H4, and 70% of those for H2A were retained upon the binding of the chimeric transcription factor GAL4-AH. This lack of complete NH_2 tail displacement is impressive considering that GAL4-AH occupies the central 90 base pairs of the core particle. These findings indicate that histone hyperacetylation does not abolish histone tail-DNA interactions even in the presence of DNA binding factors.

Mutskov et al. (1998) did demonstrate, however, that an increase in ionic strength results in a more pronounced decrease in cross-linking efficiency for hyperacetylated

nucleosomes. The authors therefore concluded that histone acetylation provokes a weakening, rather than a complete disruption of NH_2 tail-DNA associations, and that electrostatic interactions persist while nucleosomal DNA is co-occupied by transcription factors. Thus, although acetylation-induced structural changes at the lowest level of chromatin integrity are subtle, a dynamic role for the core particle in the context of gene expression is supported.

Consistent with this, numerous studies drawing from a wide variety of experimental approaches provide evidence that acetylation weakens nucleosome stability (Dunker et al. 2001; Oliva et al. 1990; Siino et al. 2003). Dunker et al., (2001) characterize the effect that a reduction in histone tail-DNA electrostatic bond strength has on nucleosomal stability by way of atomic force microscopy (AFM). With this technique, the authors were able to view hydrated nucleosomes under atmospheric pressure and increasing applied forces. They found that hyperacetylated core particles fall apart at significantly lower forces than non-acetylated nucleosomes (Dunker et al. 2001). In a separate study, Siino et al. (2003) reported thermal denaturation profiles for nucleosome core particles consisting exclusively of tetra-acetylated H4 compared to non-acetylated complexes. While two major transitions are present in both profiles as is expected for nucleosome core particles, the main transition for the tetra-acetylated H4 nucleosome is destabilized by 0.8 °C. These works suggest that acetylation mediates a decrease in the ionic and thermal stability of NH_2 tail-DNA interactions. Siino et al. (2003) also mention that the degree of thermal destabilization reported in their study is very similar to values found for globally hyperacetylated core particles in previously published works. They

thus conclude that the H4 tail may be responsible for many of the lysine-DNA contacts within the nucleosome (Siino et al. 2003).

Specific contributions of acetylated histone tails to nucleosome destabilization were examined recently by Brower-Toland et al. (2005). In this study, nucleosome arrays were acetylated to different degrees by the cellular histone acetyltransferase p300. The fibers were then mechanically stretched in order to characterize their individual nucleosomal patterns of DNA release using an optical trap. Interestingly, Brower-Toland et al. (2005) observe that within the three to four hour period of the histone acetylation reactions, the neutralization of ~ 1 lysine per H2A/H2B and H3/H4 results in a more dramatic nucleosome destabilization effect than the same level of neutralization prior to this period. The researchers proposed that this effect points to one of two possibilities. Either p300 acetylates a specific critical residue later on in a distinctly ordered fashion or their results are indicative of an acetylation threshold beyond which the tails are provoked into some type of conformational change resulting in the observed decrease in stability (Brower-Toland et al. 2005).

Evidence suggests that NH_2 tail a-helical content increases with acetylation independent of histone-DNA interactions (Wang et al. 2000). In this study, researchers were able to detect changes in secondary structure of octamers by subtracting the nucleosomal DNA's contribution to the far UV region of a circular dichroism (CD) spectrum from that of the core particle. Using this technique it was further determined that the a-helical content of H4 tail alone increases according to its degree of acetylation. By comparing their biophysical data to the predicted locations of the 23 N-terminal amino acid residues in a helical wheel, the authors conclude that lysine 16 acetylation on H4 is

the principal candidate for the resulting increase in a-helical content of this histone. Although Wang et al. (2000) do not include analyses of the individual spectral contributions of H2A/H2B or H3 as they did for H4, their results nevertheless provide support, in part, for postulations made by Brower-Toland et al. (2005). Histone acetylation indeed induces conformational changes in the nucleosome (Ausio and van Holde 1986) and nucleosomal arrays (Garcia-Ramirez et al. 1995), and a critical residue is likely to play a role. To this end, it is possible that H4 K16 acetylation functions in conjunction with other non-specific cumulative histone acetylation effects to modulate chromatin conformation making the two possibilities non-mutually exclusive (Calestagne-Morelli and Ausio 2006).

1.3 H4 K16 and the structure of chromatin

Among all the acetylatable lysines, many studies regarding the structure of chromatin have drawn special attention to H4 K16Ac. Dorigo et al., (2003) demonstrated that the N-terminal tail of histone H4 is necessary for chromatin fiber compaction *in vitro.* Compact chromatin fibers were obtained with any single histone N-terminal tail deleted except for that of histone H4. More specifically, the researchers found that residues 14-19 of histone H4's N-terminal tail are essential for proper chromatin fiber condensation (Dorigo et al. 2003). Given that histone H4 K16 acetylation is the only PTM in this region, it was hypothesized that this modification plays a fundamental role in the regulation of higher-order chromatin structure (Shia et al. 2006).

A recent study by Shogren-Knaak et al. (2006) provided the first direct evidence that acetylation at H4 K16 prevents chromatin condensation. In this work, the researchers

produced recombinant histone H4 acetylated at K16 using a chemical ligation strategy. Peptides corresponding to H4's N terminal tail (residues 1-22) with a C-terminal thioester and an acetylated K16 were synthesized by solid phase peptide synthesis. The synthesized peptides were subsequently ligated to the recombinantly expressed C-terminal of H4 harboring an arginine 23 to cysteine mutation (R23C). When the resulting synthetic full length H4 K16Ac histone was incorporated into nucleosomal arrays, Shogren-Knaak et al. (2006) observed that the modified histone prevented 30 nm chromatin fiber formation and cross-fiber interactions (Shogren-Knaak et al. 2006). This work is significant because H4 K16 acetylation is the first, and only, of all of the possible post-translational modifications to be directly linked to changes in chromatin conformation.

Although the mechanism by which H4 K16 disrupts chromatin compaction is still unknown, two distinct models have been suggested (Mutskov et al. 1998; Shia et al. 2006; Shogren-Knaak and Peterson 2006). The first model stems from the structure of the nucleosome core particle of chromatin that was solved by X-ray crystallography at 2.8 Å resolution (Luger et al. 1997). In this crystal structure, the H4 N-terminal tail of one mononucleosome was noted to make contact with an H2A/H2B acidic patch of an adjacent mononucleosome. A subsequent solution phase study of chromatin compaction demonstrated that the introduction of cysteine residues in the H4 tail allowed cross-linkage to an adjacent H2A/H2B acidic patch (Dorigo et al. 2004). It was therefore speculated that neutralization of the positive lysine residue upon acetylation of H4 K16 would disrupt the histone tail's interaction with the acidic patch and prevent chromatin condensation (Shogren-Knaak and Peterson 2006).

The second model suggests that H4 K16Ac induced chromatin decondensation is a result of the weakening of DNA-histone intra-nucleosome contacts. As mentioned previously, Mutskov et al. (1998) tested the efficiency of UV-induced histone tail-DNA cross-linking of hyperacetylated and hypoacetylated nucleosomes. They reported decreasing cross-linking efficiency for hyperacetylated nucleosomes with increasing ionic strength. These results suggest that histone acetylation weakens DNA-histone electrostatic interaction and structurally relaxes the nucleosome core particle. Unlike the first model, this mechanism would not only reduce compaction at the inter-nucleosomal (chromatin fiber) level but also at the intra-nucleosomal level (mononucleosome).

1.4 A universal role for H4 K16 acetylation

H4 K16 acetylation is a high profile PTM and many studies have examined its unique role in different organisms. The importance of H4 K16Ac in yeast, fruit flies, chickens, mice and humans is discussed below. The results from these studies and from the above mentioned study by Shogren-Knaak et al. (2006) point towards a universal role for H4 K16 acetylation in the decondensation of chromatin and in the maintenance of transcriptionally active regions.

Within the framework of long-range histone acetylation patterns, of particular interest is the profile for the acetylated H4 K16 isoform across the human, mouse, and chicken a-globin gene cluster. While levels of acetylated H4 K5, K8, and K12 isoforms across the gene cluster are enriched in erythroid cells compared to non-erythroid cells, levels of monoacetylated H4 K16 remain relatively unchanged (Anguita et al. 2001). Given that several widely expressed genes are transcribed from this domain in non-

erythroid tissues, the authors suggest that monoacetylated H4 K16 is important for the establishment of transcription potential (Anguita et al. 2001).

Consistent with this role for monoacetylated H4 K16 is the finding that non-specific changes to transcription occur as a result of an H4 K16 mutation in *Saccharomyces cerevisiae* (Dion et al. 2005). In their search for functionally redundant histone H4 acetylation sites by way of lysine-to-arginine mutagenesis, Dion et al. (2005) found that unlike for K5, K8, and K12, the mutation of K16 by itself resulted in an altered transcriptional phenotype (affecting approximately 100 genes). Strain comparison indicated that a large portion of the genes affected by the K16 ? R mutation alone were similarly affected by any of the other K ? R strains containing multiple mutations. Importantly, although the mutation of either one of the H4 K5, K8, or K12 residues does not produce an altered transcriptional phenotype, combinations of their mutation have cumulative effects on transcription.

Dion et al. (2005) defined eight transcriptional states in *Saccharomyces cerevisiae* based on the possible combinations of acetylation states of H4 K5, K8, or K12 with or without AcH4 K16. Furthermore, they argue acetylation-induced regulation of gene expression is divided into two classes: (i) the first involves 'discriminator' genes which require the modification of specific lysine residues; (ii) alternatively, the regulation of 'counter' genes is entirely dependent on the cumulative effects of hyperacetylation on the structure of chromatin (Dion et al. 2005). Dion et al's results support the previously mentioned prediction that long-range acetylation of H4 K16, as well as cumulative consequences of non-specific domain-wide hyperacetylation (see Figure 1), are likely—

and possibly non-mutually exclusive—components in the universal regulation of chromatin structure and function (Calestagne-Morelli and Ausio 2006).

Notably, over 80% of H4 K16s are acetylated in *Saccharomyces cerevisiae*, an organism in which most of the genome exists as euchromatin (Clarke et al. 1993; Smith et al. 2003; Turner and Fellows 1989; Turner et al. 1989). In fact, acetylation of H4 K16 is essential for the maintenance of euchromatic and heterochromatic boundaries in yeast (Meijsing and Ehrenhofer-Murray 2001). The histone deacetylase Sir2 is responsible for catalyzing the removal of the modification within silenced chromatin while Sas2p of the SAS complex exclusively acetylates H4 K16 at boundary loci and in active chromatin (Blander and Guarente 2004; Shia et al. 2005). Upon mutation of H4 K16 or deletion of the *sas2* gene, aberrant heterochromatinization into telomere-proximal regions occurs (Kimura et al. 2002; Suka et al. 2002). Sas2p's antagonizing activity therefore appears necessary to prevent the abnormal spreading of heterochromatin into euchromatic regions (Kimura et al. 2002). Kimura et al. (2002) observed a gradient of H4 K16 acetylation along yeast chromosomal regions near telomeres. The gradient was characterized by hypoactylated H4 K16 in transcriptionally silent chromatin close to the telomere, to highly acetylated H4 K16 in transcriptionally active regions further away (Kimura et al. 2002). The authors postulated that competition between Sir2 and Sasp2 functions to regulate transcription by acetylating and deacetylating H4 K16.

Early indications that H4 K16 acetylation mediates chromatin decondensation and gene activation arose from studies on dosage compensation in male *Drosophila* (Turner et al. 1992). XY male flies transcribe X-linked genes at twice the rate of XX females as part

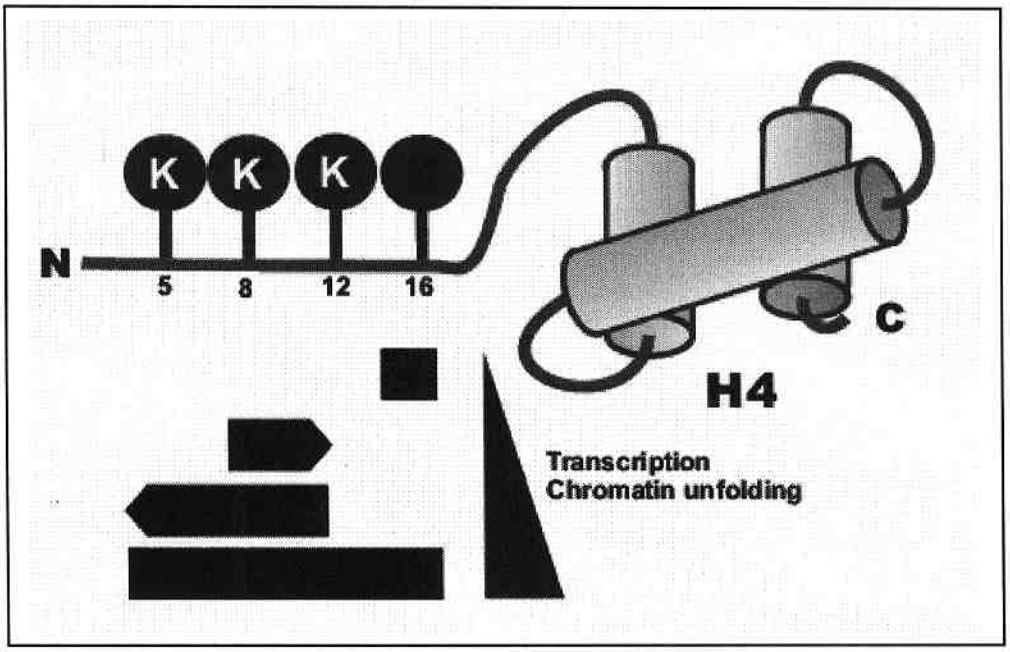

Figure 1. Histone H4 hyperacetylation and transcription. Histone H4 is acetylated at the N-terminal lysines 5, 8 12 and 16 (red circles) in a "zip" mode starting at lysine 16 (Zhang et al. 2002) followed by lysine 8 and 12 and finally lysine 5 (Thorne et al. 1990) (black boxes and boxes and arrows). Except for lysine 16 which has been shown to play a unique role in transcription (Dion et al. 2005; Shogren-Knaak et al. 2006) , histone H4 hyperacetylation appears to operate through a cumulative "charge counter" mechanism (Dion et al. 2005)(dark blue triangle) where nucleosome stability (Ausio and van Holde 1986; Dunker et al. 2001) and the extent of chromatin unfolding of the chromatin fiber (Ausio and Abbott 2004; Garcia-Ramirez et al. 1995) are dependent on the overall number of acetylated groups.

of their dosage compensation mechanism (Straub et al. 2005). The MOF subunit of the male-lethal-specific (MSL) complex binds to the X chromosome and acetylates histone H4 at K16 exclusively. MLS assembly in female flies is prevented resulting in H4 K16 hypoacetylation and a less active X chromosome (Akhtar and Becker 2000; Bone et al. 1994). In contrast, H4 K16 acetylation in male flies results in chromatin decondensation and correlates with a hyperactive X chromosome (Akhtar and Becker 2000; Bone et al. 1994). Dosage compensation in *Drosophila* therefore demonstrates not only how H4 K16 is functionally unique, but also how chromatin structure and function are intrinsically linked.

In human cells, the loss of H4 K16 acetylation is a hallmark of many cancer types including breast, lung and colon carcinomas (Fraga et al. 2005). A recent study examined acetylation levels in 25 cancer cell lines, 16 primary lymphomas tumors and 20 primary colorectal adenocarcinomas (Fraga et al. 2005). Results indicated that unlike the levels of K5, K8, and K12 acetylation which did not differ in cancer cells or tissue compared normal controls, 25 % of global H4 K16 acetylation on average was lost in cancer cell lines and primary tumors. One hypothesis regarding the role of H4 K16 in tumor suppression is that its acetylation within tumor suppressor genes prevents their transcriptional silencing in healthy cells (Shia et al. 2006). Although H4 K16Ac's role in tumorigenesis is not yet clear, recognizing patterns of specific histone modifications in cellular transformation could potentially be used as a tool in cancer diagnosis in terms of predicting the severity of the disease outcome (Seligson et al. 2005).

1.5 The role of linker histones

Linker histones bind nucleosomes at the dyad axis of symmetry and stabilize higher-order chromatin structure (Thoma et al. 1979). The linker histone H1/H5 has a central globular DNA binding domain flanked by N- and C-terminal tails. The binding of linker histones protects an additional 20 bp of chromatosome DNA from nuclease digestion, alters the path of DNA as it enters and exits the nucleosome, and restricts nucleosome mobility (Allan et al. 1980; Dou et al. 2002; Graziano et al. 1988). Although the latter is likely to strongly affect the folding of higher-order chromatin fibers, few studies have examined chromatin structure in the presence of linker histones. Their role in the modulation of chromatin organization therefore remains unclear. While acetylated chromatin fibers depleted of linker histones exhibit an unfolded conformation (Garcia-Ramirez et al. 1995; Tse et al. 1998), hyperacetylated oligonucleosome complexes containing a full complement of linker histones are only slightly less condensed than their non-acetylated counterparts (McGhee et al. 1983; Wang et al. 2001). In addition, *in vitro* studies have shown that acetylated chromatin is more refractory to histone H1 binding (Perry and Annunziato 1991; Ridsdale et al. 1990). Given that transcriptionally active chromatin has been shown to be partially depleted of linker histones (Kamakaka and Thomas 1990), the structural effects of domain-wide acetylation across both active and inactive gene cluster regions may vary contextually according to this linker histone contribution.

Evidence suggests that post-translational modifications of linker histones may also be involved in the regulation of chromatin dynamics (Ausio 2006; Catez et al. 2006). Phosphorylation is an important modification of linker histones H1 and H5 that is

correlated to changes in the structure of chromatin (Ausio 2006). Changes in the phosphorylation levels of H5 are seen during avian erythropoiesis (Wagner et al. 1977). In immature erythroblasts, H5 is highly phosphorylated and chromatin is in a relaxed state. As the erythrocyte matures, chromatin gradually condenses as H5 phosphorylation levels decrease (Wagner et al. 1977). Other instances where linker histone phosphorylation correlates to less repressive chromatin conformations include H1 phosphorylation in mammalian cells during chromatin decondensation in S-phase, H5 phosphorylation-induced rescue of SWI/SNF chromatin remodeling activities, and linker histone phosphorylation during DNA repair (Alexandrow and Hamlin 2005; Horn et al. 2002; Kysela et al. 2005; Th'ng et al. 2005).

Dou et al. (1999) demonstrated that linker histone phosphorylation mimics its partial removal from DNA by changing the overall charge of a small domain within the protein (Dou et al. 1999). The researchers hypothesized that the negative charges introduced by the phosphate group *in vivo* may increase the dissociation constant of the linker histone by weakening the DNA-histone electrostatic interaction within the nucleosome. Thus, phosphorylation could result in a population of linker histones that exchange more rapidly on the chromatin fiber while the negative charges may weaken intra- and/or inter- nucleosomal interactions. H1 phosphorylation would therefore promote chromatin decondensation and increase DNA accessibility (Dou et al. 1999).

Core histone acetylation is known to overlap with linker histone phosphorylation during avian erythrocyte differentiation (Sung et al. 1977; Yellajoshyula and Brown 2006). Notably, a similar overlap is also seen during DNA repair (Kysela et al. 2005; Tamburini and Tyler 2005). While combinations of histone post-translational

modifications are known to act synergistically in the regulation of chromatin dynamics (Strahl and Allis 2000), researchers lack a complete understanding of how the structure of chromatin is affected by multiple histone post-translational modifications. In fact, *in vitro* reconstitutions of *di-* or *multiply-* modified chromatin fibers is lacking in this field of study. Characterizing the salt-dependent conformational changes to di-modified oligonucleosomes by analytical ultracentrifuge and transmission electron microscope would clarify how linker histone phosphorylation and core histone acetylation act to modify chromatin condensation synergistically. In addition, restriction enzyme analysis of di-modified nucleosomes would reveal whether linker histone phosphorylation influences the positioning of an acetylated octamer within the nucleosome.

1.6 The study of chromatin *in vitro*: the DNA template

Besides histone and histone tail variability, linker DNA length and DNA sequence composition are additional structural components affecting nucleosome positioning and the folding of chromatin fibers (Ausio 2000). Results from studies examining salt-dependent changes in chromatin compaction using chromatin extracted from endogenous sources are often ambiguous due to sample heterogeneity (Butler and Thomas 1980; Gale and Smerdon 1988). Structural analysis of oligonucleosomes reconstituted *in vitro* using random genomic DNA fragments is similarly uninformative due to linker length variability or histone octamer close-packing (Ruiz-Carrillo et al. 1979; Steinmetz et al. 1978).

This problem regarding the *in vitro* study of the structure of chromatin beyond the level of the core particle was overcome when Simpson et al., (1985) developed more

suitable DNA substrates. They consist of long DNA fragments containing tandem repeats of the 5S rRNA gene from *Lytechinus variegatus* previously shown to precisely position the histone octamer (Simpson et al. 1985). The repeated *Lytechinus variegatus* positioning sequence allows the reconstitution of homogenous chromatin fibers with constant linker lengths (Hansen et al. 1989; Simpson et al. 1985). Since then, other tandem arrays have been constructed using an alternate nucleosome positioning sequence, the Widom 601 DNA sequence (Lowary and Widom 1998).

One pitfall regarding the study of the folding of homogenous chromatin fibers containing tandemly repeating DNA sequences is the impossibility of differentiating one region of the reconstituted nucleosomal array from another using restriction enzyme analysis. The creation of a template containing one nucleosome positioning sequence with unique restriction enzyme sites flanked on both sides by tandem repeats of an alternate nucleosome positioning sequence would allow the differentiation of the middle nucleosome within the fiber from its flanking ends. It would therefore be possible to study H1 positioning, and/or the effect of single or synergistic histone modifications on nucleosomal histone-DNA interactions in the center of a chromatin fiber.

1.7 Objectives

Given the common relationship between structure and function, careful attention should be drawn to the effects that histone post-translational modification have on chromatin's structural integrity. In the first component of this thesis I describe the creation of a DNA template that allows not only the reconstitution of homogenous

chromatin fibers with constant linker lengths but also allows the differentiation of the middle of the fiber from its flanking ends.

The second component of this thesis examines the role of H4 K16Ac in chromatin dynamics. It has been shown recently that H4 K16Ac prevents 30 nm chromatin fiber formation and cross-fiber interactions (Shogren-Knaak et al. 2006). Although the mechanism by which H4 K16 acetylation decondenses chromatin remains unknown, two alternate models have been suggested. Mutskov et al. (1998) postulate that that H4 K16 acetylation weakens DNA-histone electrostatic interactions and structurally relaxes the nucleosome, and therefore the chromatin fiber. Adopting an alternate perspective, Shogren-Knaak and Peterson (2006) suggest that acetylation of H4 K16 may disrupt a potential interaction between the H4 histone tail and an H2A/H2B acidic patch of an adjacent mononucleosome within a chromatin fiber. My objective is to evaluate these alternate hypotheses using analytical ultracentrifuge analysis (AUC) and $MgCl_2$ solubility assays. If the weakening of DNA-histone intra-nucleosome contacts plays a role in the unraveling of the chromatin fiber, it is expected that H4 K16Ac mononucleosomes would be more soluble in $MgCl_2$, and would sediment more slowly than control mononucleosomes with increasing ionic strength. In contrast, if H4 K16Ac disrupts the histone tail's interaction with an adjacent H2A/H2B acidic patch no conformational differences between mononucleosomes would be detected by AUC analysis or by $MgCl_2$ solubility experiments.

In the final component of this thesis I describe the development of a purification method for nonphosphorylated and monophosphorylated linker histone H5 as well as the

preliminary AUC analyses of control oligonucleosomes reconstituted with the isolated nonphosphorylated H5.

2.0 MATERIALS AND METHODS

2.1 The creation and characterization of the Pbsn-208(10) template

2.1.1 PCR stitching of XhoI sites onto the probasin promoter sequence

Luria Agar plates containing 100 µg/ml ampicillin (Sigma) were streaked with *E. coli* Nova Blue cells (Novagen) in 40% glycerol, 60% Luria Burtani (LB) medium (1% tryptone; 0.5% yeast extract; 43mM NaCl) containing the Puc19-Pbsn plasmid. The plates were incubated overnight at 37°C. The next morning, colonies were added to Luria Burtani (LB) medium (1% tryptone; 0.5% yeast extract; 43mM NaCl) containing 50 µg/ml ampicillin (Sigma) and the liquid cultures were placed in a shaking incubator (300 rpm) for 16 hrs at 37°C. The bacterial culture was centrifuged at 3000 x g for 15 min and the supernatant was discarded. The Puc19-Pbsn plasmid was extracted from the *E. coli* Nova Blue cells using a QIAprep® Miniprep kit (Qiagen) following the manufacturer's protocol. PCR was used to stitch *Xho*I restriction enzyme sites onto both ends of the probasin promoter sequence (Pbsn) within the Puc19 plasmid in four separate reactions. Reactions 1, 2, 3, and 4 had 0.5 µl, 1.0 µl, 1.5 µl, and 0.0 µl of the above Puc19-Pbsn plasmid miniprep template respectively. Primers: PucPro fwd 5'-CTCGAGCATCTACCATTC-3', PucPro rev 5'-CGCTCGAGTTGTACACAG-3'. PCR protocol: 94°C 3 min, 30 cycles of 94°C 45 sec, 55°C 30 sec, 72°C 30 sec, and end with 72°C 10 min. The PCR products were separated by 1.0 % low melting agarose gel electrophoresis and 206 bp bands were gel purified using a QIAquik® Gel Extraction kit (Qiagen) following the manufacturer's protocol. The final products were analysed by 1.0% agarose gel electrophoresis.

2.1.2 Ligation of XhoI-probasin promoter-XhoI sequence into TOPO vector

The purified *Xho*I-probasin promoter-*Xho*I sequence was cloned into a TOPO vector (Invitrogen, PCR 2.1 kit) using the One Shot® Chemical Transformation manufacturer's protocol. White colonies were added to Luria Burtani (LB) medium (1% Tryptone; 0.5% Yeast extract; 43 mM NaCl) containing 50 μg/ml ampicillin (Sigma) and liquid cultures were placed in a shaking incubator (300 rpm) for 16 hrs at 37°C. The next day bacterial cultures were centrifuged at 3000 x g for 15 min. The supernatant was discarded and the probasin-TOPO plasmid was extracted using a QIAprep® Miniprep kit (Qiagen) following the manufacturer's protocol. The extracted plasmids were digested with *Xho*I (NEB) at 0.5 units of enzyme per μg of DNA and were analysed by 1.0% agarose gel electrophoresis.

2.1.3 Purification of the XhoI-probasin promoter-XhoI fragment

The probasin-TOPO plasmid was digested with *Xho*I (NEB) at 0.5 units of enzyme per μg of DNA and separated by 1.0 % low melting agarose gel electrophoresis. 206 bp bands were gel extracted and purified using a QIAquik® Gel Extraction kit (Qiagen) following the manufacturer's protocol. The final product was analysed by agarose gel electrophoresis.

2.1.4 Preparation of the pIC-2085S plasmid

The pIC-2085S plasmid (25 ng) (gift from Jerry Workman) was mixed with 50 μl of a chemically competent Nova Blue (Novagen) cell suspension, incubated on ice for 2 min and plated onto pre-warmed Luria-Agar plates (37°C) containing 100 μg/ml ampicillin (Sigma). Colonies formed were added to Luria Burtani (LB) medium (1% tryptone; 0.5%

yeast extract; 43 mM NaCl) containing 50 μg/ml ampicillin (Sigma) and these liquid cultures were placed in a shaking incubator (300 rpm) for 16 hrs at 37°C. The bacterial culture was centrifuged at 3000 x g for 15 min and the supernatant was discarded. The pIC-2085S plasmid was extracted using a QIAprep® Miniprep kit (Qiagen) following the manufacturer's protocol. The plasmid was digested with *Xho*I (NEB) at 0.5 units of enzyme per μg of DNA and was separated by 1.0 % low melting agarose gel electrophoresis. 4794 bp bands were gel extracted and purified using a QIAquik® Gel Extraction kit (Qiagen) following the manufacturer's protocol. The final product was analysed by 1.0 % agarose gel electrophoresis.

2.1.5 Generation of the Pbsn-208(10) plasmid

150 ng of *Xho*I-probasin promoter-*Xho*I insert was ligated with 37.5 ng of *Xho*I digested pIC-2085S using 1 unit of T4 ligase (NEB) per 1 μg of DNA in 1 X ligase buffer (NEB) at 16°C overnight. Ligation mixture (1/10) was mixed with 50 μl of a chemically competent Nova Blue (Novagen) *E. coli* cell suspension, incubated on ice for 30 min and spread onto pre-warmed Luria Agar plates (37°C) containing 100 μg/ml ampicillin. Colonies were screened for insert by PCR. Primers: PicPro fwd 5'-CGAATCTTTAAACTCGAGCAT-3', PicPro rev 5'-GGATCCAGCGAGCTCGAGTT-3'. PCR protocol: 94°C 3 min, 30 cycles of 94°C 45 sec, 55°C 30 sec, 72°C 30 sec, and end with 72°C 10 min. All products were analysed by 1.0 % agarose gel electrophoresis and selected products were further analysed by 4% Native gel electrophoresis. Three positive colonies (numbered 1, 2, and 3) and one negative colony were selected for plasmid miniculture amplification. Colonies were added to Luria Burtani (LB) medium

(1% tryptone; 0.5% yeast extract; 43mM NaCl) containing 50 μg/ml ampicillin (Sigma). Liquid cultures were placed in a shaking incubator (300 rpm) for 16 hrs at 37°C. The bacterial culture was centrifuged at 3000 x g for 15 min. The supernatant was discarded and the Pbsn-208(10) plasmid was extracted using a QIAprep® Miniprep kit (Qiagen) following the manufacturer's protocol. The extracted Pbsn-208(10) plasmids, and a negative control unligated pIC-2085S plasmid were analysed by restriction enzyme analysis. They were digested with *Xho*I (NEB) and *Eco*RI (NEB) separately at 0.5 units of enzyme per μg of DNA and fragments were separated by 2% agarose gel electrophoresis.

2.1.6 Sequence analysis of Pbsn-208(10)

Pbsn-208(10) plasmid (8 μg) was sequenced in the Centre for Biomedical Research (CBR; University of Victoria) by Roderick Hasevoets. Primers: PicPro fwd 5'-CGAATCTTTAAACTCGAGCAT-3', PicPro rev 5'-GGATCCAGCGAGCTCGAGTT-3'. Sequence was queried using the BLASTn algorithm of BLAST (v.2.2.8; http://www.ncbi.nil.gov/BLAST) against database nt.

2.1.7 Amplification of the Pbsn-208(10) plasmid

Luria Agar plates containing 100 μg/ml ampicillin (Sigma) were streaked with Nova Blue cells (Novagen) in 40% glycerol, 60% Luria Burtani (LB) medium (1% tryptone; 0.5% yeast extract; 43mM NaCl) containing the Pbsn-208(10) plasmid. Plates were incubated overnight at 37°C. The next day, colonies were added to LB medium containing 50 μg/ml ampicillin (Sigma) and liquid cultures were incubated for 16 hrs at 37°C shaking at 300

rpm. After 16 hrs, 2 mls of LB medium containing 50 μg/ml ampicillin (Sigma) were added to each of four of the liquid cultures for 6 more hours of incubation at 37°C shaking at 300 rpm. Five mls of each liquid culture were then added to four separate flasks of 500 ml LB medium containing 50 μg/ml ampicillin (Sigma). Large liquid cultures were then incubated for 16 hrs at 37°C shaking at 300 rpm. Procedure 2.1.7 was repeated 2 times.

2.1.8 Isolation and preparation of the Pbsn-208(10) DNA template

Liquid cultures were centrifuged for 20 min x 2 at 3000 x g. The supernatant was discarded and each of the four cell pellets were dissolved in 10 mls of lysis buffer (25 mM tris (pH 7.5); 10 mM EDTA; 15% sucrose; 3 mg/ml lysozyme (Sigma) and incubated on ice for 20 min. The suspensions were then divided into 6 equal aliquots and 13.3 mls of buffer 2 (0.2 M NaOH; 1% SDS) were added to each aliquot. The mixtures were inverted vigorously and incubated on ice for 10 min. Next, 8.3 mls of 3 M sodium acetate (pH 5.2) were added to each aliquot and the tubes were inverted gently then incubated on ice for 20 min. The tubes were then centrifuged at 10 000 x g for 20 min. Next, the supernatant was filtered through cheesecloth previously soaked in 0.3 M NaAc (pH 5.2). The filtrate was centrifuged at 10 000 x g for 10 min. The supernatant was divided in two and warmed to 37°C. 200 ug of RNase A (Boehringer Mannheim) at 10 mg/ml were added to each aliquot and bottles were incubated for 1 h at 37°C. Bottles were cooled to room temperature, 0.6 volumes of isopropanol were added to each, and they were incubated at room temperature for 10 min. The bottles were then centrifuged at 10 000 x g for 15 min and the supernatant was discarded. Two resulting pellets were dried under

vacuum for 30 min and dissolved in 10 mls of sdH_2O. DNA was extracted twice with an equal volume of phenol:chloroform:isoamyl alcohol (25:24:1) and once with an equal volume of chloroform:isoamyl alcohol (24:1). After each extraction and centrifugation at 10 000 x g for 5 min the aqueous layer was transferred to new tubes. DNA was precipitated by adding 0.1 volumes of 3 M NaAc (pH 5.2) followed by 2.5 volumes of ice cold 95% EtOH. DNA was stored overnight at 20°C. The next day, the tubes were centrifuged at 10 000 x g for 10 min and the 95% EtOH supernatant was discarded. The DNA pellet was washed with 2 volumes of 70% EtOH and centrifuged at 10 000 x g for 10 min. The supernatant was discarded and the pellet was dried under vacuum for 10 min. The DNA was resuspended in a total of 4 mls of TE buffer (10 mM tris-HCl (pH 7.5), 0.5 mM EDTA). The plasmid was purified from genomic DNA by loading it onto a Sephacryl (Pharmacia) column (2.5 cm x 60 cm) and eluting with TE (pH 8) at a flow rate of 60 ml/h for 6 hrs. Fractions were analysed by 1.0 % agarose gel electrophoresis. Fractions containing plasmid only were pooled and concentrated in Amicon Ultra Centrifugal Devices (Millipore; 30 000 MW) to a final volume of 3 ml. The centrifugation of the filter devices was at 2000 x g for 3 x 20 min. Next, the isolated plasmid DNA was digested with *Cla*I (NEB), *Kpn*I (NEB) and *Hha*I (NEB) at 0.5 units of enzyme per μg of DNA and was analysed by 1.6% agarose gel electrophoresis. Digested DNA was isolated by phenol:chloroform extraction and NaAc precipitation as described above. The Pbsn-208(10) insert was separated from the digested material by loading it onto a Sephacryl (Pharmacia) column (2.5 cm x 60 cm) and eluting with TE (pH 8) at a flow rate of 60 ml/h for 6 hours. Fractions were analysed by 1.0 % agarose gel electrophoresis. Fractions containing Pbsn-208(10) only were pooled and concentrated in

Amicon Ultra Centrifugal Devices (Millipore; 30 000 MW) as described above to a final volume of 1 ml. Procedures 2.1.7 and 2.1.8 were repeated 2 times.

2.1.9 Chromatin fiber reconstitution

Native histone octamers in 2 M NaCl; 20 mM Tris (pH 7.5); 0.1 mM EDTA (18 µg prepared by Allison Maffey, Ausio lab technician) were incubated in 20 mM ß-mercaptoethanol for 30 min at room temperature. The Pbsn-208(10) DNA template in 2 M NaCl; 20 mM tris (pH 7.5); 0.1 mM EDTA was then added to the octamers at a histone:DNA ratio of 0.9. The DNA and histone were dialysed in 2 M NaCl; 20 mM tris (pH 7.5); 0.1 mM EDTA; 1 mM DTT overnight at 4°C. The next day, histone octamers were assembled onto the DNA template by step-wise salt dialysis (2 M – 0 M NaCl; 10 mM Tris (pH 7.5); 0.1 mM EDTA). Each dialysis step was 2.5 hrs at 4°C. The concentration of NaCl decreased as follows: 2 M, 1.5 M, 1.2 M, 1.0 M, 0.6 M, 0.3 M, 0 M). Fibers were stored on ice for analytical ultracentrifugation.

2.1.10 Analytical ultracentrifuge characterization

Reconstituted fibers were dialysed against 20 mM NaCl; 20 mM tris (pH 7.5); 0.1 mM EDTA and subjected to sedimentation velocity analysis using a Beckman Model XL-A ultracentrifuge, an An-55 aluminum rotor and double-sector cells with aluminum-filled Epon centerpieces. The temperature was near 20°C ± 0.1°C. A solution with an $A_{260} = 0.4$ was prepared and the data were corrected to $S_{20,w}$. The estimated value of partial specific volume was 0.65. A rotor speed of 26 000 rpm was used. The UV scans (260) were analysed using the van Holde–Weischet method to determine the distribution of

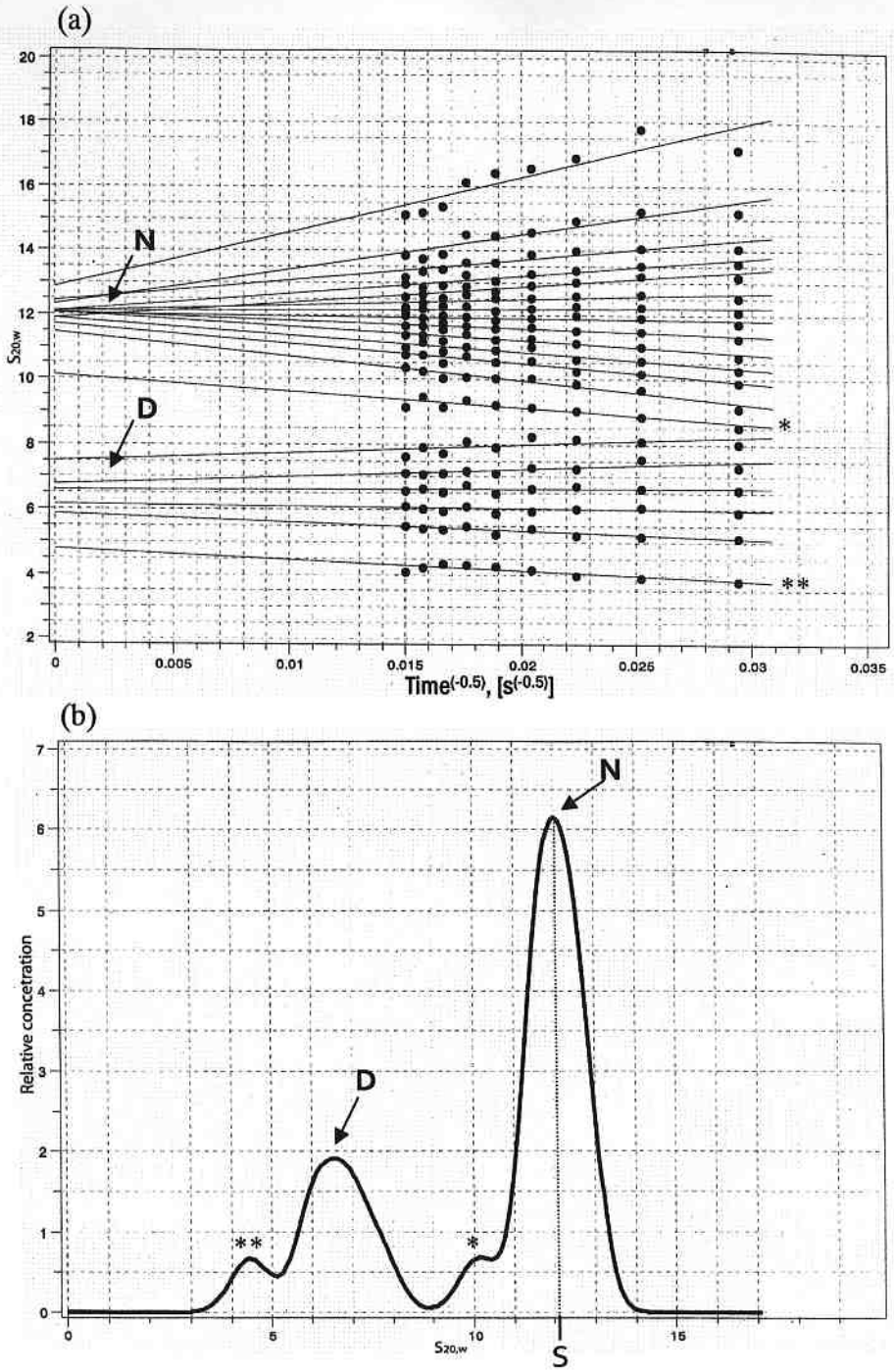

Figure 2. Example AUC 'fan plot' and 'sedimentation coefficient histogram'. (a) Fan plot sedimentation velocity analysis of 208 bp nucleosomes reconstituted with chicken histone octamers (see section 2.2.10-11). Each of the lines converging to a common $S_{20,w}$ value (in Svedberg units, S) is proportional to the fraction of sample represented. Time is in seconds. (D) proportion of sample that sediments as nucleosomal (208 bp) DNA, (N) proportion of sample that sediments as nucleosome particles. (b) Sedimentation coefficient distribution of the 208 bp nucleosomes determined by using sedimentation velocity and van Holde weischet analysis. (D) and (N) as above. S: sedimentation coefficient value extrapolated for the sample.

sedimentation coefficients for the population of fibers within a sample. The XL-A data analysis software was version 4.1 (Borries Demeler, Missoula, Montana). The sample's sedimentation coefficient value was obtained from its respective sedimentation coefficient histogram (for an example of sedimentation velocity analysis see Figure 2).

2.1.11 Gel electrophoresis

Native-PAGE gel electrophoresis was performed using 4% gels at 80 V for 45 min in 1 x E Buffer (6X: 1 M tris-HCl (pH 7.2); 0.5 M EDTA (pH 8.0); 0.12 M sodium acetate trihydrate. The acrylamide:bisacrylamide ratio was 20:1 and the 3 x sample buffer was 30% sucrose. Staining was in ethidium bromide (0.25 μg/ml) for 10 min and destaining was in water for 20 min before visualization under UV light.

Low melting temperature agarose gel electrophoresis was done at 6 V/cm using a 1.0% low temperature melting agarose; 25 mM tris-Acetate-0.5 mM EDTA (pH 8) gel and a 25 mM Tris-Acetate-0.5 mM EDTA (pH 8) running buffer. Staining was in ethidium bromide (0.25 μg/ml) for 10 min and destaining was in water for 20 min before visualization under UV light.

Regular agarose gel electrophoresis was done at 6 V/cm using a 1.0%, 1.6 %, or 2 % agarose; 25 mM tris-Acetate-0.5 mM EDTA (pH 8) gel and a 25 mM tris-Acetate-0.5 mM EDTA (pH 8) running buffer. Staining was in ethidium bromide (0.25 μg/ml) for 10 min and destaining was in water for 20 min before visualization under UV light.

2.2 H4 K16Ac and the structure of the nucleosome

2.2.1 Isolation of Native Histones

80 mls of chicken erythrocytes in 40% glycerol 0.15 M NaCl; 15 mM Na Citrate; 10 mM $NaPO_4$ (pH 7.2) were centrifuged at 2000 x g at 4°C in a Beckman® Model J2-21 centrifuge for 10 min. Pellets were resuspended in 15 mls each of Buffer II (0.1 M KCl; 50 mM Tris (pH 7.5); 1.0 mM $MgCl_2$; 0.5% Triton X-100) and 1/100 protease inhibitor mixture Complete (Roche Molecular Biochemicals) and centrifuged at 3000 x g at 4°C for 10 min. Pellets were resuspended in 20 mls each of Buffer II without Triton-X and 1/200 protease inhibitor mixture Complete (Roche Molecular Biochemicals) and centrifuged for 5 min at 3000 x g at 4°C. Pellets were resuspended in a total volume of 20 mls of Buffer III (0.1 M KCl; 50 mM Tris (7.5); 1.0 mM $CaCl_2$) to a final DNA concentration of 6.5 mg/ml. The nuclear suspension was incubated for 5 min at 37°C and digested for an additional 5 min at this temperature with micrococcal nuclease (Worhtington) at 18U/ ml. The digestion reaction was stopped by the addition of 0.5 M EDTA (pH 8.0) to a final EDTA concentration of 10 mM (on ice) and centrifuged at 10 000 x g for 10 min at 4°C. Pellets were resuspended vigorously in 0.25 mM EDTA to shear nuclei using half the volume used for the nuclease digestion. Nuclear lysis was continued for one hour at 4°C with continuous stirring. Debris was removed by centrifugation at 10 000 x g for 20 min at 4°C. Supernatant was brought to a final DNA concentration of 3 ug/µl. Linker histones were stripped by adding 5 M NaCl to a final concentration of 0.35 M while stirring vigorously. Stripped chromatin was added to CM Sephadex™ C-25 (Amersham Biosciences) resin that was previously hydrated in 0.35 M NaCl; 10 mM Tris (7.5); 0.25 mM EDTA. The chromatin was tumbled with the resin for

2 hrs at 4°C after which the resin was pelleted at 10 000 x g for 10 min at 4°C. A 1/200 A_{260} reading was taken. 48 mgs of chromatin was loaded onto a hydroxylapatite column (3.5 cm x 15 cm at a flow rate of 30 ml/h) previously equilibrated with 10 column volumes of 20 mM KPO_4 (pH6.8); 0.4 M NaCl. Histones H2A-H2B and H3-H4 were fractionated under an elution buffer gradient of 20 mM KPO_4 (pH 6.8); 0.4 M NaCl to 20 mM KPO_4 (pH 6.8); 2.5 M NaCl over 20 hrs followed by 20 mM KPO_4 (pH 6.8); 2.5 M NaCl for 2 hrs. Hydroxylapatite column chromatography fractions were analysed by SDS PAGE electrophoresis. Histones H2A-H2B and H3-H4 fractions were dialysed against 8 L of water each at 4°C (3 x 3 hrs followed by overnight dialysis). Fractions were lyophilized and kept at -80°C. procedure 2.2.1 was repeated 3 times.

2.2.2 Separation of H3 and H4

To separate histone H3 from H4 reversed phase HPLC analysis was carried out using a 5 μm Vydac C_4 column (10 mm x 250 mm): H3-H4 was dissolved in sdH_2O to final concentration of 1.5 mg/ml, loaded onto the column and eluted at a flow rate of 1 ml/min (Buffer A: 0.1% TFA; Buffer B: 100% ACN; %B gradient: 0-5% 1 min, 5-25% 10 min, 25-30% 15 min, 30-35% 20 min, 35-40% 20 min, 40-45% 10 min, 45-55% 50 min, 55-90% 5 min, 90-100% 20 min, 100-100% 5 min, 100-0% 10 min). Reversed phase HPLC fractions were analysed by SDS PAGE. H4 and H3 fractions were pooled separately and lyophilized. H3 was dissolved in sdH_2O to a final concentration of 1 mg/ml and stored at -80°C. Procedure 2.2.2 was repeated 3 times.

2.2.3 Isolation of H4 K16Ac and non-acetylated H4 K16

To separate differentially acetylated forms of H4 ionic exchange HPLC was carried out using a 6μm SynChrom Synchropak CM300 column: H4 was dissolved in sdH_2O to a final concentration of 1.5 mg/ml. Only 0.75 mg of H4 was loaded per column and a total of 6 columns were run at a flow rate of 1 ml/min (Buffer A: 8 M UREA; 23 mM NaPO4 (pH 7.0); 0.5 mM DTT; 100 mM NaCl: Buffer B: 8 M urea; 23 mM NaPO4 (pH 7.0); 0.5 mM DTT; 800 mM NaCl; %B gradient: 0-0% 5 min, 0-29% 10 min, 29-50% 40 min, 50-100% 10 min, 100-0% 5 min). Ionic exchange HPLC fractions were analysed by acid-urea PAGE. Differentially acetylated H4 fractions were pooled from all 6 columns, dialysed against 4 L of H_2O at 4°C (3 x 2 hours) and stored at -80°C.

2.2.4 Mass spectrometry of H4K16Ac

Isolated H4 K16Ac and non-acetylated H4 K16 were sent to Don Hunt (Department of Chemistry at the University of Virginia) for Tandem Mass spectrometry analysis. In summary, the N-terminus and lysines on histone H4 were propionylated before digestion with trypsin. The peptides were then loaded on a RP C-18 column and were gradient eluted into the mass spectrometer.

2.2.5 Titration of histone octamers containing either H4 K16Ac or non-acetylated H4 K16

To generate histone octamers, H4 K16Ac or non-acetylated H4 K16, and native chicken H2A-H2B, and H3 core histones in sdH_20 were mixed in stoichiometric amounts according to their individual concentrations at OD_{230} to final concentrations of 0.52 μg/μl

(octamers containing non-acetylated H4 K16) and 0.36μg/μl (H4 K16Ac-containing octamers). Octamers were analysed by SDS PAGE, lyophilized and stored at -20°C.

2.2.6 Amplification of p5S208-12 Lytechinus 5S rDNA plasmid

Luria Agar plates containing 100 μg/ml ampicillin (Sigma) were streaked with Nova Blue (Novagen) cells in 40% glycerol, 60% Luria Burtani (LB) medium (1% tryptone; 0.5% yeast extract; 43mM NaCl) containing the p5S208-12 *Lytechinus* 5S rDNA plasmid. Plates were incubated overnight at 37°C. The next day, colonies were added to LB medium containing 50 μg/ml ampicillin (Sigma). These liquid cultures were incubated for 16 hrs at 37°C shaking at 300 rpm. After 16 hrs, 2 mls of LB medium containing 50 μg/ml ampicillin (Sigma) were added to each liquid culture for 6 more hours of incubation at 37°C shaking at 300 rpm. Next, 5 mls of each liquid culture was then added separately to four flasks each containing 500mls of LB medium and 50 μg/ml ampicillin (Sigma). Large liquid cultures were then incubated for 16 hrs at 37°C shaking at 300 rpm.

2.2.7 Isolation and preparation of the 208-12 Lytechinus 5S rDNA

Isolation and preparation of the 208-12 Lytechinus 5S rDNA was completed as described in section 2.1.8 with the following change. The p5S208-12 *Lytechinus* 5S rDNA plasmid was digested with only *Hha*I (NEB) at 0.5 units of enzyme per μg of DNA. Procedures 2.2.6 and 2.2.7 were repeated 3 times.

2.2.8 Preparation of the 208 bp Lytechinus 5S rDNA monomer

208-12 *Lytechinus 5S rDNA* was digested with *Rsa*I (NEB) at 0.5 units of enzyme per µg of DNA and was analysed by 1.0 % agarose gel electrophoresis. 208 bp *Lytechinus 5S rDNA* monomer was separated from digested material by loading it onto a Bio-Gel DEAE-5-PW HPLC column 75 x 7.5 mm (BIO-RAD) and eluting at a flow rate of 1 ml/min (Buffer A: 0.1 M Tris (pH 7.5), Buffer B: 0.1 M Tris (pH 7.5); 1 M NaCl, % B gradient: 0-0% 5 min, 0-31% 15 min, 31-50% 60 min, 50-80% 10 min, 80-80% 5 min, 80-8% 5 min). 208 bp *Lytechinus 5S rDNA* monomer fractions were pooled and DNA was isolated by phenol:chloroform extraction and NaAc precipitation as described above. DNA was resuspended in sdH_20 to a final concentration of 0.328 µg/µl and stored at -20°C. The final product was analysed by 1.0 % agarose gel electrophoresis.

2.2.9 Random 146 bp genomic chicken DNA nucleosome preparation and sucrose gradient purification

Titrated H4 K16Ac and H4 nonAc octamers prepared above were denatured by dissolution in 6 M GnHCl; 50 mM Tris (7.5) to a final DNA concentration of 2 µg/µl. ß-mercaptoethanol was added to a final concentration of 20 mM and octamers were incubated at room temperature for 30 min, diluted by an equal volume of sdH_20 and dialysed against sdH_2O at 4°C 2 x 2 hrs. Octamers were then renatured by dialysis against 2 M NaCl; 50 mM Tris-HCl (7.5); 1 mM EDTA; 1 mM DTT) overnight at 4°C. The next day random 146 bp genomic chicken DNA (prepared by Allison Maffey, technician, Ausio Lab) in the same buffer minus DTT was added to both the H4 K16Ac and H4 nonAc octamers. The histone:DNA ratio was 1.12. Histone octamers were assembled

onto the DNA template by step-wise salt dialysis (2 M – 0 M NaCl; 10 mM Tris (pH 7.5); 0.1 mM EDTA). Each dialysis step was 2.5 hrs at 4°C. The concentration of NaCl decreased as follows: 2 M, 1.5 M, 1.2 M, 1.0 M, 0.6 M, 0.3 M, 0 M). The 146 bp genomic chicken DNA nucleosome were analysed by 4% native PAGE. The nucleosomes were loaded onto a 5-20% sucrose gradient in 50 mM NaCl; 10 mM Tris-HCl (pH 7.5); 0.1 mM EDTA and centrifuged at 134 000 g for 19.6 h in a Beckman SW41 rotor at 4°C. Sucrose gradient fractions were collected at 0.5 ml/min and analysed by 4% native PAGE. Hexamer-free nucleosomes were pooled, analysed by 4% native PAGE and stored on ice for analytical ultracentrifuge analysis.

2.2.10 208 bp Lytechinus 5S rDNA nucleosome preparation

Titrated H4 K16Ac and H4 nonAc histone octamers were denatured and renatured as described above with the following minor changes: 1) no DTT was added to the overnight dialysis buffer (2 M NaCl; 50 mM Tris-HCl (7.5); 1 mM EDTA), 2) DTT was added the following day to the octamers to a final concentration of 1 mM from a 1 M stock, 3) nucleosomes were incubated for 1 hr at room temperature instead of ½ hr. After this, 208 bp *Lytechinus 5S rDNA* in the same buffer minus the DTT was added to both the H4 K16Ac and H4 nonAc octamers. The histone:DNA ratio was 0.78. Histone octamers were assembled onto the DNA template by step-wise salt dialysis (2 M – 0 M NaCl; 10 mM Tris (pH 7.5); 0.1 mM EDTA). Each dialysis step was 2.5 hrs at 4°C. The concentration of NaCl decreased as follows: 2 M, 1.5 M, 1.2 M, 1.0 M, 0.6 M, 0.3 M, 0 M). Nucleosomes were analysed by 4% native PAGE and stored on ice for analytical ultracentrifuge analysis.

2.2.11 Analytical ultracentrifuge characterization

Reconstituted H4 K16Ac and H4 nonAc 146 bp and 208 bp nucleosomes were dialysed against 50 mM, 200 mM, 400 mM, and 600 mM NaCl; 20 mM Tris (pH 7.5); 0.1 mM EDTA and subjected to sedimentation velocity analysis using a Beckman Model XL-A ultracentrifuge as described in section 2.1.10. A rotor speed of 40 000 rpm was used. The UV scans (260) were analysed using the van Holde–Weischet method to determine the distribution of sedimentation coefficients for the population of nucleosomes within a sample. The XL-A data analysis software was version 4.1 (Borries Demeler, Missoula, Montana). Each sample's sedimentation coefficient value was obtained from its respective sedimentation coefficient histogram (for an example of sedimentation velocity analysis see Figure 2).

2.2.12 Magnesium chloride solubility

18.75 ug of each H4 K16Ac and H4 nonAc 208 bp *Lytechinus 5S rDNA* nucleosomes were dialysed against 20 mM Tris (pH 7.5) overnight at 4°C. Original nucleosome samples had an $A_{260} = 0.8$. Both species of nucleosomes were brought to 0.02 µg/µl (DNA) in 20 mM Tris (pH 7.5) and varying concentrations of $MgCl_2$. Final Mg^{2+} concentrations for H4 K16Ac and H4 nonAc nucleosomes were 0 mM, 2 mM, 4 mM, 6 mM, 8 mM, 10 mM, and 12 mM. The different concentrations were achieved by mixing equal volumes of the nucleosome samples in the 20 mM Tris (pH 7.5) buffer with an equal volume of a 2 X $MgCl_2$ in the same buffer. Nucleosomes were incubated for 55 min

at 4°C and centrifuged at 10 000 x g for 10 min at 4°C. Supernatant A_{260} readings were used for the calculation of % solubility.

2.2.13 Gel electrophoresis

4% Native-PAGE gel electrophoresis was performed at 80 V for 45 min in 1 x E Buffer (6X: 1 M Tris-HCl (pH 7.2); 0.5 M EDTA (pH 8.0); 0.12 M sodium acetate trihydrate. The acrylamide:bisacrylamide ratio was 20:1 and the 3 x sample buffer was 30% sucrose. Staining was in ethidium bromide (0.25 µg/ml) for 10 min and destaining was in water for 20 min before visualization under UV light.

Acid-urea PAGE (2.5 M urea; 15% acrylamide; 5% acetic acid) was performed at 100 V for 4 h in 5% acetic acid. The acrylamide:bisacrylamide ratio was 20:1. The 2 x sample buffer was 8 M urea, 10% acetic acid, and 0.3% Pyronine Dye Y. Staining was with Coomasie blue (0.25% Coomasie Brilliant Blue, 25% isopropanol, 10% acetic acid) for ½ h after which the gel was destained for 1 h (10% isopropanol; 10% acetic acid).

SDS PAGE (6% stacking, 15% separating) was performed at 100 V for 1.3 h in 1X SDS Running buffer (0.05 M Tris; 0.4 M Glycine; 0.004 M Sodium dodecyl sulphate (SDS). The acrylamide:bisacrylamide ratio was 30:0.8. The 2 x sample buffer was 0.125 M Tris (6.8); 4% SDS; 20% glycerol; 1.43 M ß-mercaptoethanol and 0.1% bromophenol blue. Staining was with Coomasie blue (0.25% Coomasie Brilliant Blue, 25% isopropanol, 10% acetic acid) for ½ h after which the gel was destained for 1 h (10% isopropanol; 10% acetic acid).

Agarose gel electrophoresis was performed at 6 V/cm using a 1.0%, agarose; 25 mM Tris-Acetate-0.5 mM EDTA (pH 8) gel and a 25 mM Tris-Acetate-0.5 mM EDTA

(pH 8) running buffer. Staining was in ethidium bromide (0.25 μg/ml) for 10 min and destaining was in water for 20 min before visualization under UV light.

2.3 The isolation of mono-phosphorylated H5

2.3.1 Preparation of native octamers

Native octamers were prepared as described in section 2.2.1 with the following change. 48 mgs of chromatin were loaded onto a hydroxylapatite column (3.5 cm x 15 cm at a flow rate of 30 ml/h) previously equilibrated with 10 column volumes of 20 mM KPO_4 (pH 6.8); 0.4 M NaCl. The column was washed with 130 mls of 20 mM KPO_4 (pH 6.8); 0.4 M NaCl and then flushed for 4 hrs with 20 mM KPO_4 (pH 6.8); 2.5 M NaCl in order to elute the octamers. Octamer fractions were pooled and concentrated using Amicon Ultra Centrifugal Devices (Millipore) 30 000 MW to a final volume of 2 mls. 1 ml of this was dialysed against 2 L of 2 M NaCl; 0.1 mM EDTA; 20 mM Tris (pH 7.5) at 4°C overnight. Prepared octamers were analysed by SDS PAGE and stored at -80°C.

2.3.2 Preparation of native H5

80 mls of chicken erythrocytes in 40% glycerol 0.15 M NaCl; 15 mM Na Citrate; 10 mM $NaPO_4$ (pH 7.2) were centrifuged at 2000 x g at 4°C in a Beckman® Model J2-21 centrifuge for 10 min. Pellets were resuspended in 15 mls each of Buffer II (0.1 M KCl; 50 mM Tris (pH 7.5); 1.0 mM $MgCl_2$; 0.5% Triton X-100) and 1/100 protease inhibitor mixture (Complete; Roche Molecular Biochemicals) and centrifuged at 3000 x g at 4°C for 10 min. Pellets were resuspended in 20 mls each of Buffer II without Triton-X and 1/200 protease inhibitor mixture Complete (Roche Molecular Biochemicals) and

centrifuged for 5 min at 3000 x g at 4°C. The pellet was dissolved in 5% PCA, dounced and centrifuged at 10 000 x g for 10 min. Supernatant was acidified to 0.25 N HCl from a 1.2 N HCl stock. This mixture was precipitated in 6 volumes of acetone at -20°C overnight. The next day, the liquid was centrifuged at 10 000 x g for 10 min and the supernatant was removed. Warm acetone was added and the pellet was redissolved and centrifuged at 10 000 x g for 10 min. The supernatant was removed and pellet was vacuum dried and stored at -20°C.

2.3.3 Isolation of differentially phosphorylated H5

To separate H1 from H5 reversed phase HPLC analysis was carried out using a 5 μm Vydac C_4 column (10 mm x 250 mm): H1-H5 was dissolved in sdH_2O to final concentration of 1.5 mg/ml, loaded onto the column and eluted at a flow rate of 1 ml/min (Buffer A: 0.1% TFA; Buffer B: 100% ACN; %B gradient: 0-5% 1 min, 5-25% 10 min, 25-30% 15 min, 30-35% 20 min, 35-40% 20 min, 40-45% 10 min, 45-55% 50 min, 55-90% 5 min, 90-100% 20 min, 100-100% 5 min, 100-0% 10 min). Fractions were analysed by SDS PAGE. H5 fractions were pooled separately and lyophilized and stored at -80°C. To separate differentially phosphorylated forms of H5 ionic exchange HPLC was carried out using a 6μm SynChrom Synchropak CM300 column: H5 was dissolved in sdH_2O to a final concentration of 1.0 mg/ml. Only 1.0 mg of H5 was loaded per column and a total of 6 columns were run at a flow rate of 1 ml/min (Buffer A: 6 M UREA; 20 mM NaPO4 (pH 5.8), Buffer B: 6 M urea; 20 mM NaPO4 (5.8); 600 mM NaCl; %B gradient: 0-0% 5 min, 0-70% 30 min, 70-100% 60 min, 100-100% 5 min, 100-0% 5 min). Different H5 fractions were pooled separately from all 6 columns, dialysed against 4 L of H_2O at 4°C

(3 x 2hours), lyophilized and stored at -80°C. Fractions were dissolved in sdH_2O and a repeat separation was done using the same column. Differentially phosphorylated forms were pooled and dialysed against 4 L of H_2O at 4°C (3 x 2 hours), lyophilized and stored at -80°C. Fractions were analysed by acid-urea PAGE.

2.3.4 Mass spectrometry of H5 species.

Matrix assisted laser desorption ionisation – time of flight (MALDI-TOF) mass spectrometry was performed by Ron Finn at the UVIC Genome BC Proteomics Center. Peptide sample in sdH_2O was dissolved 1:1 with 0.1% trifluoroacetic acid; 50% acetonitrile; 10μg/ml 3,5-Dimethoxy-4-hydroxycinnamic acid (sinapinic acid). Peptide mixture (1 μl) was analysed using a Voyager-DE™ STR BioSpectrometry Workstation (Perspective Biosystems).

2.3.5 Amplification of p5S208-12 Lytechinus 5S rDNA plasmid

Amplification of the p5S208-12 *Lytechinus* 5S rDNA plasmid was completed as described in section 2.2.6.

2.3.6 Isolation and preparation of the 208-12 Lytechinus 5S rDNA

Isolation and preparation of the 208-12 *Lytechinus* 5S rDNA was completed as described in section 2.2.7.

2.3.7 Chromatin fiber reconstitutions

Native histone octamers in 2 M NaCl; 20 mM Tris (pH 7.5); 0.1 mM EDTA octamers were incubated in 20 mM ß-mercaptoethanol for ½ hour at room temperature. The 208-12 *Lytechinus* 5S rDNA template in 2 M NaCl; 20 mM Tris (pH 7.5); 0.1 mM EDTA was then added to the octamers at a histone:DNA ratio of 0.9. The DNA and histones were dialysed in 2 M NaCl; 20 mM Tris (pH 7.5); 0.1 mM EDTA; 1 mM DTT overnight at 4°C. The next day, histone octamers were assembled onto the DNA template by step-wise salt dialysis (2 M – 0 M NaCl; 10 mM Tris (pH 7.5); 0.1 mM EDTA). Each dialysis step was 2.5 hrs at 4°C. The concentration of NaCl decreased as follows: 2 M, 1.5 M, 1.2 M, 1.0 M, 0.6 M, 0.3 M, 0 M). Fibers were stored on ice for analytical ultracentrifugation. For the histone H5 control fiber reconstitution, H5 in 0.6 M NaCl; 10 mM Tris (pH 7.5); 0.1 mM EDTA was added to the mixture at the 0.6 M NaCl; 10 mM Tris (pH 7.5); 0.1 mM EDTA dilution step. The H5:DNA ratio was 1.3.

2.3.8 Analytical ultracentrifugation characterization

Reconstituted fibers were dialysed against 0 mM, 40 mM (+H5 control) or 50 mM (-H5 control), and 100 mM NaCl; 20 mM Tris (pH 7.5); 0.1 mM EDTA and subjected to sedimentation velocity analysis using a Beckman Model XL-A ultracentrifuge as described in section 2.1.10. A rotor speed of 26 000 rpm was used. The UV scans (260nm) were analysed using the van Holde–Weischet method to determine the distribution of sedimentation coefficients for the population of fibers within a sample. The XL-A data analysis software was version 4.1 (Borries Demeler, Missoula, Montana). Each sample's sedimentation coefficient value was obtained from its respective

sedimentation coefficient histogram (for an example of sedimentation velocity analysis see Figure 2).

2.3.9 Gel electrophoresis

Acid-urea PAGE (2.5 M urea; 15% acrylamide; 5% acetic acid) was performed at 100 V for 4 h in 5% acetic acid. The acrylamide:bisacrylamide ratio was 20:1. The 2 x sample buffer was 8 M urea, 10% acetic acid, and 0.3% pyronine Dye Y. Staining was with Coomasie blue (0.25% Coomasie Brilliant Blue, 25% isopropanol, 10% acetic acid) for ½ h after which the gel was destained for 1 h (10% isopropanol; 10% acetic acid).

SDS PAGE (6% stacking, 15% separating) was performed at 100 V for 1.3 h in 1X SDS Running buffer (0.05 M Tris; 0.4 M Glycine; 0.004 M sodium dodecyl sulphate (SDS). The acrylamide:bisacrylamide ratio was 30:0.8. The 2 x sample buffer was 0.125 M Tris (6.8); 4% SDS; 20% glycerol; 1.43 M ß-mercaptoethanol and 0.1% bromophenol blue. Staining was with Coomasie blue (0.25% Coomassie Brilliant Blue, 25% isopropanol, 10% acetic acid) for 30 min after which the gel was destained for 1 h (10% isopropanol; 10% acetic acid).

Agarose gel electrophoresis was performed at 6 V/cm using a 1.0%, agarose; 25 mM Tris-Acetate-0.5 mM EDTA (pH 8) gel and a 25 mM Tris-Acetate-0.5 mM EDTA (pH 8) running buffer. Staining was in ethidium bromide (0.25 μg/ml) for 10 min and destaining was in water for 20 min before visualization under UV light.

3.0 RESULTS

3.1 The creation and characterization of the Pbsn-208(10) template

3.1.1 PCR stitching of XhoI sites onto the probasin promoter

The expected product size resulting from a PCR stitch of *Xho*I sites onto both sides of the probasin promoter using the PucProfwd and PucProrev primers is 206 bp. The integrity and purity of the PCR stitched product after gel purification was analysed by agarose gel electrophoresis: all three reactions resulted in only one product each of the expected 206 bp size (Figure 3).

3.1.2 Ligation of XhoI-probasin promoter-XhoI sequence into TOPO vector

The ligated TOPO-*Xho*I-probasin promoter-*Xho*I plasmid was successfully transformed into One Shot® *E. coli* cells (Invitrogen). The *lacZa* gene within the pCR®II-TOPO® multiple cloning site allows the detection of successful transposition by blue/white colony formation. Upon ligation of the *Xho*I-probasin promoter-*Xho*I DNA, *lacZa*'s expression is interrupted. As a result, a positive transposition event gives white colonies in the presence of X-gal and the inducer IPTG. Unsuccessful integration would result in blue colonies under these conditions (Invitrogen 2006). Figure 4 shows the electrophoretic analysis of the transposed TOPO ligant *Xho*I digests compared to an uncut TOPO ligant and an uncut Puc-probasin plasmid. Of seven white colonies that were screened by *Xho*I digestion, one did not contain the 206 bp *Xho*I-probasin promoter-*Xho*I insert (lane 3), and one did not digest (lane 4). Five of the seven colonies screened by *Xho*I digestion resulted in products of the expected 206 bp size (lanes 5-9).

3.1.3 Purification of the XhoI-probasin promoter-XhoI sequence and preparation of the pIC-2085S plasmid

Digestion of the TOPO-*Xho*I-probasin promoter-*Xho*I plasmid and the pIC-2085S plasmid with *Xho*I allowed the gel extraction of the 206 bp *Xho*I-probasin promoter-*Xho*I fragment and the linearized 4794 bp pIC-2085S plasmid. Figure 5 shows the electrophoretic analysis of the *Xho*I digest gel extractions. Gel purifications of both the TOPO-*Xho*I-probasin promoter-*Xho*I plasmid and the pIC-2085S plasmid reactions showed only one product within the predicted size range each (206 bp and 4794 bp respectively).

3.1.4 Generation of the Pbsn-208(10) plasmid

*Xho*I-probasin promoter-*Xho*I-pIC-2085S ligants were successfully transformed into Nova Blue (Novagen) *E. coli* cells. Of seventeen colonies that were screened by PCR and analysed by gel electrophoresis seven resulted in amplicons of the predicted size (227 bp). Figure 6 shows the electrophoretic analysis of amplicons from three positive PCR reactions (named ligation 1, 2, and 3) and one negative control. In all three positive PCR reactions the primary amplicon (227 bp) is most intense while the presence of a secondary amplicon is visible in lanes 2 and 3, and multiple banding is seen in lane 1.

Ligated plasmids 1, 2 and 3 from Figure 6, and two pIC-2085S negative controls were analysed further by *Xho*I to confirm insert ligation, and by *Eco*RI to determine if ligants contained more than one copy of the DNA insert. The *Eco*RI digest expected band sizes are: a) 2632, 237, and 196 for a ligant with one insert, b) 2632, 429, and 196 for a ligant with two inserts, c) 2632 and 196 for the ligated plasmid with no insert (negative control 1), d) 2632, 196 and 47 for the unligated plasmid (negative control 2). The *Xho*I

digest expected band sizes are: a) 4800 and 196 for a ligant with one or more inserts, c) 4800 for the ligated plasmid with no insert (negative control 3). Figure 7 shows the 2% agarose electrophoretic analysis of *Xho*I and *Eco*RI digests of ligants 1, 2, and 3 and the pIC-2085S negative controls compared to a positive PCR amplicon from Figure 6. *Xho*I digests of ligants (lanes 7 and 8) resulted in two bands of expected sizes for a ligant with insert (4800 bp and 196 bp) while the negative control (lane 9; negative control 3) showed no insert sized band. The presence of a secondary band of undigested plasmid is visible in lane 9 (negative control 3). *Eco*RI digestion of ligants 1, 2, and 3 (lanes 2, 3, and 4) all resulted in 3 bands of expected sizes for a ligant with one insert (2632 bp, 237 bp, and 196 bp). *Eco*RI digestion of the two negative controls resulted in bands of expected sizes for the ligated plasmid with no insert (lane 5: 2632 bp and 196 bp; negative control 1) and the unligated plasmid (lane 6: 2632 bp, 196 bp and 47 bp; negative control 2). No *Eco*RI digests resulted in bands of sizes indicative of a double integration event (2632 bp, 429 bp, and 196 bp).

3.1.5 Sequence analysis of Pbsn-208(10)

Figure 8 shows a BioEdit sequence alignment of the Pbsn-208(10) plasmid forward (picproFwdseq) and reverse (picproRevcomplseq) sequence analysis results compared to the expected *Xho*I-probasin promoter-*Xho*I cDNA (probasinXHOIstitch). Blast search of the cloned probasin promoter cDNA sequence revealed 100 % identity with the *Rattus norvegicus* probasin (Pbsn) gene promoter region, accession number AY370611. Therefore no mutation in the Pbsn sequence occurred throughout the experimental manipulation. The sequence data that extends beyond the probasin promoter DNA on

both sides has 100 % identity with the multiple cloning site on the left and right side of the *Xho*I cut site and into the first 208 *Lytechinus* 5S rDNA repeat. The sequencing results therefore indicate not only that only one copy of the insert was ligated into the pIC-2085S plasmid but also that the insert was ligated in the right direction. The plasmid was officially renamed Pbsn-208(10).

3.1.6 Isolation and preparation of the Pbsn-208(10) DNA template

Although Sephacryl column chromatography of the Pbsn-208(10) plasmid extracted from Nova Blue *E. coli* cells was meant to fractionate the plasmid DNA from bacterial genomic DNA, the elution profile in Figure 9 and the electrophoretic analysis of the fractionation in Figure 10 show that this step was not necessary. No bacterial genomic DNA appears to have been extracted along with the plasmid. Figure 11 shows the electrophoretic analysis of the *Kpn*I, *Cla*I and *Hha*I triple digestion of the concentrated Pbsn-208(10) plasmid. The digestion resulted in one 2349 bp Pbsn-208(10) insert band (lane 4) and multiple smaller bands where *Kpn*I, *Cla*I and *Hha*I digested the rest of the plasmid. Lane 4 does not contain bands of sizes denoting incomplete digestion visible in the control lanes 1-3 and 5. Sephacryl column chromatography of the Pbsn-208(10) *Kpn*I, *Cla*I and *Hha*I triple digestion allowed the fractionation of the 2349 bp Pbsn-208(10) DNA insert from the smaller pieces of the digested plasmid (Figure 12). Figure 13 shows the electrophoretic analysis of the fractionation.

3.1.7 Analytical ultracentrifuge characterization

The sedimentation velocity analysis of the Pbsn-208(10) oligonucleosomes indicates that at 20 mM NaCl the fiber's sedimentation value is 34 S.

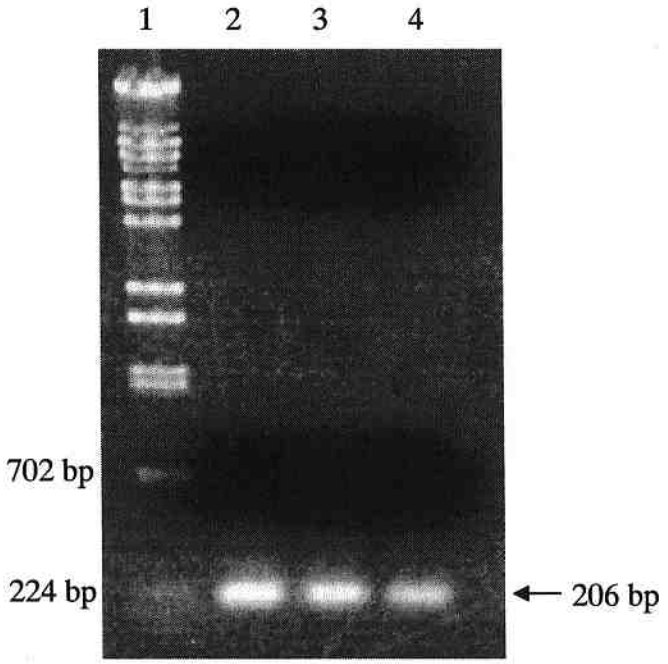

Figure 3. Gel purified products from *Xho*I PCR stitch reactions. Products were electrophoresed on a 1.0% agarose/ 25 mM Tris-Acetate 0.5 mM EDTA (pH 8) gel. The gel was stained in ethidium bromide (0.25 μg/ml) for 10 min and destained in water for 20 min then visualized under UV light. Lane 1) Lambda DNA-*Bst*E II digest (NEB); lane 2)–4) gel purified amplicons from PCR reactions 1, 2, and 3 respectively.

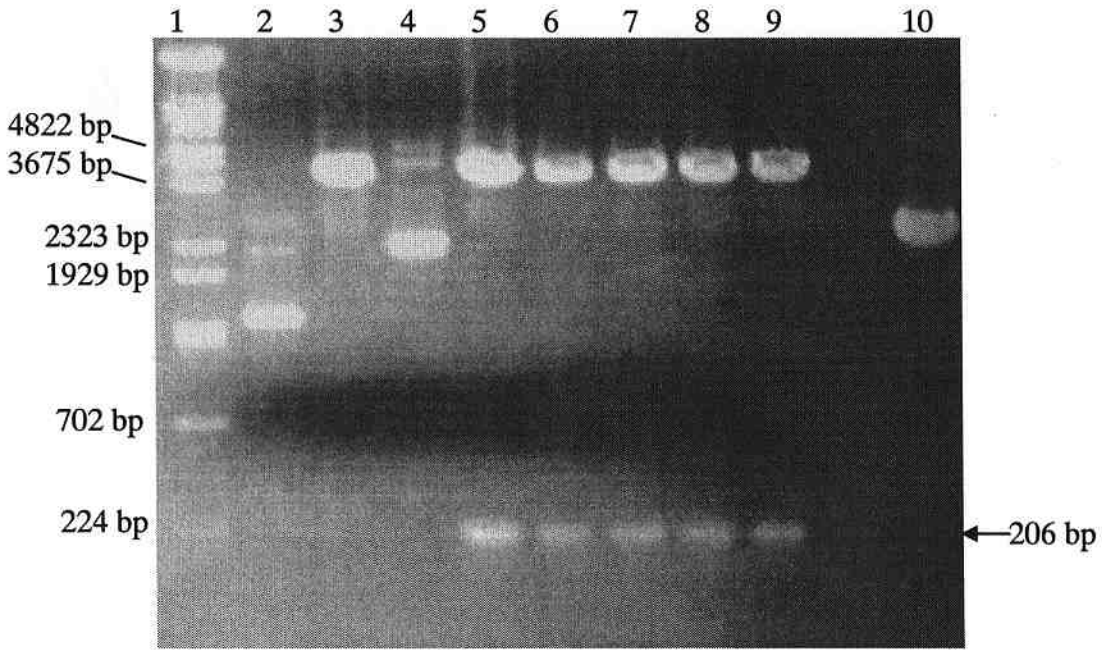

Figure 4. *Xho*I digestion products from the transformed TOPO-*Xho*I-probasin promoter-*Xho*I plasmid. Products were electrophoresed on a 1.0% agarose/ 25 mM Tris-Acetate 0.5 mM EDTA (pH 8) gel. The gel was stained in ethidium bromide (0.25 μg/ml) for 10 min and destained in water for 20 min then visualized under UV light. Lane 1) Lambda DNA-*Bst*E II digest (NEB); lane 2) uncut Puc-probasin plasmid; lane 3)-9) *Xho*I digested TOPO ligants; lane 10) uncut TOPO ligant.

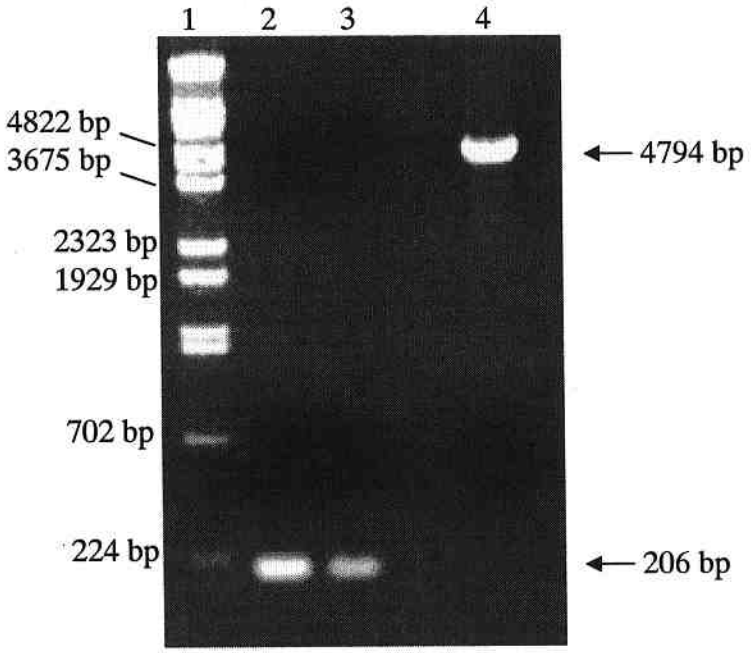

Figure 5. Gel purified products from *Xho*I digestion of the TOPO-*Xho*I-probasin promoter-*Xho*I plasmid and the pIC-2085S plasmid. Products were electrophoresed on a 1.0% agarose/ 25 mM Tris-Acetate 0.5 mM EDTA (pH 8) gel. The gel was stained in ethidium bromide (0.25 μg/ml) for 10 min and destained in water for 20 min then visualized under UV light. Lane 1) Lambda DNA-*Bst*E II digest (NEB); lane 2) & 3) gel purified *Xho*I digested TOPO-*Xho*I-probasin promoter-*Xho*I plasmid; lane 4) gel purified *Xho*I digested pIC-2085S plasmid.

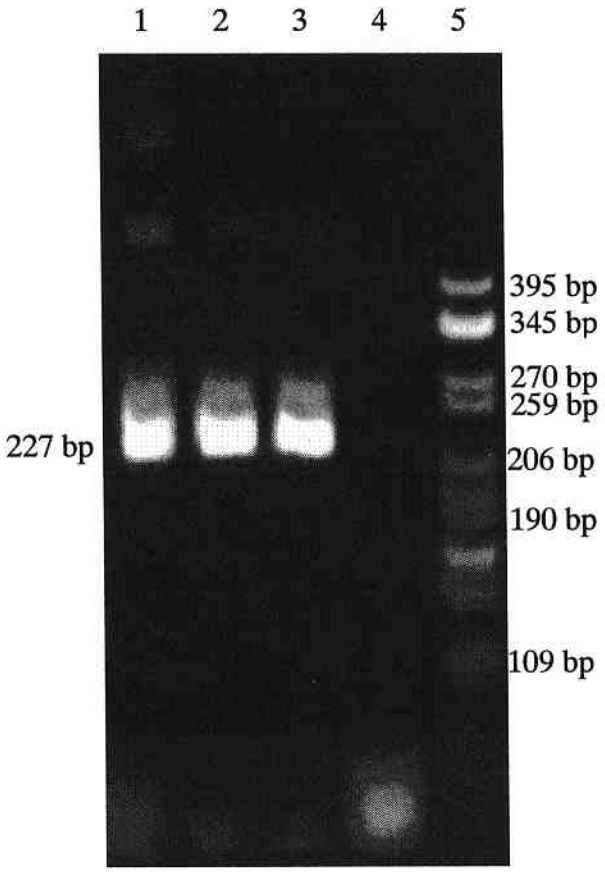

Figure 6. Amplicons from Nova Blue (Novagen) *E. coli* cells transformed with *Xho*I-probasin promoter-*Xho*I-pIC-2085S plasmid (later renamed Pbsn-208-10; see section 3.1.5). Products were electrophoresed on a 4% Native-PAGE gel electrophoresis at 80 V for 45 min in 1 x E Buffer (6X: 1 M Tris-HCl (pH 7.2); 0.5 M EDTA (pH 8.0); 0.12 M sodium acetate trihydrate. The acrylamide:bisacrylamide ratio was 20:1 and the 3 x sample buffer was 30% sucrose. Staining was in ethidium bromide (0.25 μg/ml) for 10 min and destaining was in water for 20 min before visualization under UV light. Lanes 1)-3) amplicons from ligation reaction 1, 2, and 3 respectively; lane 4) PCR negative control; lane 5) *Cfo*I pBr322 digest DNA marker.

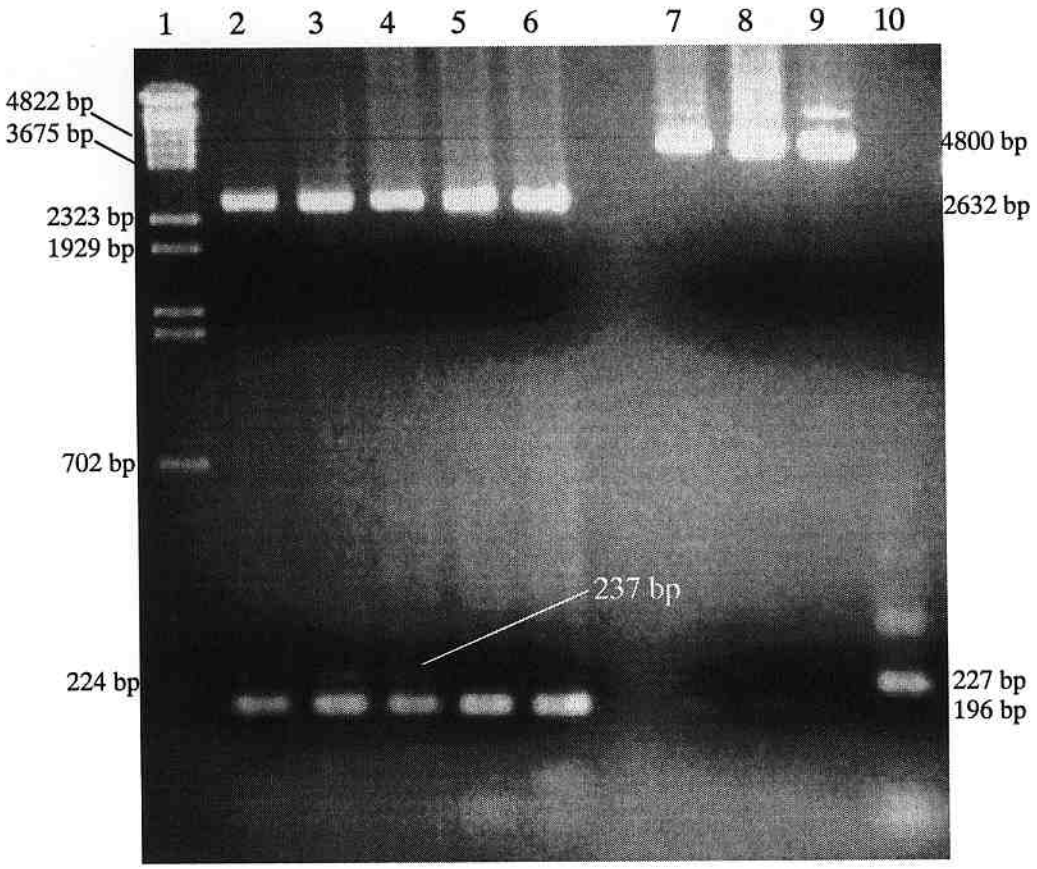

Figure 7. *Xho*I and *Eco*RI digestion products of *Xho*I-probasin promoter-*Xho*I-pIC-2085S plasmid (later renamed Pbsn-208-10; see section 3.1.5). Products were electrophoresed on a 2.0% agarose/ 25 mM Tris-Acetate 0.5 mM EDTA (pH 8) gel. The gel was stained in ethidium bromide (0.25 μg/ml) for 10 min and destained in water for 20 min then visualized under UV light. Lane 1) Lambda DNA-*Bst*E II digest (NEB); lane 2)-4) *Eco*RI digests of plasmids from ligation reactions 1, 2, and 3 respectively; lane 5) *Eco*RI digest of the pIC-2085S negative control 1 plasmid; lane 6) *Eco*RI digest of the pIC-2085S negative control 2 plasmid; lane 7)-8) *Xho*I digests of plasmids from ligation reactions 1 and 3; lane 9) *Xho*I digest of the pIC-2085S negative control 3 plasmid; lane 10) PCR amplicon from ligation reaction 1.

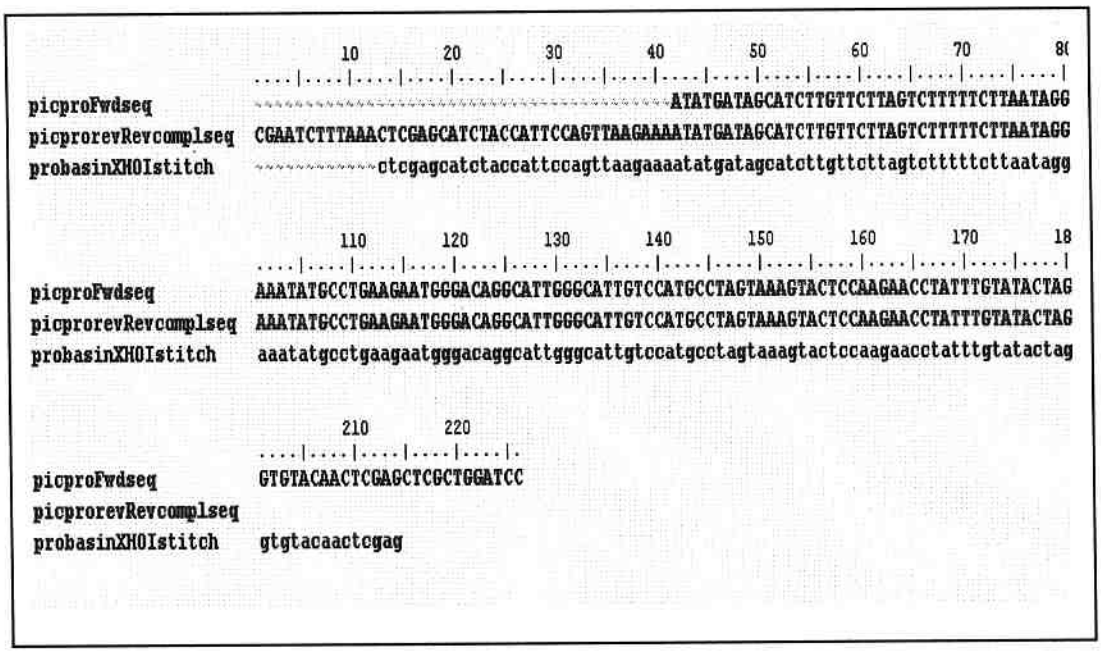

Figure 8. BioEdit sequence alignment of the Pbsn-208(10) plasmid forward (picproFwdseq) and reverse (picproRevcomplseq) sequence analysis results compared to the expected *Xho*I-probasin promoter-*Xho*I cDNA (probasinXHOIstitch).

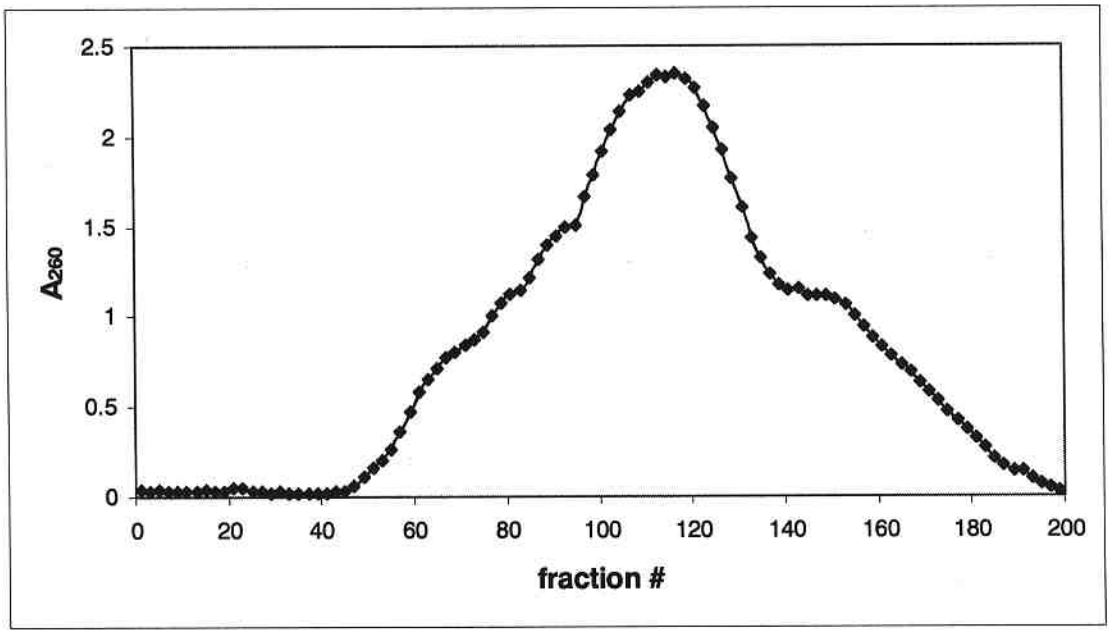

Figure 9. Sephacryl column chromatography of Pbsn-208(10) plasmid extracted from Nova Blue *E. coli* cells. DNA was loaded onto a Sephacryl column (2.5 cm x 60 cm) at a flow rate of 60 ml/h and eluted in TE in 2 ml fractions. The elution profile was recorded at a wavelength of A_{260}.

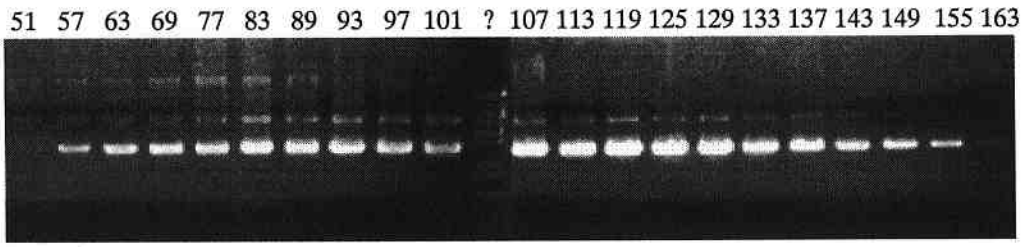

Figure 10. Electrophoretic analysis of the Pbsn-208(10) plasmid Sephacryl column fractionation. Aliquots were electrophoresed on a 1.0% agarose/ 25 mM Tris-Acetate 0.5 mM EDTA (pH 8) gel. The gel was stained in ethidium bromide (0.25 μg/ml) for 10 min and destained in water for 20 min then visualized under UV light. Lane numbers correspond to elution fraction numbers from Figure 9. ? marker is lambda DNA-*Bst*E II digest (NEB) with sizes from the bottom to top: 702 bp, 1264 bp, 1371 bp, 1929 bp, 2323 bp, 3675 bp, 4324 bp, 4882 bp, 5686 bp, 6369 bp, 7284 bp, 8454 bp.

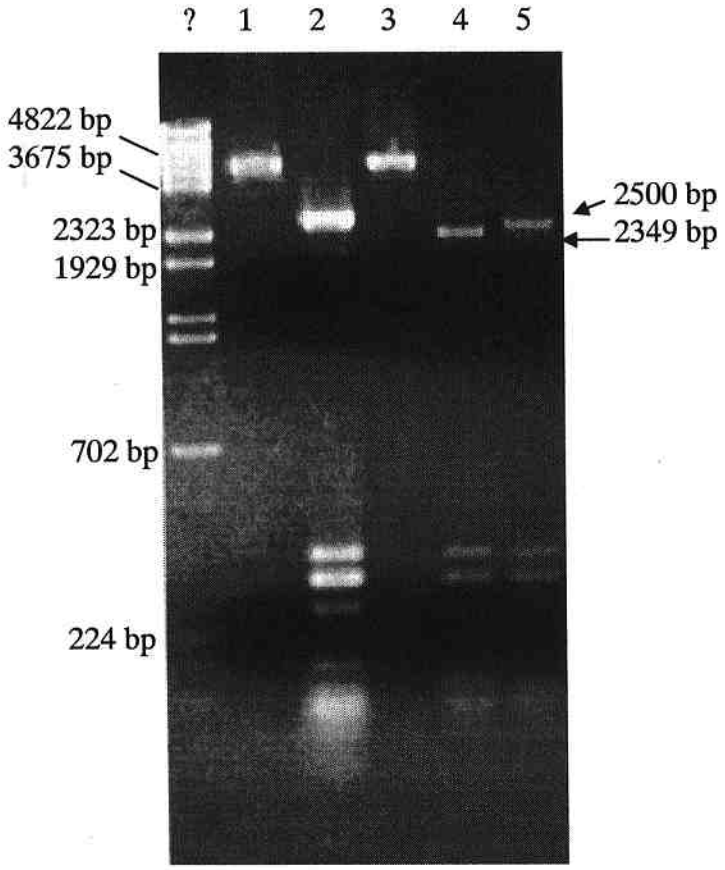

Figure 11. Electrophoretic analysis of the Pbsn-208(10) plasmid triple digest. Products were electrophoresed on a 1.6% agarose/ 25 mM Tris-Acetate 0.5 mM EDTA (pH 8) gel. The gel was stained in ethidium bromide (0.25 μg/ml) for 10 min and destained in water for 20 min then visualized under UV light. Lane 1) Pbsn-208(10) *Kpn*I control digest; lane 2) Pbsn-208(10) *Hha*I control digest; lane 3) Pbsn-208(10) *Cla*I control digest; lane 4) Pbsn-208(10) *Kpn*I, *Cla*I and *Hha*I triple digest; lane 5) Pbsn-208(10) *Cla*I and *Hha*I control digest. ? marker is lambda DNA-*Bst*E II digest (NEB).

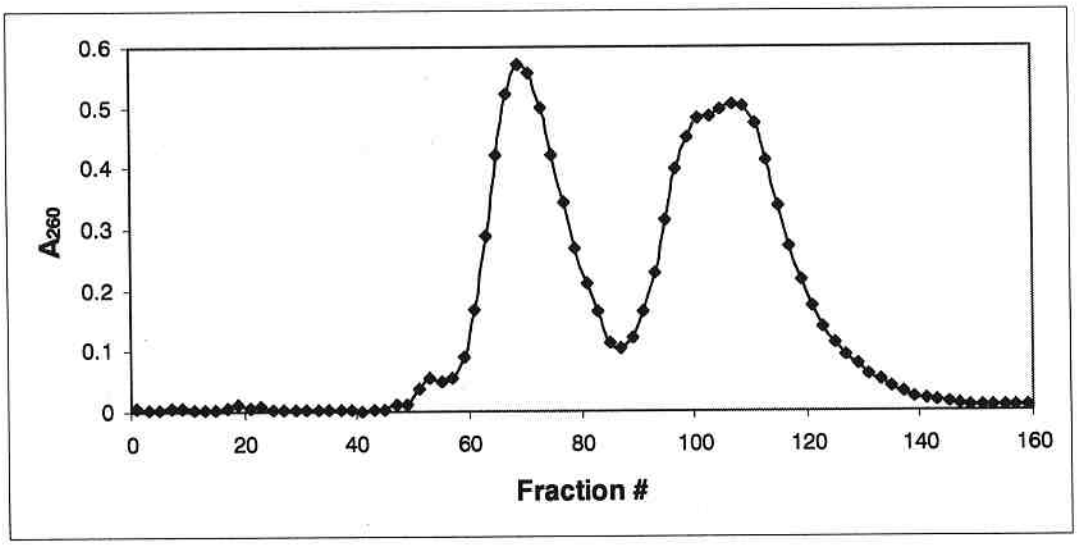

Figure 12. Sephacryl column chromatography of the Pbsn-208(10) plasmid *Cla*I, *Kpn*I, and *Hha*I triple digestion. DNA was loaded onto a Sephacryl column (2.5 cm x 60 cm) at a flow rate of 60 ml/h and eluted in TE in 2ml fractions. The elution profile was recorded at a wavelength of A_{260}.

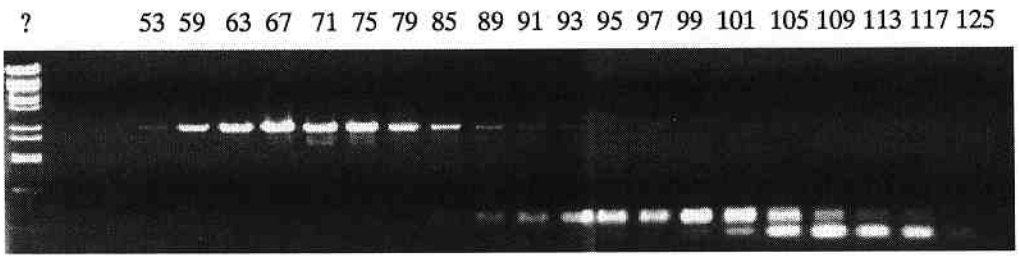

Figure 13. Electrophoretic analysis of the Pbsn-208(10) plasmid *Cla*I, *Kpn*I, and *Hha*I triple digest Sephacryl column fractionation. Aliquots were electrophoresed on a 1.0% agarose/ 25 mM Tris-Acetate 0.5 mM EDTA (pH 8) gel. The gel was stained in ethidium bromide (0.25 μg/ml) for 10 min and destained in water for 20 min then visualized under UV light. Lane numbers correspond to elution fraction numbers from Figure 12. ? marker is lambda DNA-*Bst*E II digest (NEB) with sizes from the bottom to top: 224 bp, 702 bp, 1264 bp, 1371 bp, 1929 bp, 2323 bp, 3675 bp, 4324 bp, 4882 bp, 5686 bp, 6369 bp, 7284 bp, 8454 bp.

3.2 H4 K16Ac and the structure of the nucleosome

3.2.1 Isolation of Native Histones

Hydroxylapatite column chromatography of stripped chromatin extracted from chicken erythrocytes allowed for the fractionation of natives histones under increasing salt concentrations (Figure 14). Figure 15 shows the electrophoretic analysis of the fractionation of the native histones. Histones H2A-H2B eluted separately from H3-H4 under the given elution buffer gradient. Pure histones H3 and H4 are visible from fraction # 97 onwards (Figure 15).

3.2.2 Separation of H3 and H4

Histones H3 and H4 were fractionated by reversed phase HPLC (Figure 16). Figure 17 shows the electrophoretic analysis of the fractionation. H4 from fractions represented by and including lanes 5-6 were pooled for H4 K16Ac extraction. H3 from fractions represented by and including lanes 15-16 were pooled for use in reconstitutions.

3.2.3 Isolation of H4 K16Ac and non-acetylated H4 K16

Differentially acetylated H4 was fractionated by ion exchange HPLC (Figure 18). Figure 19 shows the electrophoretic analysis of the fractionation. H4 species eluted separately from one another under the indicated elution buffer gradient. Nonacetylated H4 is seen in lanes 2 and 4 while monoacetylated H4 K16 is seen in lanes 3 and 5 of Figure 19.

3.2.4 Mass spectrometry of H4K16Ac

A summary of the tandem mass spectrometry results provided to us by Don Hunt from the department of Chemistry at the University of Virginia is shown in Table 1. The results indicate that 75% of the mono-acetylated H4 isolated by ionic exchange HPLC have their acetyl group bound at lysine 16.

3.2.5 Titration of histone octamers containing either H4 K16Ac or non-acetylated H4 K16

Figure 20 shows the electrophoretic analysis of titrated octamers. Octamers containing H4 K16Ac (lane 4) and those containing non-acetylated H4 K16 (lane 2) are both mixed in stoichiometric amounts.

3.2.6 Isolation and preparation of the 208-12 Lytechinus 5S rDNA

Sephacryl column chromatography of the p5S208-12 *Lytechinus* 5S rDNA plasmid extract allowed the separation of plasmid DNA (fractions 50 – 85; Figure 21) from genomic DNA (fractions 100 – 180: electrophoresis not shown). Figure 22 shows the electrophoretic analysis of the first peak (the plasmid peak) of the fractionation. The *Hha*I digestion of the concentrated p5S208-12 *Lytechinus* 5S rDNA plasmid resulted in one 2496 bp 208(12)-*Lytechinus* 5S rDNA band and multiple smaller bands where *Hha*I digested the rest of the p5S plasmid (lanes 1 – 3; Figure 23). Sephacryl column chromatography of the p5S208-12 *Lytechinus* 5S rDNA plasmid *Hha*I digestion allowed for the fractionation of the 2496 bp 208-12 *Lytechinus* 5S rDNA piece from the smaller

pieces of the digested p5S plasmid (Figure 24). Figure 25 shows the electrophoretic analysis of the fractionation.

3.2.7 Preparation of the 208 bp Lytechinus 5S rDNA monomer

The ion exchange HPLC fractionation of *Rsa*I digested 208(12)-*Lytechinus* 5S rDNA allowed the separation of the digested product of the predicted 208 bp size (Figure 26). The electrophoretic analysis of the 208 *Lytechinus* 5S rDNA monomer isolate is shown in Figure 27.

3.2.8 The formation and sucrose gradient purification of random 146 bp genomic chicken DNA nucleosomes

Figure 28 shows that the 146 bp nucleosome reconstitution resulted in the formation of octameric nucleosomes, hexameric nucleosomes, and free DNA for both the H4 K16Ac nucleosomes and the H4 NonAc nucleosomes. Sucrose gradient centrifugation was used to separate the hexamer products from the octameric nucleosomes. Figure 29 shows the sucrose gradient fractionation results of the 146 bp reconstitution products. The overlapping peaks in Figure 29 indicate that the sucrose gradient centrifugation did not result in a complete separation of the 146 bp hexamers from the octamers. Incomplete separation is visualized by electrophorectic analysis in Figure 30. The 146 bp nucleosome fractions least contaminated with hexamers were pooled for use in reconstitutions (fractions denoted by white arrows in Figure 30). The final pooled 146 bp H4 K16Ac nucleosomes and H4 NonAc nucleosomes are shown in Figure 31.

3.2.9 The formation of 208 bp Lytechinus 5S rDNA nucleosomes

Unlike for the 146 bp nucleosomes, the 208 bp nucleosome reconstitutions did not result in the formation of hexamers. Sucrose gradient separation was therefore not necessary. Figure 32 shows the electrophoretic analysis of the reconstituted H4 K16Ac nucleosomes and H4 NonAc nucleosomes.

3.2.10 Analytical ultracentrifuge characterization of random 146 bp genomic chicken DNA nucleosomes

The sedimentation velocity analysis of the 146 bp nucleosomes shown in Table 2 indicates that at high salt (600 mM NaCl) H4 K16Ac nucleosomes sediment more slowly than the H4 NonAc nucleosomes. At lower salt, however, (100 mM NaCl) the inverse is observed: the H4 NonAc nucleosomes sediment more slowly than the H4 K16Ac nucleosomes.

3.2.11 Analytical ultracentrifuge characterization of 208 bp Lytechinus 5S rDNA nucleosomes

The sedimentation velocity analysis of the 208 bp nucleosomes shown in Figure 33 indicates that at low (10 mM NaCl) and high salt (600 mM NaCl) H4 K16Ac nucleosomes sediment more slowly than the H4 NonAc nucleosomes. At 50 mM, 200 mM, and 400 mM NaCl, however, the inverse is observed: the H4 NonAc nucleosomes sediment more slowly than the H4 K16Ac nucleosomes.

3.2.12 Magnesium chloride solubility

The magnesium chloride solubility curves show that H4 K16Ac nucleosomes are more soluble in $MgCl_2$ than H4 NonAc nucleosomes (Figure 34).

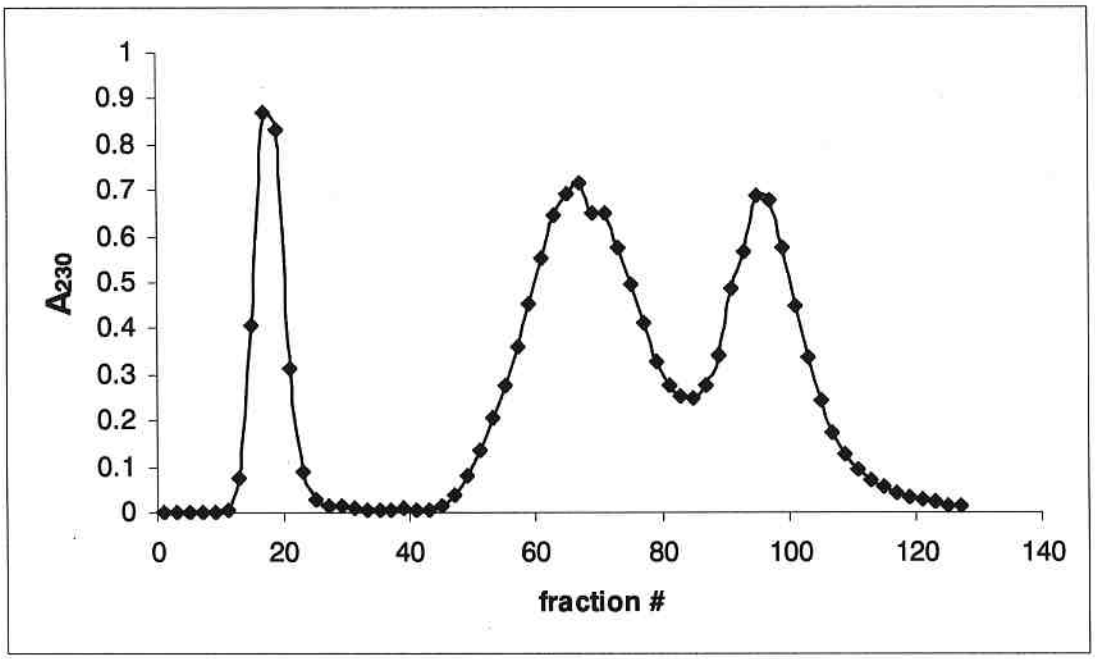

Figure 14. Hydroxylapatite column chromatography of stripped chromatin extracted from chicken erythrocytes. Chromatin was loaded onto a hydroxylapatite column (3.5 cm x 15 cm at a flow rate of 30 ml/h). The elution buffer gradient was: 20 mM KPO_4 (pH 6.8); 0.4 M NaCl to 20 mM KPO_4 (pH 6.8); 2.5 M NaCl over 20 hours followed by 20 mM KPO_4 (pH 6.8); 2.5 M NaCl for 2 hours. The elution profile was recorded at a wavelength of A_{230}.

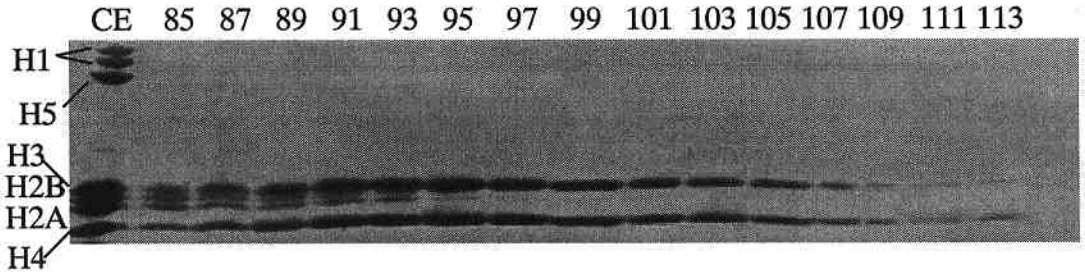

Figure 15. Electrophoretic analysis of hydroxylapatite column chromatography fractions. Histones were analysed by SDS PAGE (6% stacking, 15% separating) at 100 V for 1.3 h in 1X SDS Running buffer (0.05 M Tris; 0.4 M Glycine; 0.004 M Sodium dodecyl sulphate). The acrylamide:bisacrylamide ratio was 30:0.8. The 2 x sample buffer was 0.125 M Tris (pH 6.8); 4% SDS; 20% glycerol; 1.43 M ß-mercaptoethanol and 0.1% bromophenol blue. Staining was with Coomassie blue (0.25% Coomasie Brilliant Blue, 25% isopropanol, 10% acetic acid) for ½ h after which the gel was destained for 1 h (10% isopropanol; 10% acetic acid). Lane numbers correspond to elution fraction numbers from Figure 14. CE: chicken erythrocyte histone marker.

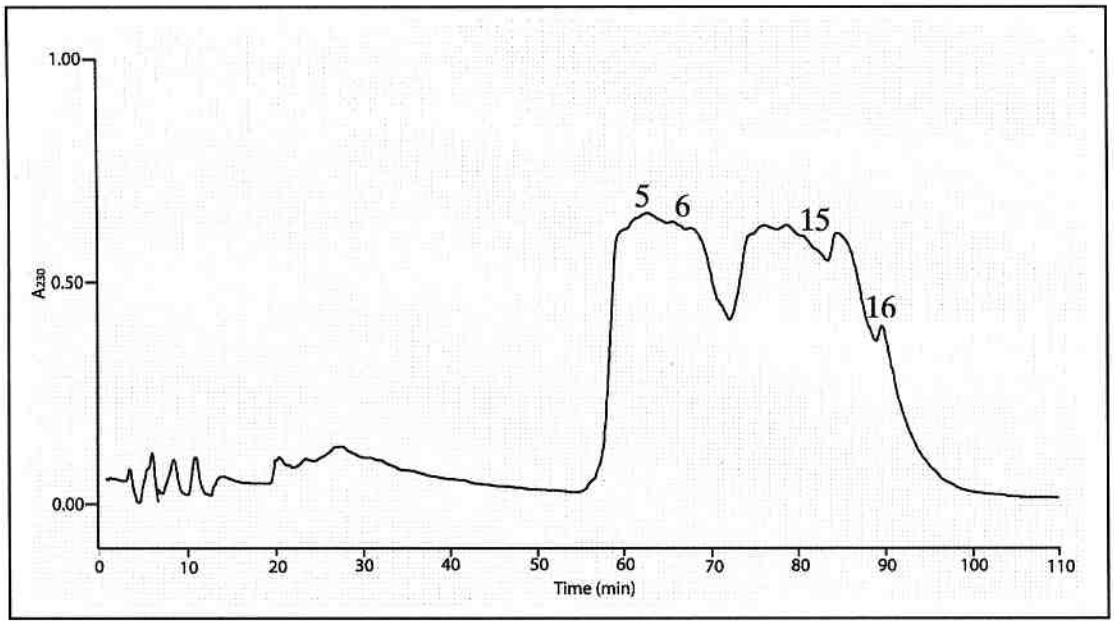

Figure 16. Reverse phase HPLC fractionation of lyophilized histone H3-H4 hydroxylapatite column fractions. Histones H3-H4 were dissolved in sdH_2O to final concentration of 1.5 mg/ml, loaded onto the 5μm Vydac C_4 column (10 mm x 250 mm) and eluted at a flow rate of 1 ml/min (Buffer A: 0.1% TFA; Buffer B: 100% ACN; %B gradient: 0-5% 1 min, 5-25% 10 min, 25-30% 15 min, 30-35% 20 min, 35-40% 20 min, 40-45% 10 min, 45-55% 50 min, 55-90% 5 min, 90-100% 20 min, 100-100% 5 min, 100-0% 10 min). The elution profile was recorded at a wavelength of A_{230}.

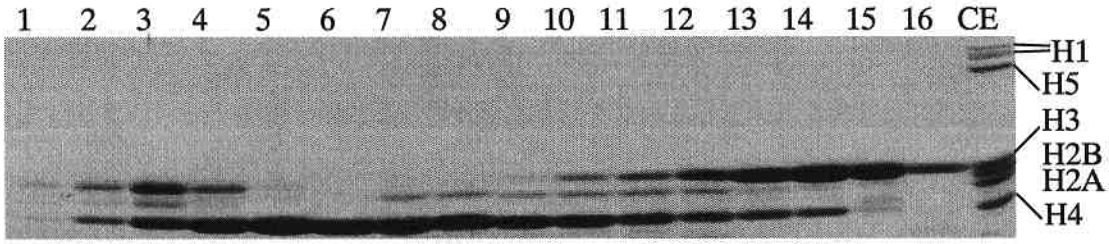

Figure 17. Electrophoretic analysis of reversed phase HPLC separation of H3-H4. Histones were analysed by SDS PAGE (6% stacking, 15% separating) at 100 V for 1.3 h in 1X SDS Running buffer (0.05 M Tris; 0.4 M Glycine; 0.004 M Sodium dodecyl sulphate). The acrylamide:bisacrylamide ratio was 30:0.8. The 2 x sample buffer was 0.125 M Tris (pH 6.8); 4% SDS; 20% glycerol; 1.43 M ß-mercaptoethanol and 0.1% bromophenol blue. Staining was with Coomassie blue (0.25% Coomasie Brilliant Blue, 25% isopropanol, 10% acetic acid) for ½ h after which the gel was destained for 1 h (10% isopropanol; 10% acetic acid). Lane numbers represent Figure 16 peak fractions from left to right. Lane numbers of interest are indicated on the chromatogram in Figure 16. CE: chicken erythrocyte histone marker.

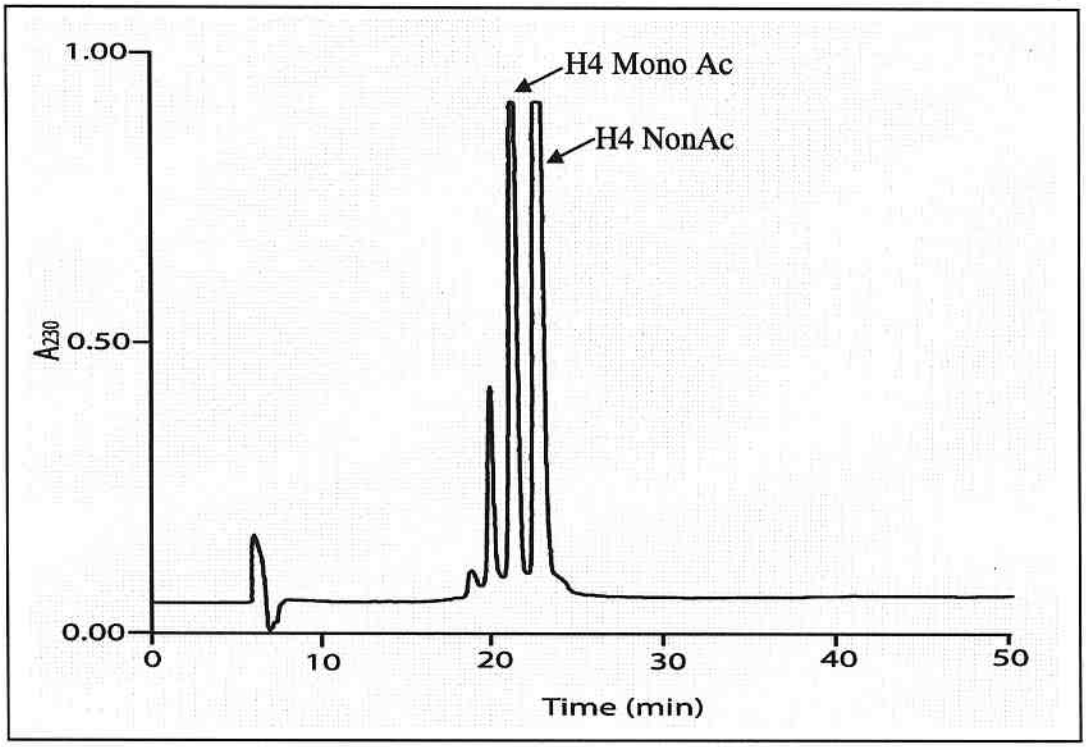

Figure 18. Ion exchange HPLC fractionation of lyophilized histone H4 from reversed phase HPLC. H4 was dissolved in sdH_2O to a final concentration of 1.5 mg/ml and loaded onto the 6 μm SynChrom Synchropak CM300 column at a flow rate of 1 ml/min (Buffer A: 8 M UREA; 23 mM NaPO4 (pH 7.0); 0.5 mM DTT; 100 mM NaCl: Buffer B: 8 M urea; 23 mM NaPO4 (pH 7.0); 0.5 mM DTT; 800 mM NaCl; %B gradient: 0-0% 5 min, 0-29% 10 min, 29-50% 40 min, 50-100% 10 min, 100-0% 5 min). The elution profile was recorded at a wavelength of A_{230}.

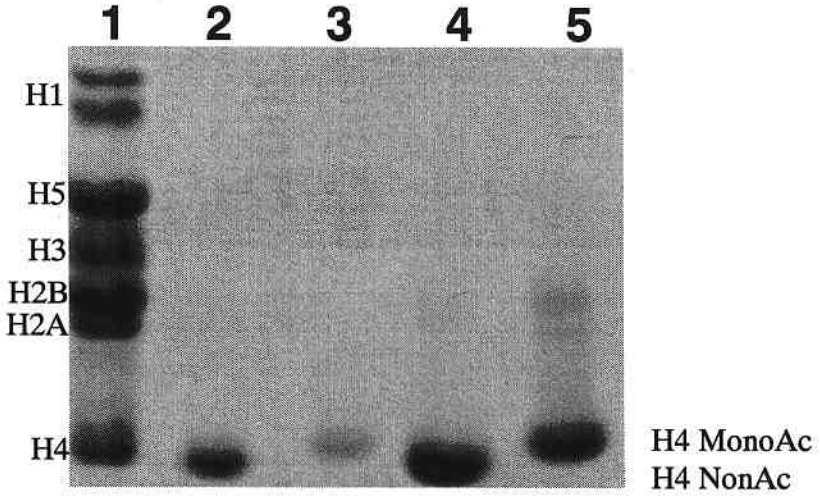

Figure 19. Electrophoretic analysis of H4 ionic exchange HPLC fractions. Fractions were analysed by acid-urea PAGE (2.5 M urea; 15% acrylamide; 5% acetic acid) at 100 V for 4 h in 5% acetic acid. The acrylamide:bisacrylamide ratio was 20:1. The 2 x sample buffer was 8M urea, 10% acetic acid, and 0.3% pyronine Dye Y. Staining was with Coomassie blue (0.25% Coomassie Brilliant Blue, 25% isopropanol, 10% acetic acid) for ½ h after which the gel was destained for 1 h (10% isopropanol; 10% acetic acid). Nonacetylated H4 is seen in lanes 2 and 4 while monoacetylated H4 K16 is seen in lanes 3 and 5. Lane 1: chicken erythrocyte histone marker.

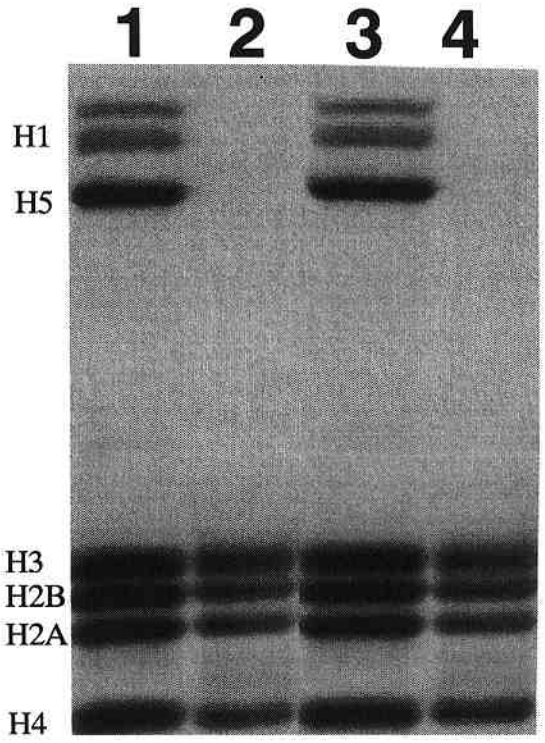

Figure 20. Titrated histone octamers containing either H4 K16Ac or non-acetylated H4 K16. Octamers were analysed by SDS PAGE (6% stacking, 15% separating) at 100 V for 1.3 h in 1X SDS Running buffer (0.05 M tris; 0.4 M Glycine; 0.004 M sodium dodecyl sulphate). The acrylamide:bisacrylamide ratio was 30:0.8. The 2 x sample buffer was 0.125 M Tris (pH 6.8); 4% SDS; 20% glycerol; 1.43 M ß-mercaptoethanol and 0.1% bromophenol blue. Staining was with Coomassie blue (0.25% Coomasie Brilliant Blue, 25% isopropanol, 10% acetic acid) for ½ h after which the gel was destained for 1 h (10% isopropanol; 10% acetic acid). Octamers containing nonacetylated H4 are seen in lane 2 and those containing H4 K16Ac are seen in lane 4. Lane 1 and 3: chicken erythrocyte histone marker.

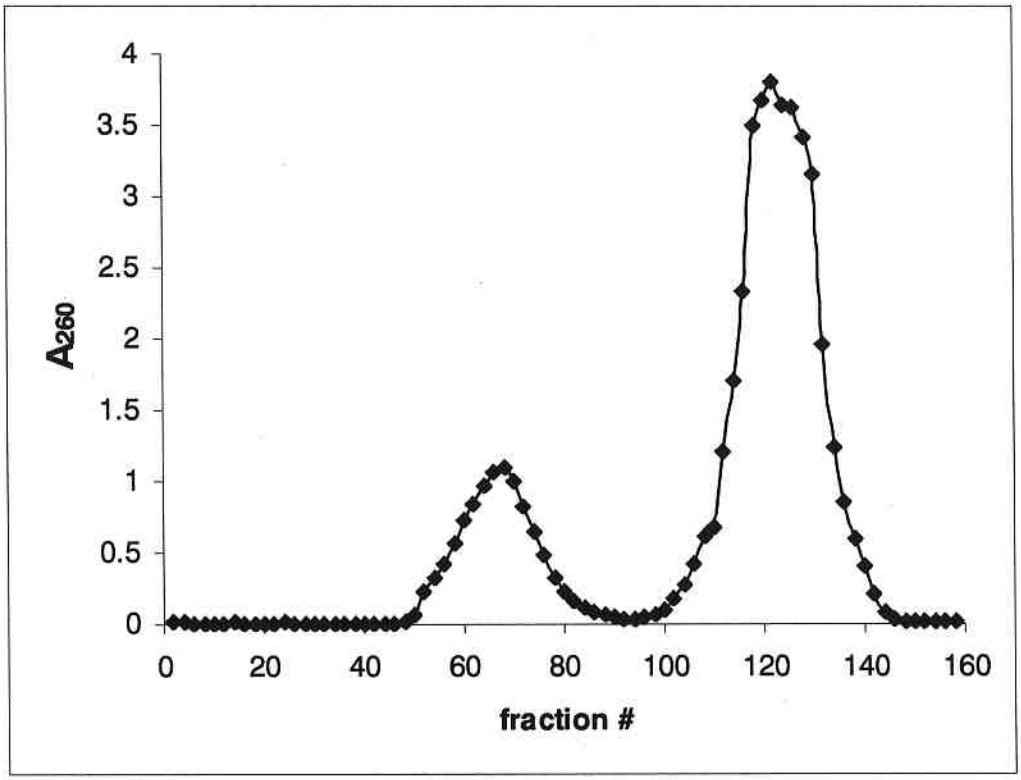

Figure 21. Sephacryl column chromatography of the p5S208-12 *Lytechinus* 5S rDNA plasmid extracted from Nova Blue *E. coli* cells. DNA was loaded onto a Sephacryl column (2.5 cm x 60 cm) at a flow rate of 60 ml/h and eluted in TE in 2ml fractions. The elution profile was recorded at a wavelength of A_{260}.

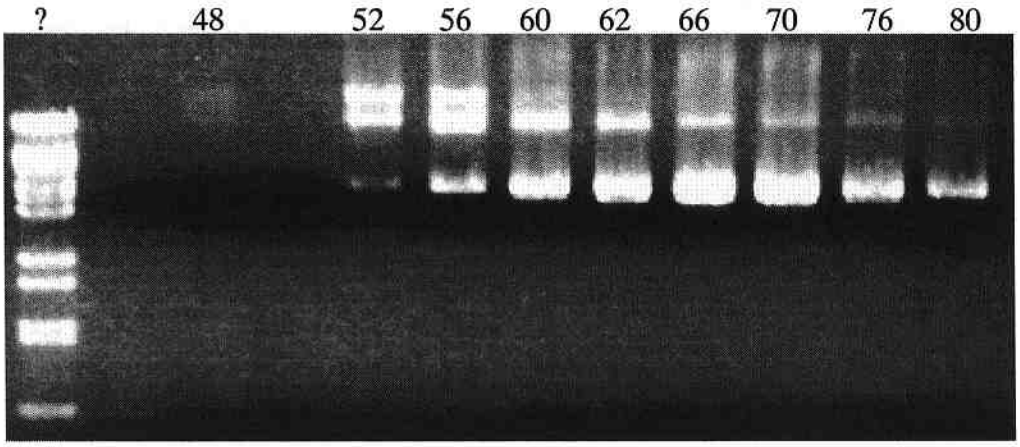

Figure 22. Electrophoretic analysis of p5S208-12 *Lytechinus* 5S rDNA plasmid Sephacryl column fractionation. Aliquots were electrophoresed on a 1.0% agarose/ 25 mM tris-acetate 0.5 mM EDTA (pH 8) gel. The gel was stained in ethidium bromide (0.25 μg/ml) for 10 min and destained in water for 20 min then visualized under UV light. Lane numbers correspond to elution fraction numbers from Figure 21. ? marker is lambda DNA-*Bst*E II digest (NEB) with sizes from the bottom to top: 702 bp, 1264 bp, 1371 bp, 1929 bp, 2323 bp, 3675 bp, 4324 bp, 4882 bp, 5686 bp, 6369 bp, 7284 bp, 8454 bp.

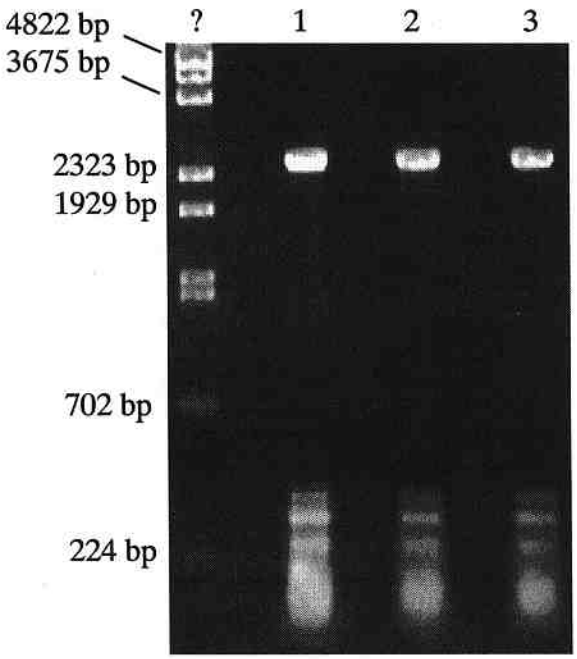

Figure 23. *Hha*I p5S208-12 *Lytechinus* 5S rDNA plasmid digestion product. Product was electrophoresed on a 1.0% agarose/ 25 mM tris-acetate 0.5 mM EDTA (pH 8) gel. The gel was stained in ethidium bromide (0.25 μg/ml) for 10 min and destained in water for 20 min then visualized under UV light. Lanes 1-3 are all p5S208-12 *Lytechinus* 5S rDNA plasmid *Hha*I digestion product. ? marker is lambda DNA-*Bst*E II digest (NEB).

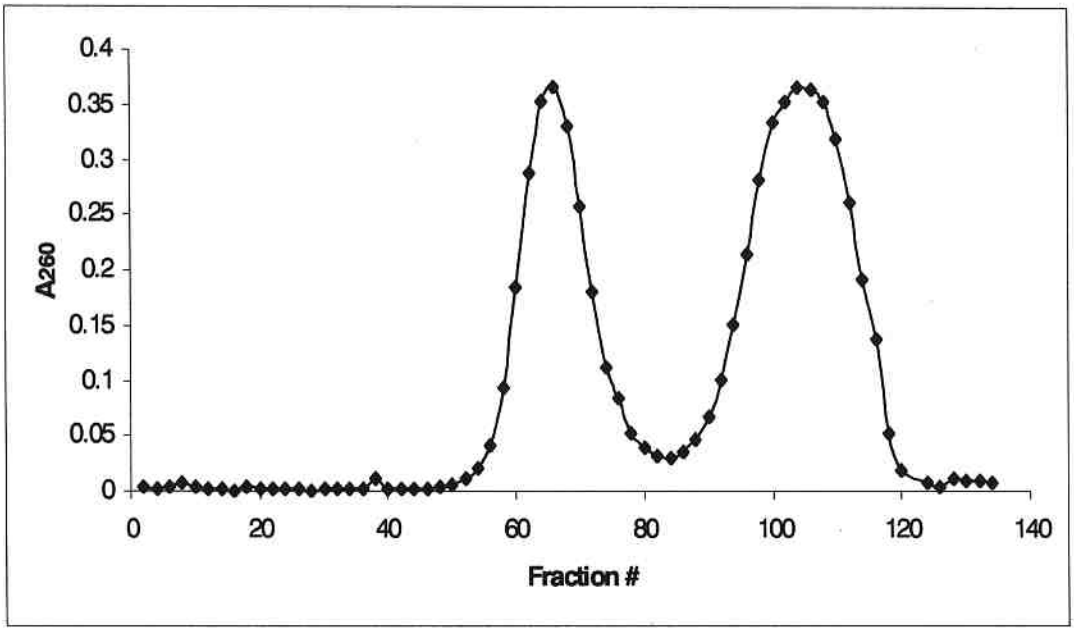

Figure 24. Sephacryl column chromatography of the p5S208-12 *Lytechinus* 5S rDNA plasmid *Hha*I digestion. DNA was loaded onto a Sephacryl column (2.5 cm x 60 cm) at a flow rate of 60 ml/h and eluted in TE in 2 ml fractions. The elution profile was recorded at a wavelength of A_{260}.

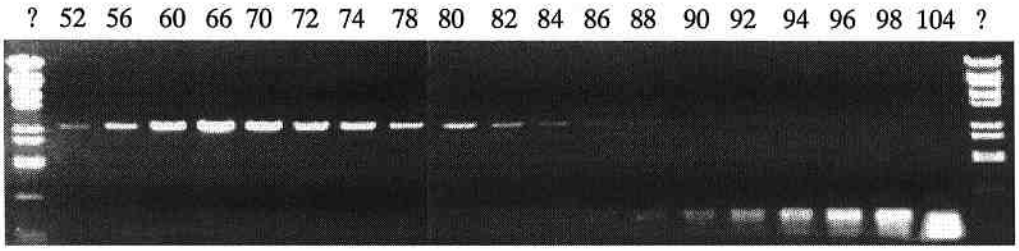

Figure 25. Electrophoretic analysis of the *Hha*I digested p5S208-12 *Lytechinus* 5S rDNA plasmid after Sephacryl column fractionation. Aliquots were electrophoresed on a 1.0% agarose/ 25 mM Tris-Acetate 0.5 mM EDTA (pH 8) gel. The gel was stained in ethidium bromide (0.25 μg/ml) for 10 min and destained in water for 20 min then visualized under UV light. Lane numbers correspond to elution fraction numbers from Figure 24. ? marker is lambda DNA-*Bst*E II digest (NEB) with sizes from the bottom to top: 702 bp, 1264 bp, 1371 bp, 1929 bp, 2323 bp, 3675 bp, 4324 bp, 4882 bp, 5686 bp, 6369 bp, 7284 bp, 8454 bp.

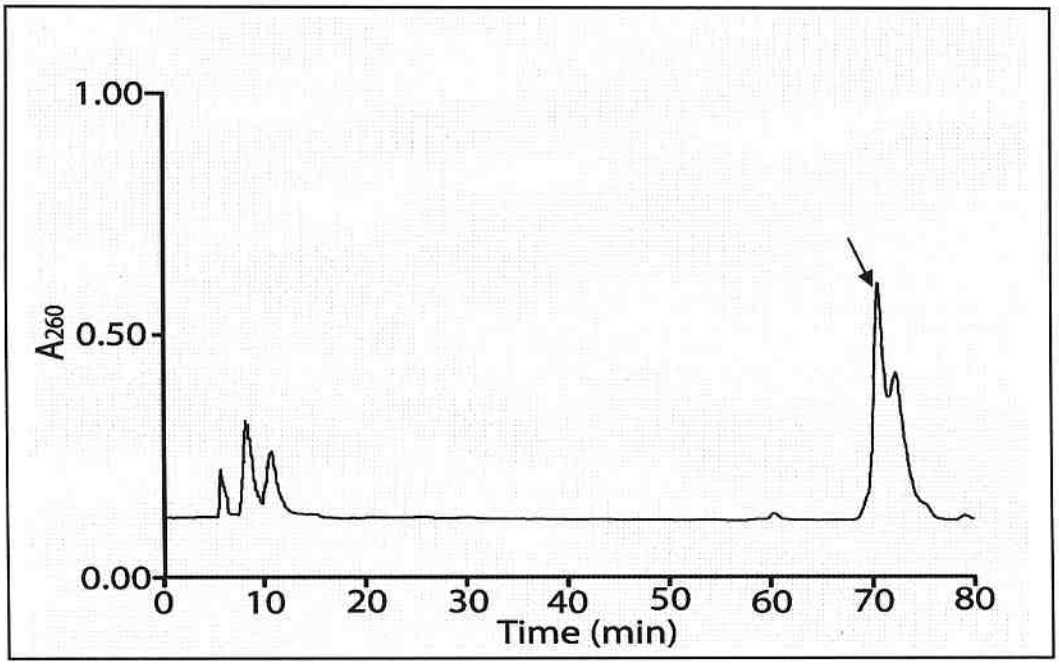

Figure 26. Ion exchange HPLC of *Rsa*I digested 208(12)-*Lytechinus* 5S rDNA. DNA was loaded onto a Bio-Gel DEAE-5-PW HPLC column (75 x 7.5 mm) and eluted at a flow rate of 1 ml/min (Buffer A: 0.1 M Tris (pH 7.5), Buffer B: 0.1 M Tris (pH 7.5); 1 M NaCl, % B gradient: 0-0% 5 min, 0-31% 15 min, 31-50% 60 min, 50-80% 10 min, 80-80% 5 min, 80-5% 5 min). The elution profile was recorded at a wavelength of A_{260}.

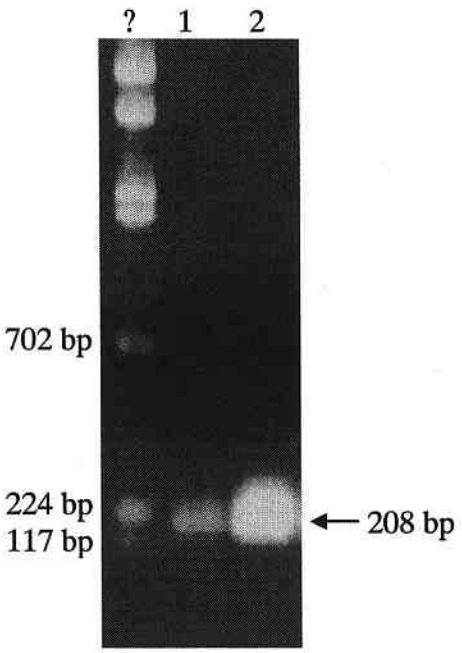

Figure 27. 208 bp *Lytechinus 5S rDNA* ionic exchange HPLC isolate. Aliquots were electrophoresed on a 1.0% agarose/ 25 mM Tris-Acetate 0.5 mM EDTA (pH 8) gel. The gel was stained in ethidium bromide (0.25 μg/ml) for 10 min and destained in water for 20 min then visualized under UV light. Lanes 1)-2) are 208 *Lytechinus 5S rDNA* aliquots from the same HPLC fraction denoted by an arrow in Figure 26. ? marker is lambda DNA-*Bst*E II digest (NEB).

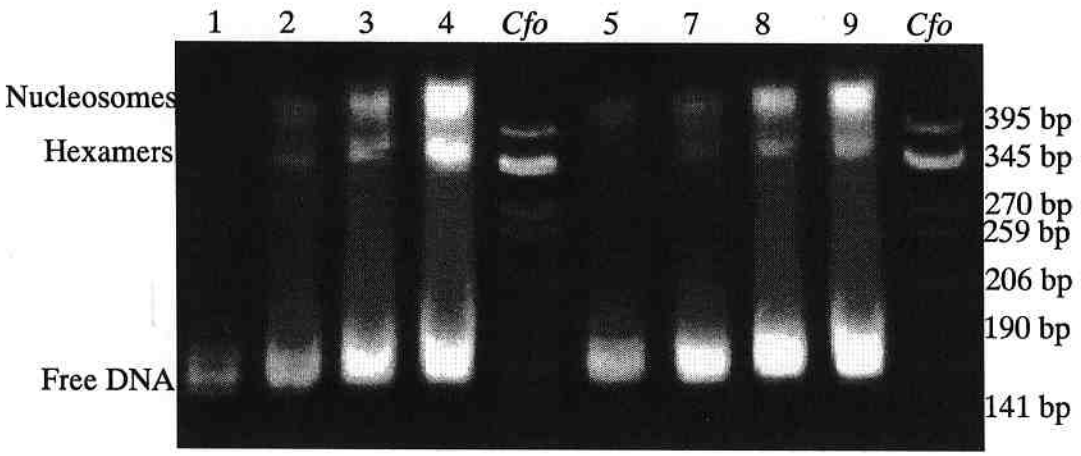

Figure 28. Electrophoretic analysis of 146 bp genomic chicken DNA nucleosome reconstitutions. Histone octamers were assembled onto the DNA template by step-wise salt dialysis (0 M – 2 M NaCl; 10 mM Tris (pH 7.5); 0.1 mM EDTA). The histone:DNA ratio was 1.12. Nucleosomes were electrophoresed on a 4% Native-PAGE gel at 80 V for 45 min in 1 x E Buffer (6X: 1 M Tris-HCl (pH 7.2); 0.5 M EDTA (pH 8.0); 0.12 M sodium acetate trihydrate. The acrylamide:bisacrylamide ratio was 20:1 and the 3 x sample buffer was 30% sucrose. Staining was in ethidium bromide (0.25 μg/ml) for 10 min and destaining was in water for 20 min before visualization under UV light. Lanes 1)-4) are NonAc H4-contaning nucleosomes; lanes 5)-9) are H4 K16Ac-containing nucleosomes. *Cfo*: *Cfo*I pBr322 digest DNA marker.

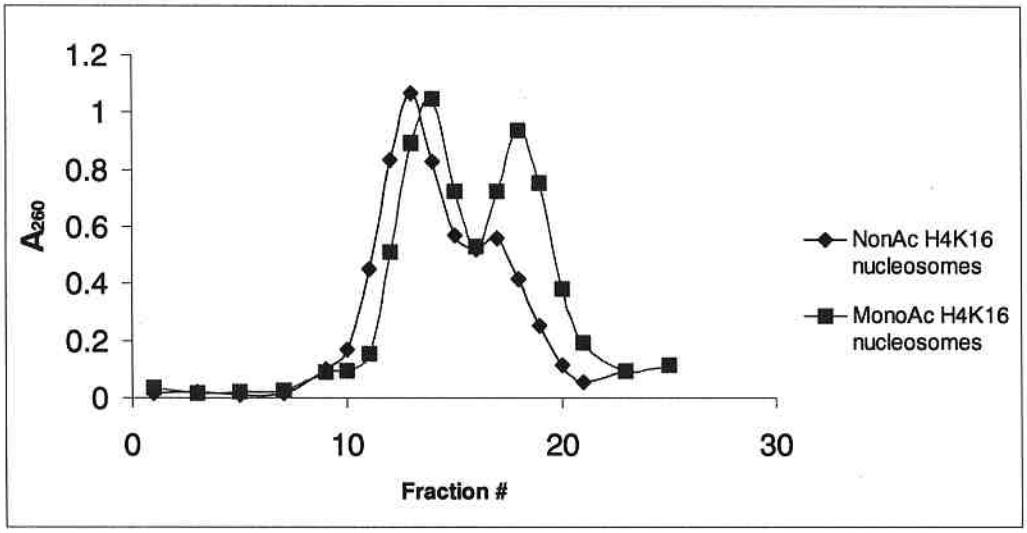

Figure 29. Sucrose gradient fractionation profile of reconstituted 146 bp nucleosomes. The 146 bp nucleosomes were loaded onto a 5-20% sucrose gradient in 50 mM NaCl; 10 mM Tris-HCl (pH 7.5); 0.1 mM EDTA and centrifuged at 134 000 g for 19.6 h in a Beckman SW41 rotor at 4°C. Sucrose gradient fractions were collected at 0.5 ml/min. The fractionation profile was recorded at a wavelength of A_{260}.

Figure 30. Electrophoretic analysis of 146 bp nucleosome sucrose gradient fractions. Aliquots were electrophoresed on a 4% native-PAGE gel at 80 V for 45 min in 1 x E Buffer (6X: 1 M Tris-HCl (pH 7.2); 0.5 M EDTA (pH 8.0); 0.12 M sodium acetate trihydrate. The acrylamide:bisacrylamide ratio was 20:1 and the 3 x sample buffer was 30% sucrose. Staining was in ethidium bromide (0.25 μg/ml) for 10 min and destaining was in water for 20 min before visualization under UV light. Lane numbers correspond to fraction numbers in Figure 29. White arrows denote fractions pooled for use in AUC analysis. *Cfo*: *Cfo*I pBr322 digest DNA marker.

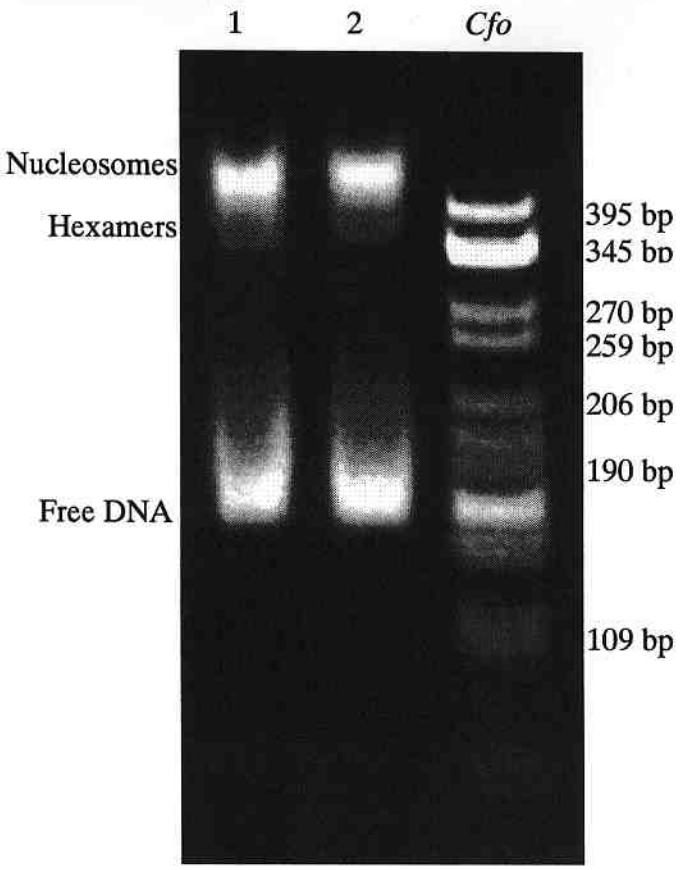

Figure 31. Electrophoretic analysis of pooled 146 bp nucleosome sucrose gradient fractions. Aliquots were electrophoresed on a 4% native-PAGE gel at 80 V for 45 min in 1 x E Buffer (6X: 1 M Tris-HCl (pH 7.2); 0.5 M EDTA (pH 8.0); 0.12 M sodium acetate trihydrate. The acrylamide:bisacrylamide ratio was 20:1 and the 3 x sample buffer was 30% sucrose. Staining was in ethidium bromide (0.25 μg/ml) for 10 min and destaining was in water for 20 min before visualization under UV light. Lane 1) pooled H4 K16Ac nucleosomes; lane 2) pooled H4 NonAc nucleosomes. *Cfo*: *Cfo*I pBr322 digest DNA marker.

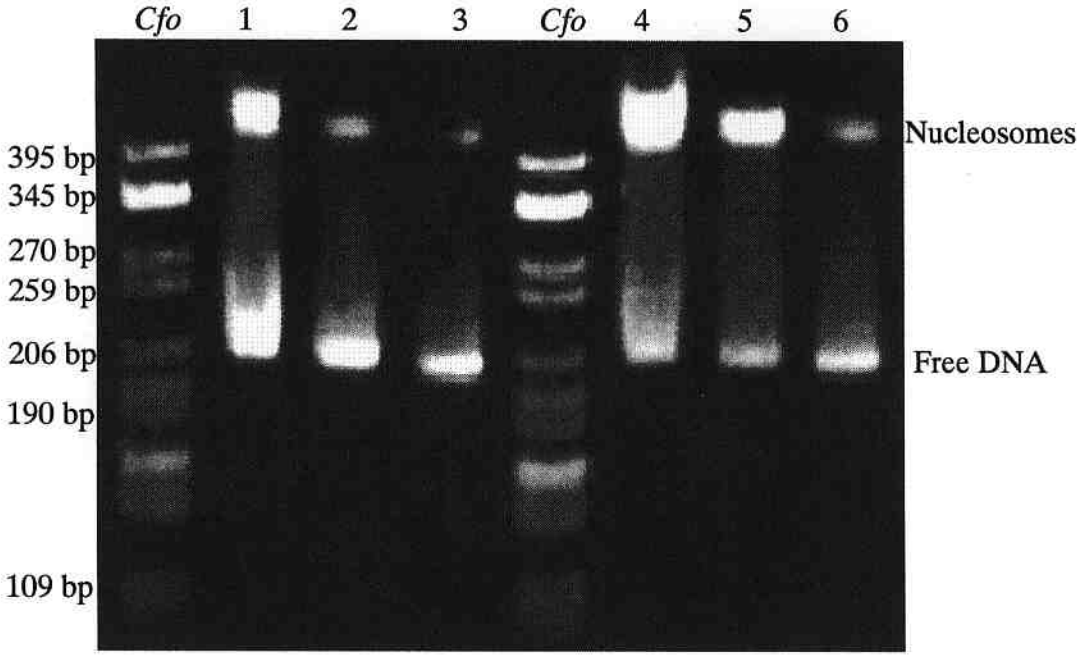

Figure 32. Electrophoretic analysis of 208 bp *Lytechinus* 5S rDNA nucleosome reconstitutions. Histone octamers were assembled onto the DNA template by step-wise salt dialysis (0 M – 2 M NaCl; 10 mM Tris (pH 7.5); 0.1 mM EDTA). The histone:DNA ratio was 0.78. Nucleosomes were electrophoresed on a 4% Native-PAGE gel at 80 V for 45 min in 1 x E Buffer (6X: 1 M Tris-HCl (pH 7.2); 0.5 M EDTA (pH 8.0); 0.12 M sodium acetate trihydrate. The acrylamide:bisacrylamide ratio was 20:1 and the 3 x sample buffer was 30% sucrose. Staining was in ethidium bromide (0.25 μg/ml) for 10 min and destaining was in water for 20 min before visualization under UV light. Lanes 1)-3) are H4 K16Ac-containing nucleosomes; lanes 4)-6) are NonAc H4-contaning nucleosomes. *Cfo*: *Cfo*I pBr322 digest DNA marker.

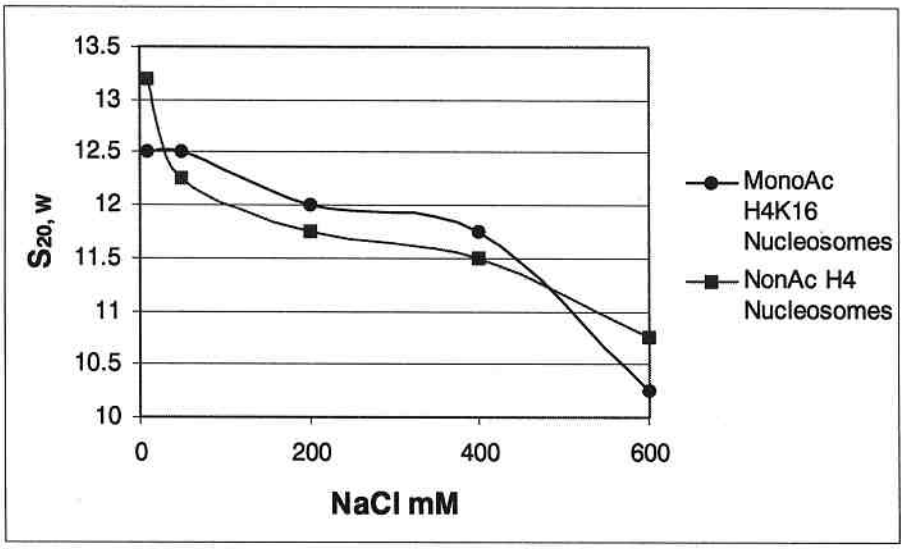

Figure 33. Dependence of the sedimentation coefficient ($S_{20,w}$) of 208 bp nucleosomes on NaCl concentration. The sedimentation velocity analysis was done using a Beckman XL-A ultracentrifuge and an An-55 aluminum rotor and double-sector cells with aluminum-filled Epon ceterpieces. The UV scans at A_{260} were analysed using the van Holde–Weischet method to determine the distribution of sedimentation coefficients for the population of nucleosomes within a sample.

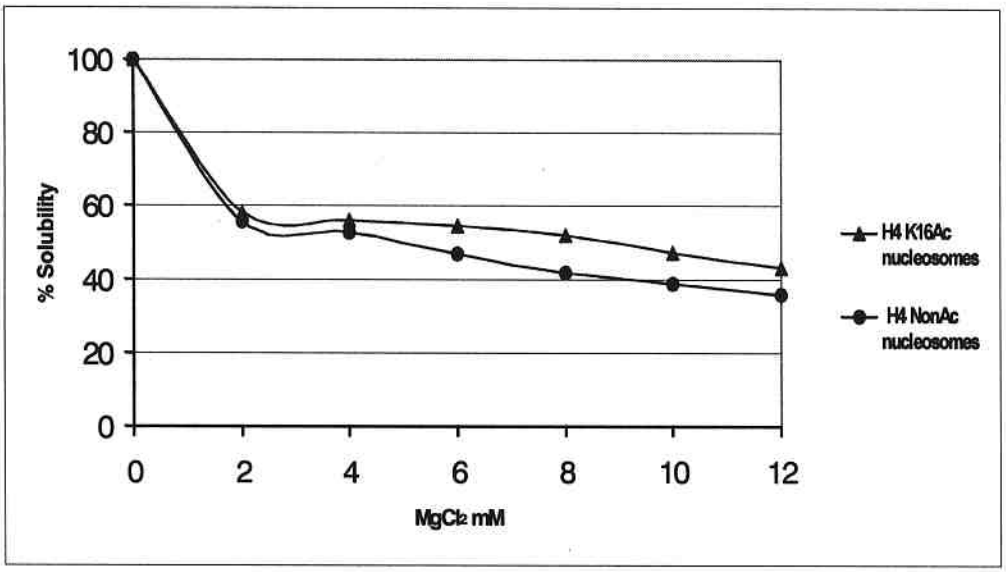

Figure 34. Nucleosome solubility in magnesium chloride. H4 K16Ac nucleosomes and H4 NonAc nucleosomes were brought to 0.02 μg/μl (DNA) in 20 mM Tris (pH 7.5) and the indicated concentrations of $MgCl_2$. Nucleosomes were incubated for 55 min at 4°C and centrifuged at 10 000 x g for 10 min at 4°C. Supernatant A_{260} values were used for the % solubility calculation.

Table 1. Site specific % acetylation of mono-acetylated H4 from tandem mass spectrometry analysis. The N-terminus and lysines on histone H4 were propionylated before digestion with trypsin. The peptides were then loaded on a RP C-18 column and were gradient eluted into the mass spectrometer.

Lysine	**% Acetylation**
K5	11
K8	4
K12	10
K16	75

Table 2. Dependence of the sedimentation coefficient ($S_{20,w}$) of 146 bp nucleosomes on NaCl concentration. The sedimentation velocity analysis was done using a Beckman XL-A ultracentrifuge and an An-55 aluminum rotor and double-sector cells with aluminum-filled Epon ceterpieces. The UV scans at A_{260} were analysed using the van Holde–Weischet method to determine the distribution of sedimentation coefficients for the population of nucleosomes within a sample.

Nucleosome type / [NaCl mM]	**Sedimentation Coefficient, $S_{20,w}$**
H4 NonAc 146 bp / 100 mM	13.2
H4 K16Ac 146 bp / 100 mM	14.0
H4 NonAc 146 bp / 600 mM	11.0
H4 K16Ac 146 bp / 600 mM	10.4

3.3 The isolation of mono-phosphorylated H5

3.3.1 Preparation of native octamers

The native histone octamers extracted from chicken erythrocytes shown in Figure 35 are free of linker histones and do not contain any degradation products.

3.3.2 Preparation of native H5

Reversed phase HPLC chromatography of 5% PCA extracted linker histones from chicken erythrocytes allowed the partial fractionation of histone H1 from H5 (Figure 36). Figure 37 shows the electrophoretic analysis of the overlapping H1 and H5 elution. H5 fractions 9 and 10, however, were pure enough for use in ion exchange HPLC separation of differentially phosphorylated species.

3.3.3 Isolation of differentially phosphorylated H5

Figure 38 shows the H5 ion exchange HPLC histone elution profile. From the last two peaks denoted by arrows in Figure 38, two species (non-phosphorylated H5 and mono-phosphorylated H5) appear to have been separated. They are visualized in lane 1, and lane 2 of Figure 39. Lane 2 protein was chosen for MALDI-TOF analysis.

3.3.4 Mass spectrometry of H5

The MALDI-TOF spectrum (Figure 40) characterized one 20680.36 Da protein (protein A) and two secondary species (20458.36 Da and 20389.81 Da). The mass of *gallus* spp. H5 is 20602.50 Da and the calculated mass of H5 with the addition of a phosphate group, HPO_3 (80 atomic mass units) is 20682.50 Da. Thus protein A is likely

monophosphorylated *gallus* spp. H5 protein despite a -2.14 Da discrepancy between the calculated mass of the H5-P the experimental mass of protein A.

3.3.5 Isolation and preparation of the 208-12 Lytechinus 5S rDNA

The isolation and preparation of the 208-12 *Lytechinus* 5S rDNA resulted in similar column profiles, identical digestion products and 208-12 *Lytechinus* 5S rDNA insert purity as described in section 3.2.6 (data not shown).

3.3.6 Analytical ultracentrifuge characterization

The sedimentation velocity analysis of the 208-12 chromatin fibers (Figure 41) indicates that at lower salt concentrations (10 mM NaCl-50mM NaCl) the H5 containing fibers sediment more quickly than the –H5 fibers. These values are similar to published S values for fibers similar in compositions to those described here (Ausio 2000). At 100 mM NaCl, however, the inverse is observed: the H5 fibers sediment more slowly than the –H5 fibers which is not consistent with published values (Ausio 2000).

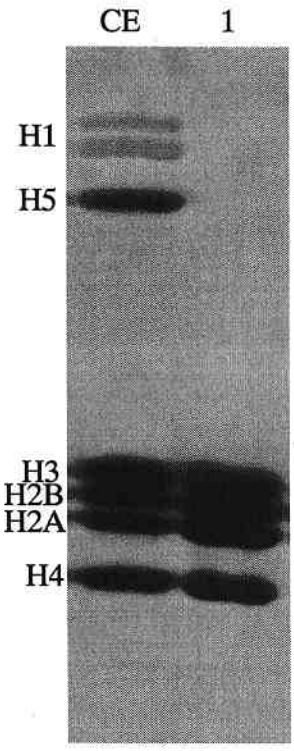

Figure 35. Electrophoretic analysis of native octamers extracted from chicken erythrocytes. Octamers were analysed by SDS PAGE (6% stacking, 15% separating) at 100 V for 1.3 h in 1X SDS Running buffer (0.05 M Tris; 0.4 M Glycine; 0.004 M sodium dodecyl sulphate). The acrylamide:bisacrylamide ratio was 30:0.8. The 2 x sample buffer was 0.125 M Tris (pH 6.8); 4% SDS; 20% glycerol; 1.43 M ß-mercaptoethanol and 0.1% bromophenol blue. Staining was with Coomassie blue (0.25% Coomassie Brilliant Blue, 25% isopropanol, 10% acetic acid) for ½ h after which the gel was destained for 1 h (10% isopropanol; 10% acetic acid). Lane 1) native chicken histone octamers extracted from chicken erythrocytes; CE: chicken erythrocyte histone marker.

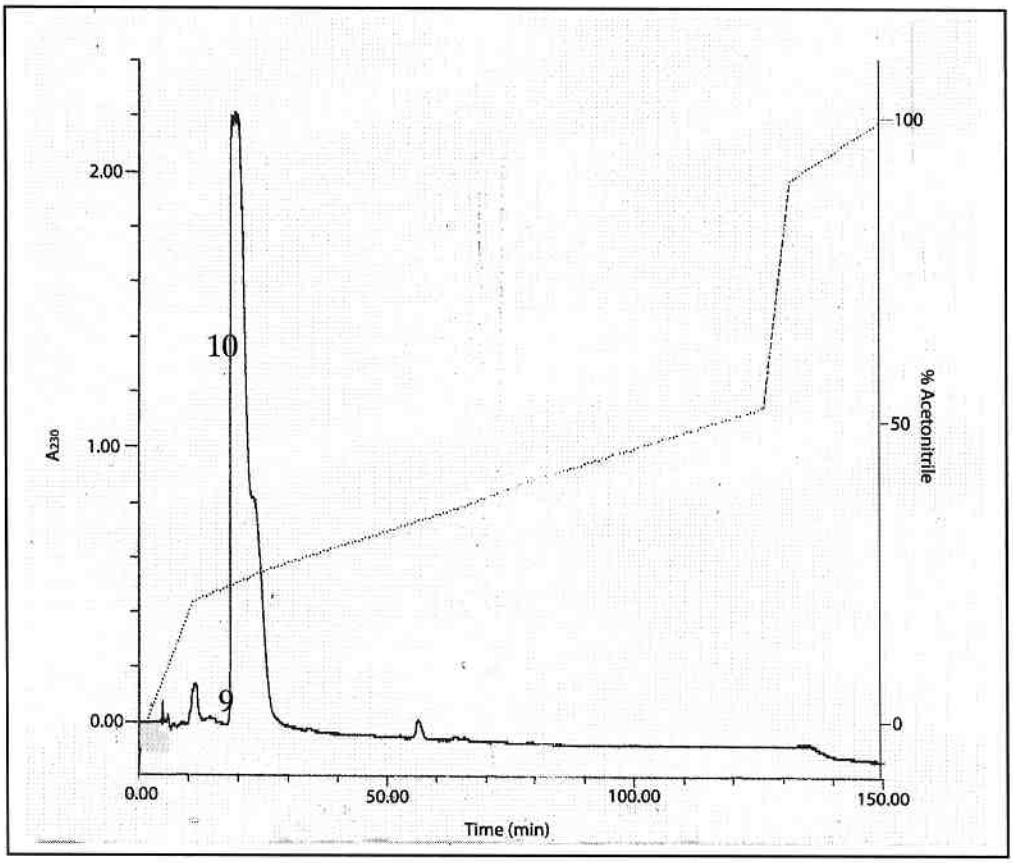

Figure 36. Reversed phase HPLC fractionation of 5% PCA extracted linker histones. Linker histones were dissolved in sdH_2O to final concentration of 1.5 mg/ml, loaded onto the 5μm Vydac C_4 column (10 mm x 250 mm) and eluted at a flow rate of 1 ml/min (Buffer A: 0.1% TFA; Buffer B: 100% ACN; %B gradient: 0-5% 1 min, 5-25% 10 min, 25-30% 15 min, 30-35% 20 min, 35-40% 20 min, 40-45% 10 min, 45-55% 50 min, 55-90% 5 min, 90-100% 20 min, 100-100% 5 min, 100-0% 10 min). The elution profile was recorded at a wavelength of A_{230}. (—): % Acetonitrile, (.....): Elution profile.

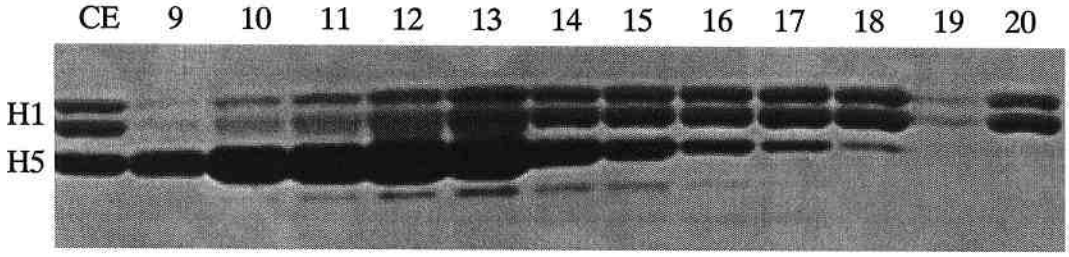

Figure 37. Electrophoretic analysis of linker histone by reversed phase HPLC. Histones were analysed by SDS PAGE (6% stacking, 15% separating) at 100 V for 1.3 h in 1X SDS Running buffer (0.05 M Tris; 0.4 M Glycine; 0.004 M Sodium dodecyl sulphate). The acrylamide:bisacrylamide ratio was 30:0.8. The 2 x sample buffer was 0.125 M Tris (pH 6.8); 4% SDS; 20% glycerol; 1.43 M ß-mercaptoethanol and 0.1% bromophenol blue. Staining was with Coomassie blue (0.25% Coomassie Brilliant Blue, 25% isopropanol, 10% acetic acid) for ½ h after which the gel was destained for 1 h (10% isopropanol; 10% acetic acid). Lane numbers represent Figure 36 peak fractions from left to right. Lane numbers of interest (9 – 10) are indicated on the chromatogram in Figure 36. CE: chicken erythrocyte histone marker.

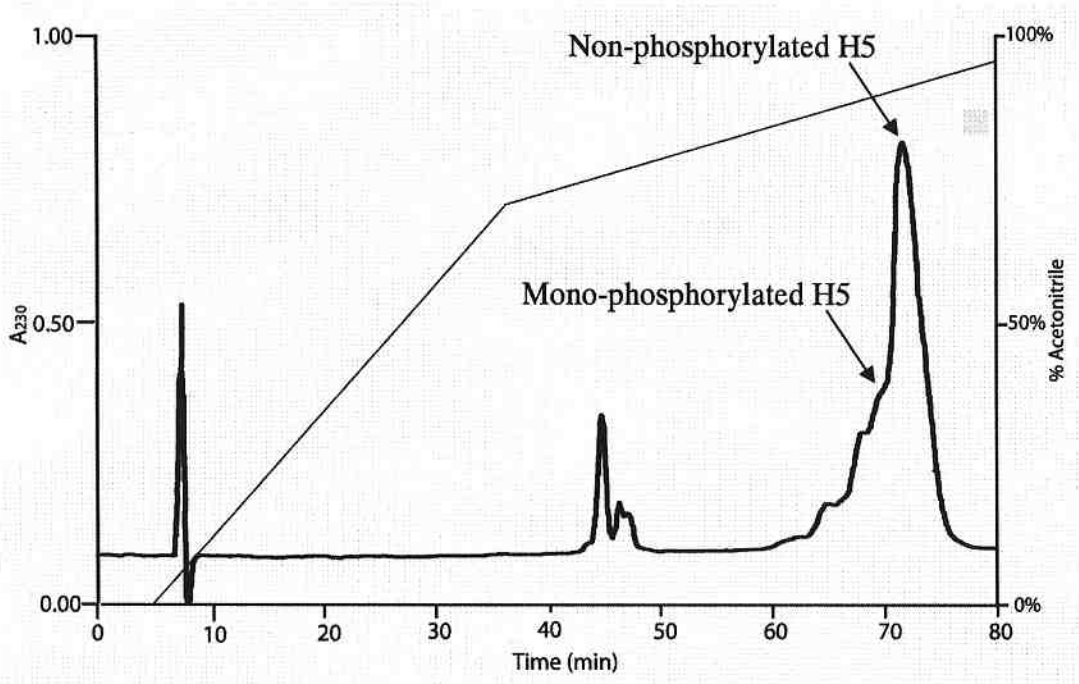

Figure 38. Ion exchange HPLC fractionation of lyophilized histone H5. H5 was dissolved in sdH_2O and loaded onto the 6 μm SynChrom Synchropak CM300 column at a flow rate of 1 ml/min (Buffer A: 6 M UREA; 20 mM NaPO4 (pH 5.8), Buffer B: 6 M urea; 20 mM NaPO4 (pH 5.8); 600 mM NaCl; %B gradient: 0-0% 5 min, 0-70% 30 min, 70-100% 60 min, 100-100% 5 min, 100-0% 5 min). The elution profile was recorded at a wavelength of A_{230}. (——): % Acetonitrile, (▬): Elution profile.

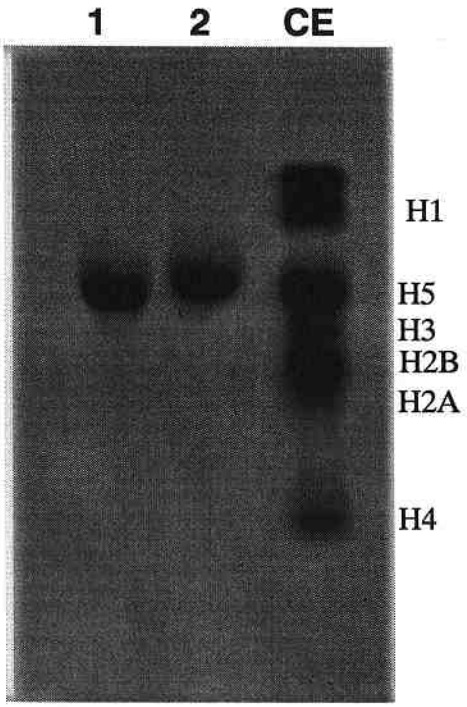

Figure 39. Electrophoretic analysis of ion H5 fractions by exchange HPLC. Fractions were analysed by acid-urea PAGE (2.5 M urea; 15% acrylamide; 5% acetic acid) at 100 V for 4 h in 5% acetic acid. The acrylamide:bisacrylamide ratio was 20:1. The 2 x sample buffer was 8M urea, 10% acetic acid, and 0.3% Pyronine Dye Y. Staining was with Coomassie blue (0.25% Coomassie Brilliant Blue, 25% isopropanol, 10% acetic acid) for ½ h after which the gel was destained for 1 h (10% isopropanol; 10% acetic acid). Lane 1) non-phosphorylated H5 fraction denoted by an arrow in Figure 38; lane 2) mono-phosphorylated H5 fraction denoted by an arrow in Figure 38. CE: Chicken erythrocyte histone marker.

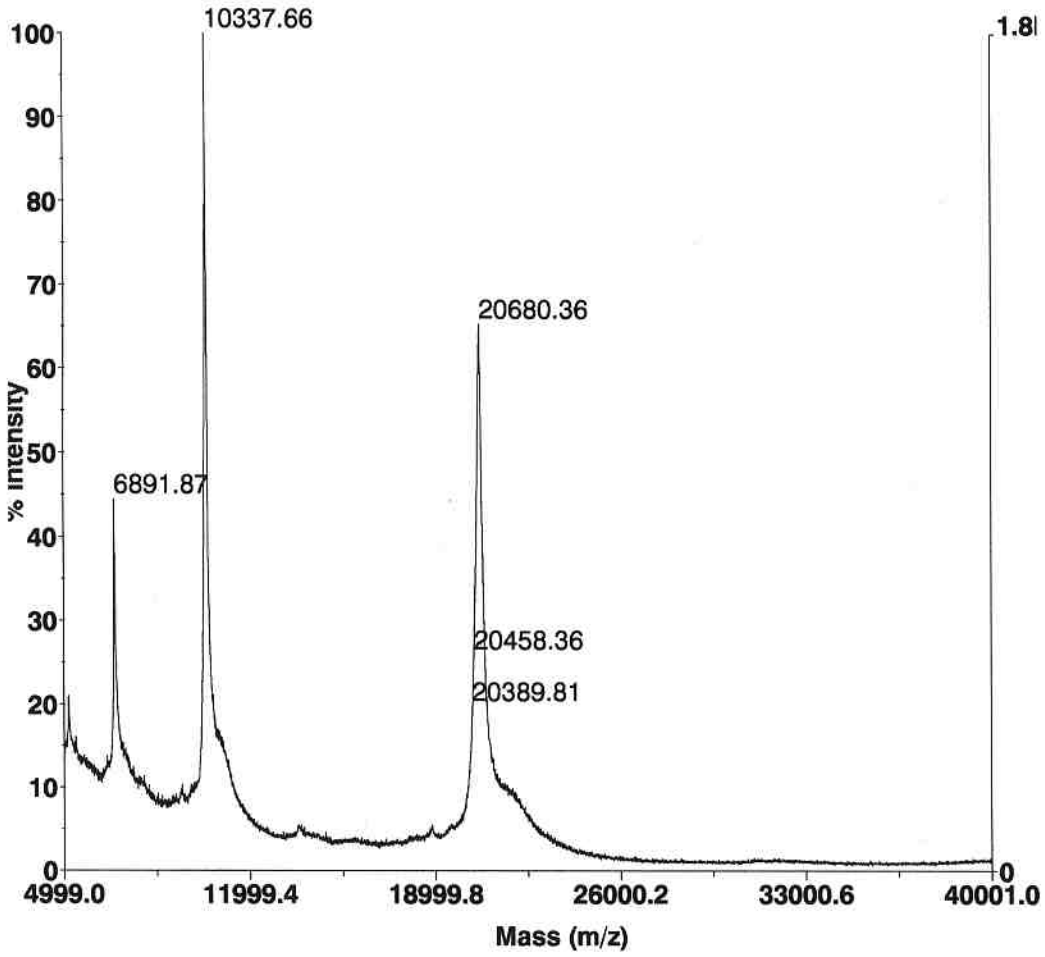

Figure 40. Matrix assisted laser desorption ionisation – time of flight (MALDI-TOF) mass spectrometry profile for monophosphorylated H5. Peptide sample in sdH_2O was dissolved 1:1 with 0.1% trifluoroacetic acid; 50% acetonitrile; 10μg/ml 3,5-dimethoxy-4-hydroxycinnamic acid (sinapinic acid). Peptide mixture (1 μl) was analysed using a Voyager-DE™ STR BioSpectrometry Workstation (Perspective Biosystems).

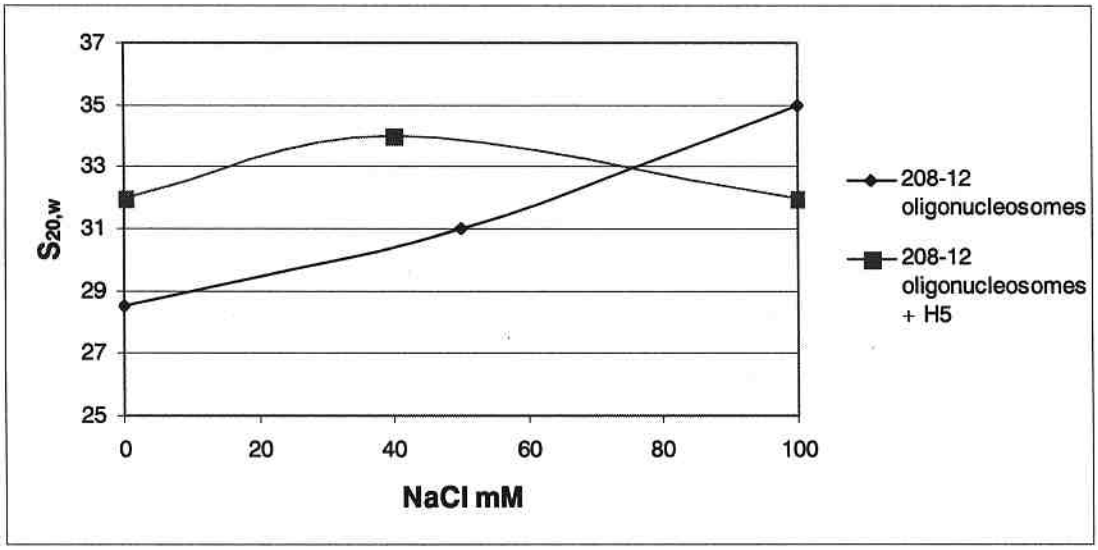

Figure 41. Dependence of the sedimentation coefficient ($S_{20,w}$) of 208-12 oligonucleosomes on NaCl concentration. The sedimentation velocity analysis was done using a Beckman XL-A ultracentrifuge and an An-55 aluminum rotor and double-sector cells with aluminum-filled Epon ceterpieces. The UV scans at A_{260} were analysed using the van Holde–Weischet method to determine the distribution of sedimentation coefficients for the population of oligonucleosomes within a sample.

4.0 DISCUSSION

4.1 The Pbsn-208(10) DNA template

Homogenous chromatin fibers with constant linker lengths are an essential component for the study of salt-dependent chromatin compaction *in vitro* (Lowary and Widom 1998; Simpson et al. 1985). Suitable DNA templates used currently consist of DNA fragments containing tandem repeats of either the *Lytechinus variegates* 5S rRNA nucleosome positioning sequence or the Widom 601 DNA nucleosome positioning sequence (Huynh et al. 2005; Shogren-Knaak et al. 2006). These templates do not permit, however, for the differentiation of one region of the reconstituted nucleosomal array from another. To this end, I have created a template containing the probasin promoter nucleosome positioning sequence from *Rattus norvegicus* flanked on both sides by tandem repeats of the nucleosome positioning 5S rRNA gene from *Lytechinus variegatus*.

One of the major challenges in the design of this DNA template involved the need to maintain relatively constant linker length between nucleosome positioning sequences. To fulfill this requirement, identical restriction enzyme sites (*Xho*I) had to flank both sides of the probasin promoter nucleosome positioning fragment (Appendix 1). This created the possibility of tandem ligation, and/or of ligation in the wrong orientation. Restriction enzyme analysis (Figure 7) and sequence data (Figure 8) indicate, however, that a template containing only one probasin promoter insert in the right orientation was created successfully. AUC analysis of the template reconstituted with native histones extracted from chicken erythrocytes show that its sedimentation coefficient (34 S) is consistent with the expected value for a chromatin fiber of that length with a high histone:DNA ratio (Ausio 2000).

The Pbsn-208(10) template is a valuable addition to the chromatin field. It provides the basis for the investigation of chromatin compaction *in vitro* using the simple approach of restriction endonuclease analysis. The central probasin promoter sequence is useful not only because it forms a strongly positioned nucleosome (Maffey et al., *In Press*), but also because it contains restriction enzyme sites that are distinct from those in the five *Lytechinus variegatus* flanking repeats to its left and right sides. Thus, the effects of PTMs on histone-DNA interactions and nucleosome conformation in the center of a chromatin fiber can now be easily investigated. In addition, the Pbsn-208(10) template can help to identify the precise location of H1/H5 within the nucleosome. Future studies using this template should include restriction endonuclease cleavage site protection assays, DNA footprinting analysis, and AUC analysis of post-translationally modified mononucleosomes isolated by restriction endonuclease digestion from the middle of the Pbsn-208(10) fiber.

4.2 H4 K16Ac and the structure of chromatin: an intra-nucleosomal affair

H4 K16 acetylation is involved in the regulation of chromatin decondensation at the structural level (Shogren-Knaak et al. 2006), and is believed to play a universal role in the maintenance of transcriptionally active domains (Calestagne-Morelli and Ausio 2006; Dion et al. 2005; Shia et al. 2006; Wang et al. 2000). The two alternate hypotheses proposed by Mutskov et al. (1998) and Shogren-Knaak and Peterson (2006) regarding the mechanism by which H4 K16 acetylation affects chromatin compaction were examined in this work using analytical ultracentrifuge analysis (AUC) and $MgCl_2$ solubility assays.

Reverse-phase and ionic-exchange HPLC purified chicken erythrocyte histones were used in the reconstitution of 146 bp and 208 bp mononucleosomes. Chicken erythrocytes proved to be a rich source of H4 K16Ac (Table 1). However, more than half of the reconstituted 146 bp mononucleosome product was not of use for subsequent AUC analysis due to a high concentration of hexameric nucleosomes (Figure 30). Possible explanations for incomplete nucleosome formation may include an insufficient GnHCl denaturing incubation period or an inadequate histone:DNA ratio.

The AUC analyses of the sucrose gradient purified 146 bp mononucleosomes indicate that the H4 K16 monoacetylated nucleosomes exhibit a more pronounced conformational change towards asymmetry with increasing ionic concentration than the nonacetylated mononucleosomes (Table 2). This suggests that H4 K16 acetylation produces a more structurally relaxed nucleosome core particle. To confirm the accuracy of this conclusion, the 146 bp mononucleosome reconstitutions and AUC analyses should be repeated. For additional confirmation, AUC analyses of the 146 bp nucleosomes at more salt concentrations should be performed.

Unlike for the 146 bp nucleosome reconstitution, the 208 bp mononucleosomes were not contaminated with hexameric nucleosomes (Figure 32). AUC results demonstrate that the H4 K16Ac 208 bp nucleosomes are less compact at both high (600 mM NaCl) and very low (10 mM NaCl) ionic concentrations compared to controls (Figure 33). Notably, the 208 bp nucleosome salt-dependent conformational changes are consistent with those observed for the 146 bp particles, which further supports the prediction that H4 K16 acetylation destabilizes the nucleosome and results in

decompaction. Once again, to confirm the significance of these results the 208 bp mononucleosome reconstitutions and AUC analyses should be repeated.

Finally, in order to further investigate the effect of H4 K16 acetylation on the structure of the nucleosome, we examined the percent solubility of H4 K16Ac compared to H4 K16NonAc 208 bp mononucleosomes in $MgCl_2$. Chromatin solubility in the presence of multivalent cations (eg. Mg^{2+}) is directly linked to the amount of linker DNA bound to the nucleosome (Ausio et al. 1986). Free DNA requires more Mg^{2+} to precipitate than DNA bound to the nucleosome (Ausio et al. 1986). In this work, H4 K16Ac 208 bp mononucleosomes were more soluble in $MgCl_2$ than H4 K16 NonAc mononucleosomes (Figure 34), which indicates that they contain more free-DNA than nucleosome bound DNA. Similar to the AUC data described previously, these results support the model whereby H4 K16 acetylation produces a less compact nucleosome particle.

Taken together, the AUC and $MgCl_2$ data presented here are consistent with the hypothesis that H4 K16 acetylation weakens intra-nucleosomal DNA-histone electrostatic interactions and structurally relaxes the dynamic association of nucleosomal DNA with the histone octamer. The weakening of DNA-histone intra-nucleosome contacts would by default also prevent compaction at the inter-nucleosomal level, which is consistent with the data presented by Shogren-Knaak et al. (2006). The salt-dependent conformational changes of the nucleosome detected in this work are not consistent with the model of chromatin decondensation proposed by Shogren-Knaak and Peterson's (2006). Thus, while H4 K16 acetylation plays a critical role in maintaining an open chromatin fiber structure, it is unlikely that the PTM exerts its modulatory effect by disrupting the histone tail's interaction with an H2A/H2B acidic patch in an adjacent nucleosome.

What is clear from this work and from the study by Wang et al. (2000) is that the following questions remain unresolved: How might the H4 K16 acetylation-induced formation of a-helices in the H4 N-terminal tail influence or alter histone tail-DNA interactions? In particular, how might this structural transition from disorder to order relax intra-nucleosomal compaction without releasing the DNA ends flanking the nucleosome (Mutskov et al. 1998; Wang et al. 2000)? The answer to these questions would help to complete our understanding of H4 K16Ac mediated chromatin decondensation.

H4 K16 acetylation is the first of all of the possible histone post-translational modifications to be directly linked to changes in chromatin conformation (Shogren-Knaak et al. 2006). It is also the only PTM to be classified as a switch regulating the transition from repressive to active chromatin (Shogren-Knaak and Peterson 2006). Given the common relationship between structure and function, attention should be drawn to the study of the functional implications of H4 K16 acetylation. In particular, it is important to examine what functional roles H4 K16 acetylation-induced structural changes in nucleosomal and chromatin structure may have in gene expression. For instance, although charge neutralization does not release histone tails completely from DNA (Mutskov et al. 1998), H4 K16 acetylation does weaken nucleosome stability and structurally relax the nucleosome particle which, in turn, could potentially improve activation kinetics (Brower-Toland et al. 2005; Dunker et al. 2001; Siino et al. 2003). In support of this, histone hyperacetylation increases the equilibrium accessibility of nucleosomal DNA target sites approximately 1.4 ± 0.1 fold *in vitro* (Anderson et al. 2001).

Besides an improvement in activation kinetics, an acetylation-induced ionic-dependent reduction in the affinity of NH_2 tails for nucleosomal DNA (Mutskov et al. 1998) may also decrease the amount of energy RNA polymerases need to transcribe through nucleosomal outer turn and off-dyad strong interactions (Brower-Toland et al. 2005; van Holde et al. 1992). Consistent with this, acetylation of H3 and H4 has been found to strongly increase RNA polymerase II's rate of elongation and to reduce transcriptional stuttering *in vitro* (Protacio et al. 2000).

Finally, it has been suggested that acetylation-induced changes in linking number are involved in the displacement of the H2A/H2B dimer from the nucleosome during elongation (Morales and Richard-Foy 2000). H4 K16Ac relaxation of the dynamic association of nucleosomal DNA with the histone octamer may facilitate the exchange of histone H2A-H2B dimers that is observed to occur during transcription (Baer and Rhodes 1983; Kireeva et al. 2002; van Holde et al. 1992). Adding to this model of nucleosome unfolding are the findings that chromatin remodeling complexes and chaperone proteins such as the heterodimer FACT (facilitates chromatin transcription) or the NAP-1 (nucleosome assembly protein 1) homodimer complex (Park and Luger 2006) function to displace H2A/H2B dimers during RNA polymerase II-driven elongation (Belotserkovskaya et al. 2003; Bruno et al. 2003; Jackson 1990; Levchenko et al. 2005).

4.3 The Isolation of Monophosphorylated Linker Histone H5

Similar to early studies on H4 K16 acetylation, evidence suggests that the phosphorylation of linker histones promotes chromatin decondensation and increases DNA accessibility (Dou et al. 1999). In an effort to initiate a study characterizing the structural effects of chromatin fibers containing phosphorylated linker histones, I have

optimized a method of purification for nonphosphorylated and monophosphorylated linker histone H5 from erythrocytes of anemic chickens. This method is valuable as it results in a high yield of pure post-translationally modified H5 product (Figure 38 and Figure 40), which is a critical component given the experimental requirements of *in vitro* chromatin investigations. Preliminary AUC data of oligonucleosomes containing the nonphosphorylated control linker histones (manipulated to the same degree as the experimental monophosphorylated linker histones) show a salt-dependent sedimentation trend that is consistent with expected values at low ionic concentrations (Figure 41)(Ausio 2000). Precipitation of the template was detected, however, at 100 mM NaCl (Figure 41). The latter suggests that an inadequate linker histone ratio was applied, a problem that would be easily resolved by either decreasing the linker histone:DNA ratio or introducing small (146 bp) fragments of competitor DNA.

Future DNA footprinting experiments using monophosphorylated histone H5 isolated in the manner described here would reveal whether linker histone phosphorylation influences the positioning of octamers within the nucleosome. In addition, the method established provides the foundation for future structural studies of di- modified fibers chromatin *in vitro*. The latter would help to clarify the structural implications of the core histone acetylation and linker histone phosphorylation overlap observed during cellular differentiation and DNA repair (Kysela et al. 2005; Sung et al. 1977; Tamburini and Tyler 2005).

4.4 Concluding remarks

Since 1964 it has been frequently postulated that histone acetylation induces chromatin decondensation. Until recently, however, experimental evidence for this hypothesis was lacking. H4 K16 acetylation is the first of all of the possible post-translational modifications to be directly linked to changes in chromatin conformation (Shogren-Knaak et al. 2006). Data from the work described here suggests that H4 K16Ac structurally relaxes the association of nucleosomal DNA with the histone octamer by weakening intra-nucleosomal DNA-histone electrostatic interaction. Confirming that this is indeed the mechanism by which H4 K16Ac affects chromatin structure will be a monumental step in the chromatin field.

Increasingly, barriers to the study of chromatin structure are being overcome. The creation of suitable DNA templates for *in vitro* experiments, and the more recent large-scale and genome-wide approaches to the study of chromatin modification are only a few of the tools that have contributed towards our knowledge of the structural parameters involved in gene expression. The development of the Pbsn-208(10) template and the purification method for monophosphorylated H5 described here will add to the existing chromatin experimental toolbox and help to answer questions that have fascinated researchers in the chromatin field for many years.

The structural effects of post-translational histone modifications deserve special consideration as they are likely to have implications for the functional component of chromatin regulation. H4 K16Ac modified histones, for instance, are generally found genome-wide (yeast) or across entire domains (mice, humans, chicken) and are likely involved in the maintenance of transcriptionally poised domains. Given the high number

of possible histone modifications, it is highly probable that others are also involved in regulating the structure of chromatin. Much research is needed to characterize the dynamic and possibly redundant structural roles of other histone tail modifications. Advances in this field are promising, however, and will certainly add to a better understanding of eukaryotic gene expression.

5.0 LITERATURE CITED

Akhtar, A. and P. B. Becker 2000. Activation of transcription through histone H4 acetylation by MOF, an acetyltransferase essential for dosage compensation in Drosophila. Mol Cell **5**: 367-375.

Alexandrow, M. G. and J. L. Hamlin 2005. Chromatin decondensation in S-phase involves recruitment of Cdk2 by Cdc45 and histone H1 phosphorylation. J Cell Biol **168**: 875-886.

Allan, J., P. G. Hartman, C. Crane-Robinson and F. X. Aviles 1980. The structure of histone H1 and its location in chromatin. Nature **288**: 675-679.

Allfrey, V. G., R. Faulkner and A. E. Mirsky 1964. Acetylation And Methylation Of Histones And Their Possible Role In The Regulation Of Rna Synthesis. Proc Natl Acad Sci U S A **51**: 786-794.

Anderson, J. D., P. T. Lowary and J. Widom 2001. Effects of histone acetylation on the equilibrium accessibility of nucleosomal DNA targets. Journal of Molecular Biology. **307**: 977-985.

Anguita, E., C. A. Johnson, W. G. Wood, B. M. Turner and D. R. Higgs 2001. Identification of a conserved erythroid specific domain of histone acetylation across the a–globin gene cluster. Proceedings of the National Academy of Sciences in the United States of America **98**: 12114-12119.

Ausio, J. 2000. Analytical ultracentrifugation and the characterization of chromatin structure. Biophys Chem **86**: 141-153.

Ausio, J. 2006. Histone variants--the structure behind the function. Brief Funct Genomic Proteomic **5**: 228-243.

Ausio, J. and D. W. Abbott (2004). The Role of histone variability in chromatin stability and folding. Chromatin Structure and Dynamics: State-of-the-Art.: 241- 290.

Ausio, J., V. Ramakrishnan and G. Fasman 1986. Biochemical and Physiochemical Characterization of Chromatin Fractions with Different Degrees of Solubility Isolated from Chicken Erythrocyte Nuclei. Biochemistry **25**: 1981-1988.

Ausio, J. and K. E. van Holde 1986. Histone hyperacetylation: its effects on nucleosome conformation and stability. Biochemistry **25**: 1421-1428.

Baer, B. W. and D. Rhodes 1983. Eukaryotic RNA polymerase II binds to nucleosome cores from transcribed genes. Nature **301**: 482-488.

Baxter, E. W., W. J. Cummings and R. E. Fournier 2005. Formation of a large, complex domain of histone hyperacetylation at human 14q32.1 requires the serpin locus control region. Nucleic Acids Res **33**: 3313-3322.

Belotserkovskaya, R., S. Oh, V. A. Bondarenko, G. Orphanides, V. M. Studitsky and D. Reinberg 2003. FACT facilitates transcription dependent nucleosome alteration. Science **310**: 1090-1093.

Bernstein, B. E., M. Kamal, K. Lindblad-Toh, S. Bekiranov, D. K. Bailey, D. J. Huebert, S. McMahon, E. K. Karlsson, E. J. Kulbokas, 3rd, T. R. Gingeras, S. L. Schreiber and E. S. Lander 2005. Genomic maps and comparative analysis of histone modifications in human and mouse. Cell **120**: 169-181.

Blander, G. and L. Guarente 2004. The Sir2 family of protein deacetylases. Annu Rev Biochem **73**: 417-435.

Bone, J. R., J. Lavender, R. Richman, M. J. Palmer, B. M. Turner and M. I. Kuroda 1994. Acetylated histone H4 on the male X chromosome is associated with dosage compensation in Drosophila. Genes Dev **8**: 96-104.

Brower-Toland, B., D. A. Wacker, R. M. Fulbright, J. T. Lis, W. L. Kraus and M. D. Wang 2005. Specific contributions of histone tails and their acetylation to the mechanical stability of nucleosomes. Journal of Molecular Biology. **346**: 135 -146.

Bruno, M., A. Flaus, C. Stockdale, C. Rencurel, H. Ferreira and T. Owen-Hughes 2003. Histone H2A/H2B dimer exchange by ATP-dependent chromatin remodeling activities. Molecular Cell **12**: 1599-1606.

Butler, P. J. and J. O. Thomas 1980. Changes in chromatin folding in solution. J Mol Biol **140**: 505-529.

Calestagne-Morelli, A. and J. Ausio 2006. Long-range histone acetylation: biological significance, structural implications, and mechanisms. Biochem Cell Biol **84**: 518-527.

Catez, F., T. Ueda and M. Bustin 2006. Determinants of histone H1 mobility and chromatin binding in living cells. Nat Struct Mol Biol **13**: 305-310.

Chambeyron, S. and W. A. Bickmore 2004. Chromatin decondensation and nuclear reorganization of the *HoxB* locus upon induction of transcription. Genes and Development **18**: 1119-1130.

Chang, S. and T. M. Aune 2005. Histone hyperacetylated domains across the Ifng gene region in natural killer cells and T cells. Proc Natl Acad Sci U S A **102**: 17095-17100.

Chowdhury, D. and R. Sen 2001. Stepwise activation of the immunoglobin μ heavy chain gene locus. EMBO **20**: 6394-6403.

Clarke, D. J., L. P. O'Neill and B. M. Turner 1993. Selective use of H4 acetylation sites in the yeast Saccharomyces cerevisiae. Biochem J **294 (Pt 2)**: 557-561.

Clayton, A. L., C. A. Hazzalin and L. C. Mahadevan 2006. Enhanced histone acetylation and transcription: a dynamic perspective. Mol Cell **23**: 289-296.

Dion, M. F., S. J. Altschuler, L. F. Wu and O. J. Rando 2005. Genomic characterization reveals a simple histone H4 acetylation code. Proceedings of the National Academy of Sciences in the United States of America **102**: 5501-5506.

Dorigo, B., T. Schalch, K. Bystricky and T. J. Richmond 2003. Chromatin fiber folding: requirement for the histone H4 N-terminal tail. J Mol Biol **327**: 85-96.

Dorigo, B., T. Schalch, A. Kulangara, S. Duda, R. R. Schroeder and T. J. Richmond 2004. Nucleosome arrays reveal the two-start organization of the chromatin fiber. Science **306**: 1571-1573.

Dou, Y., J. Bowen, Y. Liu and M. A. Gorovsky 2002. Phosphorylation and an ATP-dependent process increase the dynamic exchange of H1 in chromatin. J Cell Biol **158**: 1161-1170.

Dou, Y., C. A. Mizzen, M. Abrams, C. D. Allis and M. A. Gorovsky 1999. Phosphorylation of linker histone H1 regulates gene expression in vivo by mimicking H1 removal. Mol Cell **4**: 641-647.

Dunker, A. K., J. D. Lawson, C. J. Brown, R. M. Williams, P. Romero, J. S. Oh, C. J. Oldfield, A. M. Campen, C. R. Ratliff, K. W. Hipps, J. Ausio, M. S. Nissen, R. Reeves, C. H. Kang, C. R. Kissinger, R. W. Bailey, M. D. Griswold, M. Chiu, E. C. Garner and Z. Obradovic 2001. Intrinsically disordered protein. Journal of Molecular Graphics and Modelling **19**: 26-59.

Eberharter, A. and P. B. Becker 2002. Histone acetylation: a switch between repressive and permissive chromatin. EMBO **3**: 224-229.

Elefant, F., Y. Su, S. A. Liebhaber and N. E. Cooke 2000. Patterns of histone acetylation suggest dual pathways for gene activation by a bifunctional locus control region. EMBO **19**: 6814-6822.

Forsberg, E. C., K. M. Downs, H. M. Christensen, H. Im, P. A. Nuzzi and E. H. Bresnick 2000. Developmentally dynamic histone acetylation pattern of a tissue-specific chromatin domain. Proc Natl Acad Sci U S A **97**: 14494-14499.

Fraga, M. F., E. Ballestar, A. Villar-Garea, M. Boix-Chornet, J. Espada, G. Schotta, T. Bonaldi, C. Haydon, S. Ropero, K. Petrie, N. G. Iyer, A. Perez-Rosado, E. Calvo, J. A. Lopez, A. Cano, M. J. Calasanz, D. Colomer, M. A. Piris, N. Ahn, A. Imhof, C. Caldas,

T. Jenuwein and M. Esteller 2005. Loss of acetylation at Lys16 and trimethylation at Lys20 of histone H4 is a common hallmark of human cancer. Nat Genet **37**: 391-400.

Gale, J. M. and M. J. Smerdon 1988. UV-induced pyrimidine dimers and trimethylpsoralen cross-links do not alter chromatin folding in vitro. Biochemistry **27**: 7197-7205.

Garcia-Ramirez, M., C. Rocchini and J. Ausio 1995. Modulation of chromatin folding by histone acetylation. The Journal of Biological Chemistry **270**: 17923-17928.

Gorisch, S. M., M. Wachsmuth, K. F. Toth, P. Lichter and K. Rippe 2005. Histone acetylation increases chromatin accessibility. J Cell Sci **118**: 5825-5834.

Graziano, V., S. E. Gerchman and V. Ramakrishnan 1988. Reconstitution of chromatin higher-order structure from histone H5 and depleted chromatin. J Mol Biol **203**: 997-1007.

Hansen, J. C., J. Ausio, V. H. Stanik and K. E. van Holde 1989. Homogeneous reconstituted oligonucleosomes, evidence for salt-dependent folding in the absence of histone H1. Biochemistry **28**: 9129-9136.

Hebbes, T. R., A. L. Clayton, A. W. Thorne and C. Crane-Robinson 1994. Core histone hyperacetylation co-maps with generalized DNase I sensitivity in the chicken beta-globin chromosomal domain. Embo J **13**: 1823-1830.

Horn, P. J., L. M. Carruthers, C. Logie, D. A. Hill, M. J. Solomon, P. A. Wade, A. N. Imbalzano, J. C. Hansen and C. L. Peterson 2002. Phosphorylation of linker histones regulates ATP-dependent chromatin remodeling enzymes. Nat Struct Biol **9**: 263-267.

Huynh, V. A., P. J. Robinson and D. Rhodes 2005. A method for the in vitro reconstitution of a defined "30 nm" chromatin fibre containing stoichiometric amounts of the linker histone. J Mol Biol **345**: 957-968.

Invitrogen 2006. TOPO TA Cloning® User's Manual. 1-27.

Jackson, V. 1990. In vivo studies on the dynamics of histone-DNA interaction: evidence for nucleosome dissolution during replication and transcription and a low level of dissolution independent of both. Biochemistry **29**: 719-731.

Jenuwein, T. and C. D. Allis 2001. Translating the histone code. Science **293**: 1074-1080.

Kamakaka, R. T. and J. O. Thomas 1990. Chromatin structure of transcriptionally competent and repressed genes. Embo J **9**: 3997-4006.

Katan-Khaykovich, Y. and K. Struhl 2002. Dynamics of global histone acetylation and deacetylation in vivo: rapid restoration of normal histone acetylation status upon removal of activators and repressors. Genes and Development **16**: 743-752.

Kimura, A., T. Umehara and M. Horikoshi 2002. Chromosomal gradient of histone acetylation established by Sas2p and Sir2p functions as a shield against gene silencing. Nat Genet **32**: 370-377.

Kireeva, M. L., W. Walter, V. Tchernajenko, V. Bondarenko, M. Kashlev and V. M. Studitsky 2002. Nucleosome remodeling induced by RNA polymerase II: loss of the H2A/H2B dimer during transcription. Mol Cell **9**: 541-552.

Korzus, E., J. Torchia, D. W. Rose, L. Xu, R. Kurokawa, E. M. McInerney, T. M. Mullen, C. K. Glass and M. G. Rosenfeld 1998. Transcription factor-specific requirements for coactivators and their acetyltransferase functions. Science **279**: 703-707.

Krebs, J. E., C. J. Fry, M. L. Samuels and C. L. Peterson 2000. Global role for chromatin remodeling enzymes in mitotic gene expression. Cell **102**: 587-598.

Kuo, M., E. Baur, K. Struhl and D. Allis 2000. Gcn4 activator targets Gcn5 histone acetyltransferase to specific promoters independently of transcription. Molecular Cell **6**: 1309-1320.

Kurdistani, S. K., S. Tavazoie and M. Grunstein 2004. Mapping global histone acetylation patterns to gene expression. Cell **117**: 721-733.

Kysela, B., M. Chovanec and P. A. Jeggo 2005. Phosphorylation of linker histones by DNA-dependent protein kinase is required for DNA ligase IV-dependent ligation in the presence of histone H1. Proc Natl Acad Sci U S A **102**: 1877-1882.

Letting, D. L., C. Rakowski, M. J. Weiss and A. B. Gerd 2003. Formation of a tissue-specific histone acetylation pattern by the hematopoietic transcription factor GATA-1. Molecular and Cellular Biology **23**: 1334-1340.

Levchenko, V., B. Jackson and V. Jackson 2005. Histone release during transcription: displacement of the two H2A-H2B dimers in the nucleosome is dependent on different levels of transcription-induced positive stress. Biochemistry **44**: 5357-5372.

Litt, M. D., M. Simpson, F. Recillas-Targa, M. Prioleau and G. Felsenfeld 2001. Transition in histone acetylation reveal boundaries of three separately regulated neighboring loci. EMBO **20**: 2224-2235.

Lowary, P. T. and J. Widom 1998. New DNA sequence rules for high affinity binding to histone octamer and sequence-directed nucleosome positioning. J Mol Biol **276**: 19-42.

Luger, K., A. W. Mader, R. K. Richmond, D. F. Sargent and T. J. Richmond 1997. Crystal structure of the nucleosome core particle at 2.8 angstrom resolution. Nature **389**: 251-260.

McGhee, J. D., J. M. Nickol, G. Felsenfeld and D. C. Rau 1983. Histone hyperacetylation has little effect on the higher order folding of chromatin. Nucleic Acids Res **11**: 4065-4075.

Meijsing, S. H. and A. E. Ehrenhofer-Murray 2001. The silencing complex SAS-I links histone acetylation to the assembly of repressed chromatin by CAF-I and Asf1 in Saccharomyces cerevisiae. Genes Dev **15**: 3169-3182.

Morales, V. and H. Richard-Foy 2000. Role of N-terminal tails and their acetylation in nucleosome dynamics. Molecular and Cellular Biology **20**: 7230-7237.

Mutskov, V., D. Gerber, D. Angelov, J. Ausio, J. Workman and S. Dimitrov 1998. Persistent interactions of core histone tails with nucleosomal DNA following acetylation and transcription factor binding. Molecular and Cellular Biology **18**: 6293-6304.

Myers, F. A., D. R. Evans, A. L. Clayton, A. W. Thorne and C. Crane-Robinson 2001. Targeted and extended acetylation of histones H4 and H3 at active and inactive genes in chicken embryo erythrocytes. J Biol Chem **276**: 20197-20205.

Oliva, R., D. P. Bazett-Jones, L. Locklear and G. H. Dixon 1990. Histone hyperacetylation can induce unfolding of the nucleosome core particle. Nucleic Acids Res **18**: 2739-2747.

Parekh, B. S. and T. Maniatis 1999. Virus infection leads to localized hyperacetylation of histones H3 and H4 at the IFN-beta promoter. Mol Cell **3**: 125-129.

Park, Y. J. and K. Luger 2006. The structure of nucleosome assembly protein 1. Proc Natl Acad Sci U S A **103**: 1248-1253.

Perry, C. A. and A. T. Annunziato 1991. Histone acetylation reduces H1-mediated nucleosome interactions during chromatin assembly. Exp Cell Res **196**: 337-345.

Perry, M. and R. Chalkley 1982. Histone acetylation increases the solubility of chromatin and occurs sequentially over most of the chromatin. A novel model for the biological role of histone acetylation. J Biol Chem **257**: 7336-7347.

Protacio, R. U., G. Li, P. T. Lowary and J. Widom 2000. Effects of histone tail domains on the rate of transcriptional elongation through a nucleosome. Molecular and Cellular Biology **20**: 8866-8878.

Rastegar, M., L. Kobrossy, E. N. Kovacs, I. Rambaldi and M. Featherstone 2004. Sequential histone modifications at Hoxd4 regulatory regions distinguish anterior from posterior embryonic compartments. Mol Cell Biol **24**: 8090-8103.

Reid, J., Z. Moqtaderi and K. Struhl 2004. Regulates the global pattern of histone acetylation in *Saccharomyces cerevisiae*. Molecular and Cellular Biology **24**: 757-764.

Ridsdale, J. A., M. J. Hendzel, G. P. Delcuve and J. R. Davie 1990. Histone acetylation alters the capacity of the H1 histones to condense transcriptionally active/competent chromatin. J Biol Chem **265**: 5150-5156.

Roh, T., S. Cuddapah and K. Zhao 2005. Active chromatin domains are defined by acetylation islands revealed by genome-wide mapping. Genes and Development **19**: 542-552.

Roh, T., W. C. Ngau, K. Cui, D. Landsman and K. Zhao 2004. High resolution genome-wide mapping of histone modifications. Nature Biotechnology **22**: 1013-1016.

Ruiz-Carrillo, A., J. L. Jorcano, G. Eder and R. Lurz 1979. In vitro core particle and nucleosome assembly at physiological ionic strength. Proc Natl Acad Sci U S A **76**: 3284-3288.

Schubeler, D., C. Francastel, D. M. Cimbora, A. Reik, D. I. Martin and M. Groudine 2000. Nuclear localization and histone acetylation: a pathway for chromatin opening and transcriptional activation of the human beta-globin locus. Genes Dev **14**: 940-950.

Seligson, D. B., S. Horvath, T. Shi, H. Yu, S. Tze, M. Grunstein and S. K. Kurdistani 2005. Global histone modification patterns predict risk of prostate cancer recurrence. Nature **435**: 1262-1266.

Shia, W. J., S. Osada, L. Florens, S. K. Swanson, M. P. Washburn and J. L. Workman 2005. Characterization of the yeast trimeric-SAS acetyltransferase complex. J Biol Chem **280**: 11987-11994.

Shia, W. J., S. G. Pattenden and J. L. Workman 2006. Histone H4 lysine 16 acetylation breaks the genome's silence. Genome Biol **7**: 217.

Shogren-Knaak, M., H. Ishii, J. M. Sun, M. J. Pazin, J. R. Davie and C. L. Peterson 2006. Histone H4-K16 acetylation controls chromatin structure and protein interactions. Science **311**.

Shogren-Knaak, M. and C. L. Peterson 2006. Switching on chromatin: mechanistic role of histone H4-K16 acetylation. Cell Cycle **5**: 1361-1365.

Siino, J. S., P. M. Yau, B. S. Imai, J. M. Gatewood and E. M. Bradbury 2003. Effect of DNA length and H4 acetylation on the thermal stabilty of reconstituted nucleosome particles. Biochemical and Biophysical Research Communications **302**: 885-891.

Simpson, R. T., F. Thoma and J. M. Brubaker 1985. Chromatin reconstituted from tandemly repeated cloned DNA fragments and core histones: a model system for study of higher order structure. Cell **42**: 799-808.

Smith, C. M., P. R. Gafken, Z. Zhang, D. E. Gottschling, J. B. Smith and D. L. Smith 2003. Mass spectrometric quantification of acetylation at specific lysines within the amino-terminal tail of histone H4. Anal Biochem **316**: 23-33.

Spotswood, H. T. and B. M. Turner 2002. An increasingly complex code. The Journal Of Clinical Investigation. **110**: 577-582.

Steinmetz, M., R. E. Streeck and H. G. Zachau 1978. Reconstituted histone--DNA complexes. Philos Trans R Soc Lond B Biol Sci **283**: 259-268.

Strahl, B. and C. D. Allis 2000. The language of covalent histone modifications. Nature **403**: 41-45.

Straub, T., I. K. Dahlsveen and P. B. Becker 2005. Dosage compensation in flies: mechanism, models, mystery. FEBS Lett **579**: 3258-3263.

Suka, N., K. Luo and M. Grunstein 2002. Sir2p and Sas2p opposingly regulate acetylation of yeast histone H4 lysine16 and spreading of heterochromatin. Nat Genet **32**: 378-383.

Sung, M. T., J. Harford, M. Bundman and G. Vidalakas 1977. Metabolism of histones in avian erythroid cells. Biochemistry **16**: 279-285.

Tamburini, B. A. and J. K. Tyler 2005. Localized histone acetylation and deacetylation triggered by the homologous recombination pathway of double-strand DNA repair. Mol Cell Biol **25**: 4903-4913.

Th'ng, J. P., R. Sung, M. Ye and M. J. Hendzel 2005. H1 family histones in the nucleus. Control of binding and localization by the C-terminal domain. J Biol Chem **280**: 27809-27814.

Thoma, F., T. Koller and A. Klug 1979. Involvement of histone H1 in the organization of the nucleosome and of the salt-dependent superstructures of chromatin. J Cell Biol **83**: 403-427.

Thorne, A. W., D. Kmiciek, K. Mitchelson, P. Sautiere and C. Crane-Robinson 1990. Patterns of histone acetylation. European Journal of Biochemistry **193**: 701-713.

Topalidou, I., M. Papamichos-Chronakis and G. Thireos 2003. Post-TATA binding protein recruitment clearance of Gcn5-dependent histone acetylation within promoter nucleosomes. Molecular and Cellular Biology **23**: 7809-7817.

Tse, C., T. Sera, A. P. Wolffe and J. C. Hansen 1998. Disruption of higher-order folding by core histone acetylation dramatically enhances transcription of nucleosomal arrays by RNA polymerase III. Mol Cell Biol **18**: 4629-4638.

Turner, B. M. 1993. Decoding the nucleosome. Cell **75**: 5-8.

Turner, B. M. 2005. Reading signals on the nucleosome with a new nomenclature for modified histones. Nat Struct Mol Biol **12**: 110-112.

Turner, B. M., A. J. Birley and J. Lavender 1992. Histone H4 isoforms acetylated at specific lysine residues define individual chromosomes and chromatin domains in Drosophila polytene nuclei. Cell **69**: 375-384.

Turner, B. M. and G. Fellows 1989. Specific antibodies reveal ordered and cell-cycle-related use of histone-H4 acetylation sites in mammalian cells. Eur J Biochem **179**: 131-139.

Turner, B. M., L. P. O'Neill and I. M. Allan 1989. Histone H4 acetylation in human cells. Frequency of acetylation at different sites defined by immunolabeling with site-specific antibodies. FEBS Lett **253**: 141-145.

van Holde, K. E. (1989). Chromatin. NewYork, Springner Verlag.
van Holde, K. E., D. E. Lohr and C. Robert 1992. What happens to nucleosomes during transcription? Journal of Biological Chemistry. **267**: 2837-2840.

Vignali, M., D. J. Steger, K. E. Neely and J. L. Workman 2000. Distribution of acetylated histones resulting from Gal4-VP16 recruitment of SAGA and NuA4 complexes. EMBO **19**: 2629-2640.

Vogelauer, M., J. Wu, N. Suka and M. Grunstein 2000. Global histone acetylation and deacetylation in yeast. Nature **408**: 495-498.

Wagner, T. E., J. B. Hartford, M. Serra, V. Vandegrift and M. T. Sung 1977. Phosphorylation and dephosphorylation of histone (V (H5): controlled condensation of avian erythrocyte chromatin. Appendix: Phosphorylation and dephosphorylation of histone H5. II. Circular dichroic studies. Biochemistry **16**: 286-290.

Wang, X., C. He, S. C. Moore and J. Ausio 2001. Effects of histone acetylation on the solubility and folding of the chromatin fiber. The Journal of Biological Chemistry. **276**: 12764-12768.

Wang, X., S. C. Moore, M. Laszckzak and AusioJ. 2000. Acetylation increases the a-helical content of the histone tails of the nucleosome. The Journal of Biological Chemistry **275**: 35013-35020.

Waterborg, J. H. 2000. Steady-state levels of histone acetylation in Saccharomyces cerevisiae. J Biol Chem **275**: 13007-13011.

Waterborg, J. H. 2002. Dynamics of histone acetylation in vivo. A function for acetylation turnover? Biochem Cell Biol **80**: 363-378.

Yellajoshyula, D. and D. T. Brown 2006. Global modulation of chromatin dynamics mediated by dephosphorylation of linker histone H1 is necessary for erythroid differentiation. Proc Natl Acad Sci U S A **103**: 18568-18573.

Zhang, K., K. E. Williams, L. Huang, P. Yau, J. S. Siino, E. M. Bradbury, P. R. Jones, M. J. Minch and A. L. Burlingame 2002. Histone acetylation and deacetylation: identification of acetylation and methylation sites of HeLa histone H4 by mass spectrometry. Molecular and Cellular Proteomics **1**: 500-508.

Zhou, W., S. Chang and T. M. Aune 2004. Long-range histone acetylation of the Ifng gene is an essential feature of T cell differentiation. Proceedings of the National Academy of Sciences in the United States of America **101**: 2440-2445.

Appendix 1

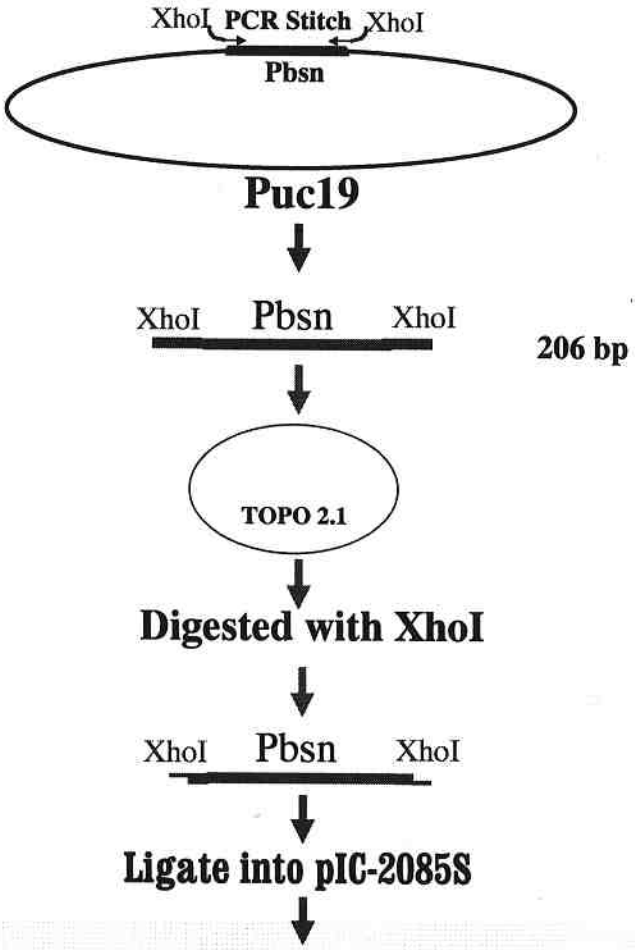
XhoI
PCR Stitch
XhoI
Pbsn
Puc19
XhoI
Pbsn
XhoI
206 bp
TOPO 2.1
Digested with XhoI
XhoI
Pbsn
XhoI
Ligate into pIC-2085S

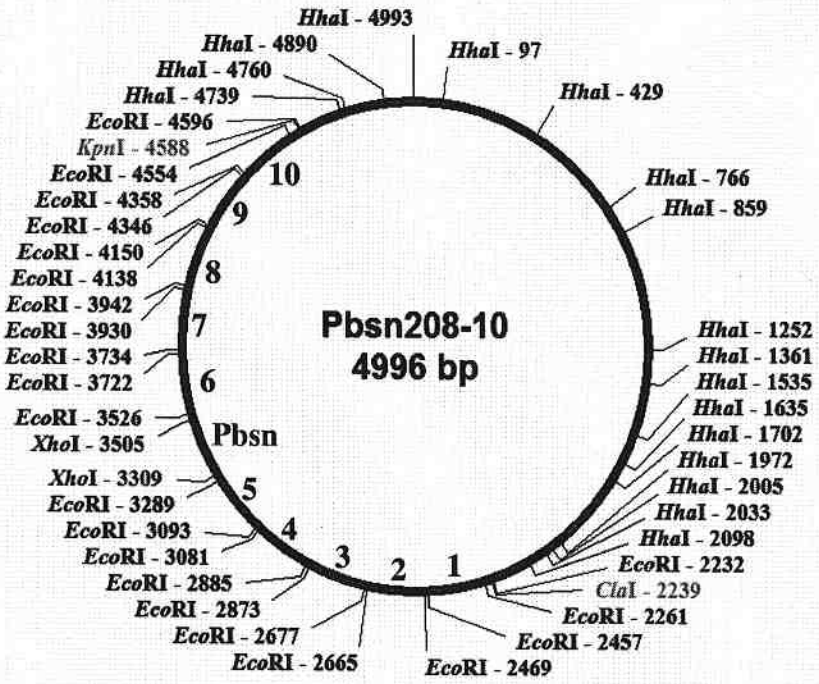
HhaI - 4993
HhaI - 4890
HhaI - 4760
HhaI - 4739
EcoRI - 4596
KpnI - 4588
EcoRI - 4554
EcoRI - 4358
EcoRI - 4346
EcoRI - 4150
EcoRI - 4138
EcoRI - 3942
EcoRI - 3930
EcoRI - 3734
EcoRI - 3722
EcoRI - 3526
XhoI - 3505
XhoI - 3309
EcoRI - 3289
EcoRI - 3093
EcoRI - 3081
EcoRI - 2885
EcoRI - 2873
EcoRI - 2677
EcoRI - 2665
HhaI - 97
HhaI - 429
HhaI - 766
HhaI - 859
HhaI - 1252
HhaI - 1361
HhaI - 1535
HhaI - 1635
HhaI - 1702
HhaI - 1972
HhaI - 2005
HhaI - 2033
HhaI - 2098
EcoRI - 2232
ClaI - 2239
EcoRI - 2261
EcoRI - 2457
EcoRI - 2469
Pbsn208-10
4996 bp
Pbsn
10
9
8
7
6
5
4
3
2
1